2018

Surface Coat Replacement Dynamics and Antigen Glycosylation in T. Brucei Influence Evasion of the Host Antibody Response

Jason M. Pinger

SURFACE COAT REPLACEMENT DYNAMICS AND ANTIGEN GLYCOSYLATION IN *T. BRUCEI* INFLUENCE EVASION OF THE HOST ANTIBODY RESPONSE

A Thesis Presented to the Faculty of

The Rockefeller University

in Partial Fulfillment of the Requirements for

the degree of Doctor of Philosophy

by

Jason M. Pinger

June 2018

SURFACE COAT REPLACEMENT DYNAMICS AND ANTIGEN GLYCOSYLATION IN *T. BRUCEI* INFLUENCE EVASION OF THE HOST ANTIBODY RESPONSE

Jason M. Pinger, Ph.D.

The Rockefeller University 2018

The protozoan parasite *Trypanosoma brucei,* a causative agent of human and animal trypanosomiasis, evades host immunity through antigenic variation of its variant surface glycoprotein (VSG) coat. During infection, the VSG coat elicits a robust antibody response, but the parasite escapes antibody-mediated clearance by repeatedly accessing its large genomic *VSG* repertoire and switching expression to antigenically distinct *VSGs*. Much of our knowledge of the process of VSG switching and the extent of VSG diversity has come from genetic analyses, but deep understanding of the *T. brucei* host-pathogen interface also requires examination of these topics at the protein level. In this thesis, I describe two protein-based studies of the VSG coat that reveal factors influencing trypanosome evasion of the host antibody response.

First, I discuss my examination of the dynamics of VSG coat replacement following a genetic *VSG* switch, and the impact of this process on the parasite's ability to escape the escalating host antibody response. Using a flow cytometry-based measurement strategy, I evaluated the rate of VSG replacement at the trypanosome surface, and showed that full coat replacement requires several days to complete. I then demonstrated through *in vivo* infection assays that parasites undergoing coat replacement are only vulnerable to clearance via early IgM antibodies for a limited time. Finally, IgM binding analyses and molecular modeling indicated that IgM loses its ability to mediate trypanosome clearance at unexpectedly early stages of coat replacement based on a critical density threshold of its cognate VSGs on the parasite surface.

In the second part of this thesis, I describe a collaborative body of work examining the biochemical features of VSG3 (also termed MITat1.3 and VSG224) and their relevance to parasite interactions with host immunity. The crystal structure of VSG3 was solved, and analysis of the high-resolution structure revealed a glycan of a form previously unidentified in *T. brucei*, which was centrally located within a region likely to be involved in VSG-antibody interactions. Subsequent mouse infection and antibody binding analyses demonstrated that this VSG modification increases parasite virulence and facilitates evasion of host antibodies.

Together, these studies increase our understanding of *T. brucei* infection dynamics and reveal that additional layers of VSG diversity can affect parasite immune evasion. The identification of an antigen density threshold for *in vivo* IgM functionality may also inform other systems in which IgM plays a crucial role. These results affirm that much remains to be learned about the interactions of the VSG coat with the host antibody response. Further examination of VSG biochemical diversity and the VSG-antibody interface may provide additional insights into *T. brucei* pathogenesis and potentially carry implications for other host-pathogen interactions or immune interactions in general.

ACKNOWLEDGEMENTS

I would first like to thank my advisor, Nina Papavasiliou, for her support throughout my graduate studies. Nina believed in my ideas and allowed me to pursue my interests while also giving me the opportunity to independently make (and resolve) mistakes. Her encouragement, insight, and patience as I solved each new set of problems helped me develop as a researcher and expand my belief in my own scientific abilities.

I also thank George Cross for the vast amount of advice and support he has provided. His broad knowledge on *T. brucei*-related literature afforded many key insights and often provided me with crucial direction to further my research. His thoughtful critical analyses helped me know when to reevaluate my work, and were also a source of great encouragement.

I thank the other members of my faculty committee, Howard Hang, and Kirk Deitsch for their time, direction, and for pressing me to expand my abilities in project planning and experimental design. Their annual evaluations were crucial to the formation of my research into a cohesive body of work. Additionally, I thank Christian Tschudi for serving as external examiner during my thesis defense.

I am very grateful to the collaborators who have contributed to the work presented here: Dragana Nešić, Liaqat Ali, Michael A. J. Ferguson, and C. Erec Stebbins. Of these collaborators, I worked most closely with C. Erec Stebbins in data analysis, and manuscript and figure preparations, and I thank him very much for all of his efforts and thoughtful commentary throughout our interactions. I am also grateful to the Rockefeller Flow Cytometry Resource Center staff for assisting me with my many flow cytometry experiments. In particular, I thank FCRC director Svetlana Mazel for her interest in the progression of my work, and for imparting

some of her flow cytometry wisdom to me. I also would like to thank Michael Mitchell for his help in statistical analyses.

I could not have done this without the support of my labmates. Upon first joining the lab, Pete Stavropoulos assisted me in generating constructs to develop VSG sortagging, helping me appreciate the value of combining rational design and brute force to solve engineering problems. Galadriel Hovel-Miner and Hee-Sook Kim provided me with trypanosome cell lines and plasmids prior to their publication, and also provided instruction on how to use them for my purposes. Francisco Aresta-Branco made key contributions to our study on VSG3 glycosylation. These labmates, along with the rest of the *T. brucei* crew, Monica Mugnier and Danae Schulz, were a constant source of valuable feedback and support as well as being excellent companions in lab and at conferences. It was a privilege to mentor my enthusiastic SURF student (and later technician) Shanin Chowdhury, whose efforts in mouse immunizations and infections and antibody binding analyses contributed greatly to both studies presented in this thesis. I want to thank my other labmates, Violeta Rayon Estrada, Maryam Zaringhalam, Linda Molla, Dimitris Garyfallos, Gianna Triller, Anita Ramnarain, Dewi Harjanto, and Nick Economos for helping make work so enjoyable, for lab dinner outings, and for being great friends.

For so many fun times, amazing memories, and being there for me when I've needed it, many thanks to my friends Doug Deutsch, Lee Hecht, Kevin Gavidia, Elaine O'Connell, and Josh Horwitz, and my girlfriend Atarah Joshua.

To Judy, Dan, Elliott, Julie, Anna Rose and Taylor (my family in all but name); Uncle Larry and Aunt Ann; my sister-in-law Sabine; and my brother Nathan: these past seven years have taught me about the depth of the meaning of family. I am so grateful for the warmth, understanding, and stability you have provided me. I'm lucky to have you all in my life.

Finally, to my parents: thank you for your love and support, for your unyielding interest in my long-winded explanations of my work, for visiting me in New York and making my visits home still feel like home, for constantly encouraging me to pursue my interests, and for always believing in me. I can't express enough gratitude for all you have done for me.

TABLE OF CONTENTS

LIST OF FIGURES

LIST OF ABBREVIATIONS

AAT – animal African trypanomiasis
BES – bloodstream form expression site
BIR – break-induced replication
bp – base pair
C/PD – cells per population doubling
CTR – co-transposed region
Dox – doxycycline
DSB – double strand DNA break
ESAG – expression site associated gene
ESB – expression site body
GC – gene conversion
GPI – glycosylphosphatidylinositol
GPI-PLC – GPI phospholipase C
HAT – human African trypanosomiasis
HR – homologous recombination
MESF – Molecules of equivalent soluble fluorochrome
MFI – Mean fluorescence intensity
SM – single marker, a VSG2-expressing Lister 427 trypanosome cell line. This cell line has a T7 RNA polymerase gene, a Tet repressor gene, and a neomycin resistance gene inserted into a β tubulin locus.
Sortase – Sortase A, derived from *S. pyogenes*
TE – telomere exchange
TLF – trypanosome lytic factor
TLR – Toll-like receptor
UTR – untranslated region
VSG – variant surface glycoprotein
VSG2 = MITat 1.2, Lister 427-2, VSG221. GenBank # X56762
VSG3 = MITat 1.3, Lister 427-3, VSG224. GenBank # AY935575

Chapter 1

Introduction

1.1 African trypanosomes and trypanosomiasis

Human African trypanosomiasis (HAT), also known as African sleeping sickness, is an infectious disease that affects large regions of sub-Saharan Africa. It is transmitted between hosts by the bite of the tsetse fly (*Glossina* spp.), and the habitat range of this vector defines the geographical distribution of HAT endemic regions[1]. The disease can also transmit between different mammalian species, and infections in non-human hosts are known as animal African trypanosomiasis (AAT) or nagana[2]. In humans, the disease is almost invariably fatal if untreated[1].

HAT and AAT are caused by a group of unicellular, protozoan parasites known as African trypanosomes. Only two subspecies of African trypanosome, *Trypanosoma brucei gambiense*, and *T. brucei rhodesiense* are capable of infecting humans, and infections with both of these subspecies proceed in two stages. First, the parasite inhabits the blood, lymph, and interstitial fluids of its host, and recent evidence suggests it can also invade fatty tissues[3]. Symptoms at this stage are non-specific to trypanosomiasis (e.g. intermittent fever, aches), which complicates early diagnosis. In the second stage, the parasite crosses the blood-brain barrier and invades the central nervous system. First stage symptoms persist, accompanied by additional neurological symptoms such as psychiatric disorders and disturbance of the sleep cycle (originating the name "African sleeping sickness"), which intensify as the disease progresses. Drug treatment is possible at both stages, but the comparatively milder drugs used to treat first stage disease cannot cross the blood-brain barrier, requiring the use of different drugs for second stage treatment, which are more toxic and difficult to administer[1,4,5]. The time course of HAT pathogenesis varies depending on the *T. brucei* subspecies causing the infection. *T. b. gambiense*,

which is found in western and central Africa, causes a chronic, slowly progressing infection lasting up to several years. *T. b. rhodesiense*, found in eastern and southern Africa, typically causes acute infection, progressing to second stage within weeks, and death within 6 months[1]. The vast majority (~97%) of HAT cases are caused by *T. b gambiense*[6].

HAT was a cause of significant mortality through much of the 20th century, but control measures (including improved diagnosis and disease surveillance, access to treatment, and vector control) have dramatically reduced the spread of human infection in recent years, with the number of new reported HAT cases falling from ~40,000 in 1998 to only 2804 in 2015[1,5]. However, the number of reported cases is considered to represent only a fraction of the actual number of infected individuals, and ~60 million people are still estimated to be at risk of infection [4,7]. Furthermore, the utility of current HAT treatment options is increasingly threatened by the development of drug resistance, necessitating continued efforts to discover novel anti-trypanosomal drugs[8].

A more diverse set of African trypanosomes infect animal hosts, including both human-infectious *T. brucei* subspecies, another subspecies *T. brucei brucei,* and other members of the *Trypanosoma* genus, *T. congolense*, *T. vivax, T. evansi*, and *T. equiperdum* [2] (although recent phylogenetic analyses suggest that *T. evansi* and *T. equiperdum*, which have long been considered individual species, may more accurately be described as *T. brucei* subspecies[9]). In contrast to the human-infectious trypanosomes, many animal-infectious trypanosomes, including *T. vivax*, *T. evansi*, and *T. equiperdum*, have evolved transmission mechanisms through vectors other than the tsetse fly. These adaptations have allowed these trypanosomes to spread outside of Africa into South and Central America, Asia, and parts of southern Europe. The animal-infectious trypanosome species show diversity in predominant host species affected, disease

pathogenicity, vector, and geographical distribution, and collectively they impose a significant burden on global agricultural economies due to death and morbidity of cattle and other livestock[2]. In Africa alone, the annual economic losses due to AAT are estimated at ~1-5 billion USD[4,10]. Additionally, these animal infections may function as a reservoir for human-infectious parasites, threatening efforts to eradicate African trypanosomiasis as a public health concern[11].

The reason many animal-infectious trypanosomes cannot infect humans is that human blood contains two innate immune complexes, trypanosome lytic factor 1 (TLF-1) and TLF-2, which have trypanocidal properties[12-14]. On rare occasions, humans can become infected with animal-infectious parasites[15]. In some cases the individual's susceptibility to these infections can be attributed to mutations in TLF components[16], but in other cases the cause of susceptibility is unknown[17]. Human-infectious *T. brucei gambiense* and *T. brucei rhodesiense* have both evolved mechanisms of inhibiting the action of the TLFs[18-22], and the possibility remains that additional trypanosome species may evolve resistance mechanisms which allow transfer of these infections to humans. While the animal-infectious African trypanosome species are all clearly important to global agriculture and animal health, this thesis will be primarily focused on *T. brucei*, the species more relevant to human infection and the most intensely studied of the African trypanosomes.

1.2 *T. brucei* life cycle and transmission

T. brucei inhabits extracellular spaces within both the vector and the mammalian host. In order to survive in each of these environments and successfully transfer between hosts, the parasite undergoes a sequence of life cycle stages with adaptive morphologies, proliferative capacities, and gene expression patterns. The *T. brucei* life cycle begins when an infected tsetse fly takes a blood meal, and metacyclic form parasites are transferred into the host bloodstream

through the fly's saliva. These trypanosomes first differentiate into their slender bloodstream form. Slender form parasites are highly proliferative, and divide rapidly until a quorum sensing mechanism initiates transformation of some parasites into a non-proliferative stumpy bloodstream form[23,24]. The mixture of slender, stumpy, and intermediary (transitioning from slender to stumpy) bloodstream forms is known as "pleomorphism". Recent *T. brucei* field isolates and some lab strains are capable of pleomorphism, but many lab adapted cell lines (including the Lister 427 cell line used for experiments presented in this thesis) are generally thought to have lost the ability to differentiate to stumpy forms[25]. During infection, the growth arrest of stumpy forms helps prevent rapid host death from slender form overgrowth, which would threaten subsequent parasite transmission[26,27]. Stumpy form cells are also especially adapted for reuptake into the tsetse fly midgut during a subsequent blood meal. They are resistant to the acidic environment of the midgut[28], and their surface receptor profiles and stage of cell-cycle arrest prime them for rapid differentiation into the next life cycle stage, the procyclic form, upon receiving midgut environmental cues[29,30]. Procyclic form trypanosomes develop in the fly gut, sequentially expressing a set of surface proteins called procyclins that protect the parasite from digestive enzymes[31]. These parasites migrate towards the salivary glands, differentiate again to the epimastigote stage, and attach to the salivary gland epithelium. At this point, epimastigotes can undergo meiosis and sexual exchange of genetic material[32,33]. Finally, the parasites mature again to the mammalian-infectious metacyclic forms, and reside in the salivary glands until transferring to another host.

1.3 Antigenic variation - the variant surface glycoprotein (VSG) coat

Because *T. brucei* lives extracellularly within its mammalian host, it is continually exposed to attack from host immune factors. Long-term parasite persistence in this environment

is made possible via antigenic variation of the dense, variant surface glycoprotein (VSG) coat that covers the trypanosome in its bloodstream form. Each parasite expresses one *VSG* gene at a time from a genomic repertoire containing thousands of *VSG* genes [34], and is densely coated with ~10^7 VSGs[35,36]. VSGs are highly immunogenic. During infection, the host develops potent VSG-specific antibodies that mediate trypanosome clearance, but a minority of parasites evade clearance by accessing their *VSG* repertoire and changing their coats to antigenically distinct *VSGs*[35,37] in a process known as VSG "switching". These switched parasite populations then expand within the host until they are cleared, after which additional populations expressing distinct VSGs emerge again. This cyclical process results in characteristic waves of parasitemia occurring at approximately 5-8 day intervals during infection, with parasite suppression in sync with and mediated by the development of repeated primary, VSG-specific antibody responses[37-41].

All species of African trypanosomes express VSG coats and use antigenic variation as a survival strategy, although there are differences between species in the evolution of the genetic *VSG* repertoire[9,42], and there appear to be some species-dependent differences in the genetic mechanisms regulating VSG diversification[43]. Other pathogens also utilize similar mechanisms of antigenic variation to evade host immunity, including *Giardia lamblia*, which alters its variant surface protein (VSP) coat, and *Plasmodium falciparum*, which alters the PfEMP1 proteins it transports to the surface of infected erythrocytes[44,45]. Examination of antigenic variation and the host-pathogen interface in *T. brucei* may thus provide insights that can be applied to additional clinically relevant pathogens.

The work presented in this thesis will focus on the *T. brucei* host-pathogen interface, and particularly on host antibody interactions with the VSG coat. The remaining sections of this introduction will therefore predominately describe the current knowledge of the VSG coat,

including its structure, functional attributes, mechanisms of diversification, and interactions with host immunity.

1.4 Structure of the VSG coat and basis of immune shielding function

VSGs are large surface proteins (50-60 kDa) that are bound to the exterior face of the *T. brucei* plasma membrane by a glycosylphosphatidylinositol (GPI) anchor. They are the most abundant protein in bloodstream form *T. brucei*, accounting for about 10% of the total protein content of the cell, and at least 95% of the protein on the cell surface [46-48]. All VSGs consist of two domains: a highly variable N-terminal domain (350-400 residues), and a smaller, more conserved C-terminal domain (20-40 residues) to which the GPI anchor is attached[49,50]. The two domains are connected by a flexible linker[51]. Despite the fact that VSG N-terminal domains typically share low sequence homology, early structural analyses of the N-terminal domains of two VSG variants revealed that the VSGs had a conserved structural motif[50,52]: the VSGs formed homodimers, and each monomer was structured in a two-lobed, "dumbbell" arrangement, with the "top" (facing away from the pathogen) and "bottom" regions separated by an elongated 3-helix bundle. However, the sequences and specific architectures of each VSG varied considerably, in accordance with their function as antigenic variants. Each VSG also contains at least one N-linked oligosaccharide[53], and in all known structures these glycans are linked to residues in the bottom lobe of the N-terminus.

Our current model of the larger structure of the VSG coat has been formed and refined by a series of measurements and observations spanning the past several decades. Early cross-sectional electron microscopy images of the trypanosome plasma membrane showed a dense exterior coat with a thickness of 12-15nm[54]. This measurement, along with later determinations of VSG dimensions (derived from VSG crystal structures[50,55,56]) provided evidence that

individual VSG homodimers extend vertically from the cell surface. Further calculations based on estimates of the surface area of a vertically-oriented VSG homodimer, the total trypanosome cell surface area, and the VSG per cell copy number revealed that the VSGs are extremely tightly packed, physically occluding the vast majority of the cell surface[35,36,48]. Most recently, a study found that VSGs can adopt two conformations based on flexibility in the orientations of the C-terminal domain and linker region[51]. VSGs were identified in either a taller and thinner "compact" structure, or a shorter, more expansive "relaxed" structure. The authors concluded that shifting between these two conformations allows the VSG coat to accommodate variations in the total amount of surface VSGs while still maintaining occlusion of the plasma membrane.

Dense VSG packing is crucial to the immune shielding function of the VSG coat. Studies using VSG-specific monoclonal antibodies have shown that only a portion of antibodies generated against soluble VSGs are able to bind VSGs expressed on living trypanosomes[49,57-59]. The common interpretation of this phenomena is that close packing between VSGs limits antibody access to surfaces other than the highly variable "top" of the molecule, leaving the more conserved C-terminal domain and many epitopes of the N-terminal domain hidden by steric hindrance. However, it has also been suggested that some antigenic differences between soluble and membrane-bound VSG may be due to conformational changes in the soluble VSG resulting from delipidation of the VSG anchor[60]. Studies attempting to map the epitopes of individual monoclonal antibodies have not conclusively determined how much of the VSG N-terminus is accessible (reviewed in[49]). One notable study, which mapped the binding epitope of an IgG class antibody using chimeric VSG constructs, found that the antibody recognized a region on the "lower" lobe (proximal to the parasite) of the N-terminus[61]. This result demonstrates that at least in some cases, much of the VSG N-terminal domain may be accessible. In contrast, a study

examining polyclonal antisera raised against two VSG C-terminal domains found no binding against live trypanosomes[62], suggesting that these more conserved domains are indeed protected from immune recognition. It is often stated that the VSG coat also hides other invariant surface antigens from immune surveillance, and this is likely true for membrane proteins with small extracellular domains[49]. However, antibodies recognizing invariant surface proteins with large extracellular domains have been detected in the antisera of mice and humans infected with *T. brucei*[63,64]. Still, most of these antibodies do not effectively bind intact trypanosomes (suggesting that many of the epitopes are still occluded by the VSG coat), and antibodies elicited against invariant proteins do not produce protective immunity[49,63].

The VSG coat also protects the parasite from innate immune components. While alternative complement pathway activation and binding of complement components to the trypanosome surface have been identified following incubation in human serum, the complement cascade does not proceed to parasite lysis[65]. A report showing that a *T. congolense* cell line lacking a VSG coat, as well as procyclic forms of *T. congolonse* and *T. brucei brucei* could all be lysed by human complement provided evidence that the VSG coat itself may be necessary for restricting procession of the complement cascade[66], but the molecular basis of this restriction is unknown. Complement mediated trypanosome lysis can occur, however, through antibody binding and activation of the classical complement pathway[67].

1.5 Fluidity and recycling of the VSG coat

The VSG coat is a highly fluid array, and individual VSGs are free to rapidly diffuse throughout the plasma membrane. The VSG lateral diffusion coefficient ensures complete randomization of the entire VSG coat (via diffusion-based rearrangement alone) in a period of about 40 minutes[68]. Additionally, the VSG coat is in a constant state of flux, with individual

VSGs constantly being shuttled on and off the cell surface. All endo- and exocytosis in T. brucei occurs at the flagellar pocket, a specialized structure that makes up 2 % of the total surface membrane, and is situated at the base of the flagellum at the posterior end of the cell. VSGs at the flagellar pocket are internalized by endocytosis in clathrin-coated vesicles[69] and delivered to RAB5-positive early endosomes. The vast majority are then sorted to RAB11- positive recycling endosomes (directly or via RAB7-positive late endosomes) where they are delivered back to the flagellar pocket and reemerge onto the cell surface[70-73]. Roughly 9 % of the total cellular VSG content is in this internal recycling pathway at steady state. Despite the high abundance of surface VSGs, this process is rapid and efficient. The entire surface coat goes through one round of internalization and redistribution to the cell surface in approximately 12.5 min, indicating that the VSG coat is more efficiently randomized by this process than by lateral VSG diffusion[73].

It has long been observed that live trypanosomes rapidly redistribute surface- bound antibody to the flagellar pocket[57]. VSG and bound antibody are then internalized together, but upon internalization, the antibody is separated from the VSG, transported to the lysosome, and degraded[71,74]. It is not entirely clear how VSGs are specifically sorted from other proteins in the endosome, but the current model suggests that this selection is based on default sorting of GPI-anchored proteins to the recycling pathway[70,72]. VSG recycling thus provides a mechanism for rapid clearance of host antibodies from the trypanosome surface. Trypanosomes have been demonstrated to fully remove a single layer of surface-bound IgG in 120 s at 37 C[75], far faster than the rate of internalization of the VSG coat. This increased antibody clearance rate has been accounted for by the influence of hydrodynamic forces created by parasite motility. Beating of the trypanosome flagellum produces forward motion, causing bound antibodies to act as "molecular sails," which preferentially drives VSG–antibody complexes to the posteriorly

located flagellar pocket[75]. Overall, the high rate of endocytosis and surface coat recycling appears to be another adaptation for immune evasion in the mammalian host.

Still, the relative contribution of surface antibody clearance to immune evasion has not been determined. The notion that this process is, in fact, an immune evasion strategy is supported by observed differences in endocytosis rates between bloodstream form trypanosomes and those in other life cycle stages, which are not subject to similar immune pressure. Bloodstream form trypanosomes induced to differentiate to the tsetse fly midgut-inhabiting procyclic form show downregulation of components of the endocytic pathway and a concurrent tenfold reduction in endocytosis rate[76]. One study has indicated that mice infected with trypanosomes with a motility defect that prevented the internalization of bound antibody did not have a survival advantage over mice infected with motile trypanosomes[77]. However, the trypanosomes used for these experiments were derived from the highly virulent Lister 427 strain, and all mice succumbed to infection within 2 weeks. Thus, the importance of antibody internalization has not been addressed in a model of chronic infection. It has also been proposed that antibody internalization may be more crucial to preventing effector functions of antibodies recognizing invariant surface proteins, rather than those recognizing the VSG coat[49].

1.6 VSG release via the GPI phospholipase C

In its bloodstream form, *T. brucei* expresses an endogenous phospholipase (GPI phospholipase C; GPI-PLC) which can hydrolyze the GPI anchor of surface VSGs, releasing membrane-bound VSG into solution[78]. The GPI-PLC is activated following cell death or stress, and it rapidly releases the entire VSG coat from the plasma membrane within a period of a few minutes[79,80]. It is unclear whether the GPI-PLC also releases VSG from live cells: the enzyme is constitutively expressed and always localizes to the plasma membrane[81], and there is evidence

that VSG is shed at a low rate from live cells[82,83], but no evidence that this type of shedding is catalyzed by the GPI-PLC. GPI-PLC knockout (GPI-PLC$^{-/-}$) cell lines cannot shed VSG, and maintain intact coats following cell death or stress[84,85]. The lack of GPI-PLC does not affect parasite virulence in the monomorphic Lister 427 *T. brucei* strain[84], but was shown to slightly decrease parasite virulence in another cell line (EATRO 1125)[85].

1.7 The genetic basis of VSG expression and VSG switching

1.7.1 VSG monoallelic expression

VSG genes are exclusively expressed from one of ~15-20 telomeric Bloodstream Expression Sites (BES). All BESs contain *VSG* genes, but only one is BES is transcriptionally active at any given time. The BESs are highly homologous to one another, each having a set of similar features: a single promoter located at the telomere-distal end, followed by a group of expression site associated genes (*ESAG*s), a stretch of repetitive DNA known as the 70 base pair (70bp) repeats, and finally the *VSG* gene at the telomere-proximal end[86,87]. BESs vary in the number and type of *ESAG* genes they contain, and some BESs also contain multiple 70bp repeat regions and incomplete *VSG* "pseudogenes" upstream of the active *VSG*. The entire BES is expressed in a polycistronic pre-mRNA transcript, which is later spliced into individual mature mRNA transcripts with each gene flanked by a common 5' splice-leader sequence and 3' poly-A tail[88-90]. Interestingly, while mRNA is exclusively transcribed by RNA polymerase (pol) II in most eukaryotes, the active *T. brucei* BES is transcribed by RNA pol I (which typically only transcribes ribosomal RNA) [91,92].

The molecular mechanisms underlying the maintenance of monoallelic expression are incompletely understood, but nuclear localization and chromatin state appear to play a major role. The active BES is transcribed from an extranucleolar site known as the expression site body

(ESB) [93], in which chromatin is unstructured and depleted of nucleosomes[94,95]. A recently identified protein called VEX1 localizes to the ESB and can regulate allelic exclusion[96], but its mechanism of action is unknown. It is also unclear how the ESB forms or how a given BES is chosen for inclusion. There is a great deal of evidence that the silencing of inactive BESs is at least partially mediated by chromatin state. RNAi screens have identified a number of genes that are required for repression of silent BESs, and most of these encode chromatin remodeling or histone modifying proteins (reviewed in[97]). Telomeric silencing also appears to play a role, as RNAi knockdown of the telomere-associated protein RAP1 also leads to derepression of silent BESs[98].

1.7.2 The genomic VSG repertoire

The *VSG*s located in BESs represent a tiny fraction of the entire genomic *VSG* repertoire. The most completely characterized *T. brucei* genome is that of the Lister 427 strain of *T. brucei brucei,* which has been found to contain more than 2,000 *VSG* genes[34]. The *VSG* repertoires of other *T. brucei* subspecies (and other African trypanosome species) are less well characterized, but appear to be of comparable size[42]. In *T. brucei*, the majority (~80%) of the VSG-encoding sequences are incomplete genes or pseudogenes, though these sequences can still contribute to antigenic variation (discussed in section 1.7.4). Apart from the BESs, *VSG*s are located throughout the genome within the 11 megabase chromosomes, several intermediate chromosomes (typically 1-7), and ~100 minichromosomes[34,99]. Non-BES *VSG*s are located within internal arrays in the larger chromosomes, while those in minichromosomes are subtelomeric.

1.7.3 Mechanisms of VSG switching

There are two genetic mechanisms by which trypanosomes can undergo a VSG switch: (1) Transcriptional switching (also known as *in situ* switching) occurs when the active BES is silenced, and another BES is transcriptionally activated, and (2) Recombinatorial switching occurs when a *VSG* from elsewhere in the genome is copied or swapped into the active BES. Transcriptional switching only allows expression of those *VSG*s that are located within BESs (14-19 *VSG*s), while recombinatorial switching allows access to the entirety of the genomic *VSG* repertoire. Thus, recombinatorial switching is far more important for the maintenance of long-term infections, in which expression of many VSGs is required for continual evasion of host immunity. Measurements of the relative frequencies of transcriptional and recombinatorial switching have varied considerably between studies, but recombinatorial switching is generally considered to be the dominant mechanism[100-104].

Neither the mechanism by which transcriptional switching occurs nor the conditions that trigger this type of switch are well characterized. Transcriptional switching must involve chromatin remodeling as the active BES is excluded from the ESB and replaced with another BES, but the molecular basis of this process is unknown. One study demonstrated that artificial inactivation of the active BES (via a Tet repressor) triggered a transcriptional switch[105]. This suggests that loss of transcription of the *VSG* gene or some other BES component may signal a transcriptional switch, but again, does not inform the mechanism or how this may occur in a natural setting.

The mechanisms of recombinatorial switching are comparatively better understood, and this type of switch can proceed in several ways. In telomere exchange (TE), a crossover event occurs between two chromosome ends, resulting in the active *VSG* swapping locations with a

subtelomeric silent *VSG*[106]. In duplicative gene conversion (GC), a DNA region containing a silent *VSG* is copied into the active BES, and the previously active *VSG* gene is lost from the genome. GC is typically mediated by homologous recombination (HR), a DNA repair mechanism that is activated following a double strand DNA break (DSB). HR can occur via junctions at two homologous regions flanking the original and replacement *VSG*s, or via a single upstream homologous region with DNA replacement proceeding through the telomere (also known as break-induced replication (BIR))[97]. Studies have demonstrated reduced switching frequency in strains lacking HR-related proteins, including the homologous strand exchange protein RAD51[107], BRCA2 (which mediates RAD51 function) [108], and a RAD51 paralogue[109,110]. However, RAD51-independent GC switching also occurs, and this is likely mediated by a secondary DSB repair process called microhomology-mediated end joining[111,112].

GC switching can be induced by artificially introducing a DSB in the active BES, and switching efficiency increases substantially when this break occurs near the 70bp repeat region[112,113]. 70bp repeats are found upstream of more than 90% of genomic *VSG*s and have been demonstrated to be crucial sites of homology for allowing access to most of the *VSG* repertoire[43,114]. GC switching can also occur in trypanosome lines in which the 70bp repeats have been deleted at the active BES, but in these cases switching is restricted to *VSG*s in other BESs where regions of homology can still be found[43,115]. In natural settings, double strand DNA breaks have been proposed to occur in the active BES due to errors in the procession of DNA replication machinery and inherent fragility of subtelomeric genomic locations, with the 70bp repeats representing a particularly susceptible region[103,112,113,116,117]. Still, the possibility remains that the trypanosome may express factors, such as an unidentified endonuclease, that promote switching in a targeted fashion. It is also unclear whether regulation of *VSG* switching is purely

stochastic or whether environmental stimuli (e.g. host-dependent factors) affect switching frequency, but the fact that switching occurs *in vitro* suggests that there is at least some stochastic element to the process[118,119]

1.7.4 Mosaic VSGs

Most of the genomic *VSG* repertoire consists of incomplete *VSG* pseudogenes[34], and these gene segments contribute to *T. brucei* antigenic variation by recombining with one another or with complete *VSG*s to generate functional "mosaic" *VSG*s. Mosaic *VSG*s are formed by segmental GC events, and single mosaics can originate from as many as four donor pseudogenes[120-123]. Donor sequences contributing to the same mosaic typically share substantial homology (as would be expected for mosaic formation mediated by HR), but in some unusual cases the borders of segmental GC events share little or no apparent homology[120]. Many aspects of mosaic formation are uncharacterized, including whether it is a directed or stochastic process, whether it occurs in the active BES or elsewhere in the genome, and when it occurs during infection. However, one study[37] showed that three mosaic genes were not detectable within a parasite population during infection until trypanosomes actively expressing those *VSG*s emerged, suggesting that at least in some cases formation occurs shortly before expression. Overall, mosaic *VSG*s appear to contribute to antigenic variation in a manner that is greater than the sum of their parts, as mosaics with substantial sequence similarity can still be antigenically distinct from one another[120].

1.7.5 Rates of switching

In lab-adapted cell lines, *VSG* switching occurs at a rate of 10^{-5} - 10^{-6} cells per population doubling (C/PD) [113,118,119,124]. However, these rates may drastically underestimate the frequency of

switching in natural infections, as switching frequencies as high as 10^{-3} C/PD have been measured in recent field isolates[125]. Interestingly, lab adapted cell lines have been shown to increase switching rates 100-1000 fold following passage through the tsetse vector, suggesting that switching frequency might be affected by environmental cues or differentiation between life cycle stages[126].

1.7.6 Dynamics of VSG expression in vivo

Several studies have demonstrated that *VSG*s are expressed in a probabilistic order during infection[41,127-129]. The order appears to be related to genomic location, as expression of BES *VSG*s typically occurs early in infection, followed by minichromosomal *VSG*s, and finally *VSG*s from internal arrays[41,129]. The mechanism underlying this pattern is unknown, but a number of factors may contribute. BES *VSG*s can be activated by both transcriptional and recombinatorial switching, and the high homology between BESs[87] gives many potential locations for HR between these sites. Further, BESs contain complete *VSG* genes[87], and a disproportionally high percentage (85%) of minichromosomal *VSG*s are also complete, as opposed to only ~20% in the *VSG* repertoire as a whole[34]. Trypanosomes switching to these complete, functional *VSG*s would presumably have an early selective advantage. Conversely, many chromosome internal *VSG*s are incomplete and can only be accessed by mosaic formation, which is evident at much greater frequency late in infection[120,123]. The prevalence of mosaic *VSG*s late in infection is likely a consequence of the parasite's need to generate additional antigenic diversity once the existing repertoire has been exhausted[122].

Mugnier et al.[37] analyzed the diversity of *VSG*s expressed within trypanosome populations at varying time points throughout several *T. brucei* infections. Trypanosome populations showed highly diverse VSG expression at each time point, with as many as 83 VSGs

expressed concurrently within a single infection. However, within the first 30 days of infection roughly half of the VSGs were expressed only transiently, never comprising as much as 1% of the total population. Most VSGs that appeared only transiently in one infection comprised large portions of the population in another infection, suggesting that the discrepancy did not result from inherent VSG "fitness". The authors proposed that VSG cross-reactivity was a potential cause of this phenomenon, such that a VSG's fitness might depend on whether it were antigenically similar to a VSG the host had seen before. If that were true, the high diversity of VSG expression would likely be necessary for sustained infection: each switched population might need to express a multitude of VSGs to ensure that at least one is suitable for the immune environment, despite the fact that this high diversity exhausts the available *VSG* repertoire more quickly.

1.8 *T. brucei* interactions with host immune factors

1.8.1 The B cell response

VSG-specific antibodies are the key functional components in the immune response to *T. brucei*, as they are the only immune factors that mediate clearance of peaks of parasitemia. Studies in which B cell-deficient mice were infected with pleomorphic *T. brucei* showed that the parasites expanded exponentially within the host before reaching a consistently high level of parasitemia that increases very slowly until mouse death[130,131]. As the authors of these studies noted, the stabilization of parasitemia is at least partially due to parasite differentiation to non-proliferative stumpy bloodstream forms (see section 1.2). *T. brucei* can be activate B cells to produce VSG-specific antibodies via T cell-dependent (TD) and T cell-independent (TI) pathways[132]. TD B cell responses are typical against protein antigens, but the ability of *T. brucei* to stimulate a TI B cell response is likely based on the density and regularity of the VSG coat[133].

Soluble VSG and VSG coats disrupted by formalin fixation do not stimulate TI responses, and different VSG coats stimulate TI responses with varying efficiency[132].

Of all the immunoglobulin (Ig) classes, VSG-specific IgM plays a dominant role in mediating trypanosome clearance. One study which followed IgM and IgG titers during *T. brucei* infection showed that IgM was detectable during the first peak of parasitemia, but the parasitemia peak was already cleared before IgG was detectable[40]. Furthermore, the rough 5-8 day periodicity of parasitemia waves[37,38,41] aligns with the expected time frame of successive IgM responses. Still, the importance of IgM in trypanosome clearance has been the subject of some controversy. Experimental infections in IgM-deficient (but IgD-expressing, and thus also termed "IgD-only") mice[134] have shown mild phenotypes in parasitemia progression as compared to infections in wild-type mice, prompting the conclusion that IgG may be more responsible for parasite suppression[130,131]. However, the IgM-deficient mice generated compensatory IgD antibodies (normally absent in wild-type mice) with the same dynamics as a typical IgM response. Thus, an alternative explanation for these results is that trypanosome clearance is mediated by the earliest arising antibody response, and that IgD is largely capable of performing this function in place of IgM.

Antibody-mediated parasite clearance occurs in two ways: complement-mediated parasite lysis, and opsonization by phagocytes. Complement-mediated trypanosome lysis does not occur in the absence of VSG-specific antibody (discussed in section 1.4); it is dependent on antibody-mediated activation of the classical complement pathway[67]. Parasite opsonization is predominately carried out by macrophages in the liver, with smaller contributions from macrophages in other locations such as the spleen[40,135]. Studies examining whether opsonization requires deposition of complement components (for complement receptor-mediated uptake), or

whether it can be mediated by antibody (Fc) receptors alone have produced conflicting results. Macaskill et al.[136] reported that depletion of complement component C3 reduced trypanosome clearance by hepatic macrophages in passively immunized mice, while Dempsey et al.[40] depleted C3 by the same method in directly immunized mice and saw no change in parasite clearance.

1.8.2 Innate immunity

In addition to human innate trypanolytic agents TLF-1 and 2, which protect against many African trypanosome species (discussed in section 1.1), other innate immune factors also influence the progression of *T. brucei* infection. Very early in infection, trypanosome-derived factors activate macrophages to produce nitric oxide and pro-inflammatory cytokines such as TNF-α, IL-1, IL-6, and IL-12. Of these, TNF-α appears to play a particularly important role in limiting parasite growth and maximum parasitemia levels[137-139]. However TNF-α also has negative effects, as it has been shown to suppress T cell proliferation during infection[140]. *T. brucei* DNA appears to be an important factor in inducing macrophage activation, and this occurs in a Toll-like receptor 9 (TLR9)-dependent manner[141,142]. Mice deficient in TLR-9 and MyD88 (an important molecule in TLR signaling) showed increased parasitemia levels and decreased survival time following *T. brucei* infection[142]. The VSG GPI anchor also signals macrophage cytokine production[143], and it is likely that other trypanosome-derived factors stimulate innate immune responses as well[142].

1.8.3 The T cell response

While T cell help is known to be important for the development of optimal VSG-specific antibody responses[132], and purified VSG can produce protective immunity[35], T cells isolated from *T. brucei*-infected animals typically show poor proliferation in response to VSG[144,145]. However,

VSG-specific T cells have been identified. One study demonstrated that a set of VSG-specific T cells only recognized peptides from variant N-terminal portions of the VSG (rather than conserved C-terminal regions), suggesting that antigenic variation might affect T cell recognition in addition to B cell and antibody recognition[146].

T cells also produce of IFNγ, which has been shown to be a crucial factor in host resistance during *T. brucei* infections[147]. IFNγ is predominately produced by $CD4^+$ T cells, rather than $CD8^+$ T cells, and its protective effects are likely exerted through macrophage activation[130,144,148]. Despite its importance to parasite resistance, IFNγ also produces deleterious effects. Like macrophage-produced TNFα (described above), IFNγ has been shown to inhibit T cell proliferation during *T. brucei* infection[140]. Further, excessive IFNγ production causes systemic inflammation and early mortality in trypanosome infections; the pro-inflammatory effects of this cytokine must be balanced by anti-inflammatory action of IL-10[135,148].

1.8.4 T. brucei-*mediated immunosuppression*

Beyond antigenic variation, another way *T. brucei* evades host immunity is by perturbation of the function of host immune factors. Two trypanosome-derived factors, TbKHC1 and TbAdC, have been shown to facilitate *T. brucei* infection by modulation of host innate immune responses[149,150]. Another trypanosome-derived protein, TSIF, causes suppression of T cell proliferation and anti-inflammatory IL-10 production, contributing to pathogenesis[151]. Detrimental effects on B cell function and the maintenance of B cell populations have also been observed at multiple stages of infection. Starting early in infection, non-specific, polyclonal B cell activation and proliferation occurs (likely through B Cell TLR signaling initiated by trypanosomal CpG DNA or the VSG GPI anchor), which may exhaust or suppress B cell ability to generate antigen-specific antibodies[152-155]. As infection progresses, lymphopoiesis in the bone

marrow is impaired, and transitional B cells (those developing from immature to mature B cells), follicular B cells, and marginal zone B cells are depleted in the spleen via both polyclonal activation and induction of apoptosis[156-158]. While the mechanisms behind these phenomena are unclear, follicular B cell apoptosis has been demonstrated to be IFN-γ dependent, and induction of transitional B cell apoptosis appears to require direct trypanosome-B cell contact[156]. Finally, B cell memory and protective antibody titers have been shown to be weakened or abolished several weeks into *T. brucei* infection. At these later time points, mice re-challenged with parasites expressing a VSG that they have previously established immunity against show impaired secondary antibody responses and decreased control of the re-administered parasites[159,160]. Mice vaccinated against *B. pertussis* also lose the protective effect of vaccination when challenged with *B. pertussis* following *T. brucei* infection[160]. Collectively, these results suggest that B cell depletion and exhaustion of the B cell repertoire contribute to the pathogenesis of *T. brucei* infection by reducing the ability of the host to mount a humoral immune response against successive waves of parasitemia, particularly at later stages of infection.

1.9 Open questions

1.9.1 VSG switching at the protein level

Most analyses of the antigenic variation process in *T. brucei* have focused on genetic factors regulating *VSG* expression and diversification, but protein dynamics also influence the host-pathogen interface and successful immune evasion. Following a genetic *VSG* switch, trypanosomes must replace their entire VSG coat. During this period, trypanosomes simultaneously express both pre- and post-switch VSGs on their surface, a phenomenon that has been observed in infection isolates[161]. This coat replacement process is critical for the survival of

recently switched cells because initial VSGs remain targets for the escalating host antibody response, but the dynamics of VSG replacement remain poorly understood. VSG half-life measurements suggest that initial VSGs may persist on the surface of genetically switched trypanosomes for several days[82,83]. However, this estimate assumes that VSG turnover is identical in recently switched and non-switched trypanosomes. It has been proposed that trypanosomes might expedite VSG turnover during VSG switching as an immune evasion strategy[162], but the rate of VSG coat replacement has not been experimentally determined due to the low switching frequencies observed in lab adapted trypanosome cell lines *in vitro*[113,118,119,124] (discussed in section 1.7.5). Furthermore, the vulnerability of trypanosomes with partially replaced coats to antibody-mediated clearance has not been directly investigated. Thus, the specific mechanisms that allow switched trypanosomes to successfully escape the mounting antibody response are yet undetermined. In Chapter 2 of this thesis, I describe my examination of the dynamics of VSG coat replacement and identification of a key factor influencing the susceptibility of cells undergoing coat replacement to antibody-mediated clearance.

1.9.2 VSG structural diversity and VSG classes

Structural information and VSG sequence alignments have been used to allocate the variable N-terminal domains of VSGs into three different classes (major classes A and B, and minor class C) based on the presence of analogous cysteine residues[123,163], and C-terminal domains have also been grouped into six classes based on conserved sequence features[114,123,163]. The two early N-terminal domain structures of VSG2 (also termed MITat1.2 and VSG221) and ILTat1.24, and a more recently published structure (VSG M1.1, which is highly homologous to VSG2[51]) all belong to N-terminal class A. Sequence analyses of class B VSGs show that they contain some similar features as the class A VSGs (such as long antiparallel α-helices)[50], but it is

unclear whether these VSGs also share the conserved structural motif which has been identified in the VSG structures published to date. Because detailed VSG structural information is limited to a handful of variants out of the thousands of known *VSG* genes, it is quite possible that VSGs contain structural elements or confirmations that have not been identified. In Chapter 3 of this thesis, I describe a collaborative body of work in which the crystal structure of a class B VSG (VSG3, also termed MITat1.3 and VSG224) was solved, yielding unexpected findings regarding the diversity of VSG post-translational modifications and the role of these modifications in host-parasite interactions.

Chapter 2

VSG density defines an immune evasion threshold for African trypanosomes undergoing antigenic variation

2.1 Introduction

Following a genetic *VSG* switch, trypanosomes must replace their VSG coat to evade host antibodies that target the initial (pre-switch) VSG. Using published VSG half-life values[82,83], I calculated that full VSG coat replacement would take approximately 5.7 days. Because VSG-specific IgM antibodies can be detected as early as 4 days post infection[40], this timeline suggested that genetically switched trypanosomes would still display cognate initial VSGs on their surface as the antibody response developed. I therefore reasoned that a detailed examination of VSG coat replacement could improve our understanding of *T. brucei* infection dynamics, and potentially reveal unidentified factors influencing parasite immune evasion. In this chapter, I describe two experimental avenues by which I evaluated the coat replacement process. First, I directly compared VSG turnover in recently switched and non-switched trypanosomes to determine whether the parasites might expedite VSG turnover immediately post-switch as an immune evasion strategy. Second, I performed *in vivo* infection experiments and *in vitro* antibody binding analyses to examine the susceptibility of trypanosomes at intermediate stages of coat replacement to IgM-mediated clearance.

2.2 Identification of switched populations undergoing VSG coat replacement by flow cytometry

To examine the possibility that trypanosomes expedite VSG turnover following a *VSG* switch, I first needed a method to identify switched trypanosomes soon after the change in *VSG* expression occurred. Historically, it has been difficult to observe such cells because VSG

switching occurs at a low frequency *in vitro (*10^{-5} - 10^{-6} cells per population doubling [C/PD]) [113,118,119,124]. However, a transgenic cell line recently published by our group can be induced to switch at a very high frequency[43]. The cell line (Δ70) has deleted 70 bp repeats (described in sections 1.7.1-1.7.3) and an inserted I-SceI restriction site upstream of the active *VSG* (*VSG2,* a.k.a. *Lister 427-2*, *VSG221*) (Fig. 2.1a), as well as a tet-inducible *I-SceI* gene in a spacer region within the rDNA. Doxycycline (Dox) induction initiates an I-SceI-mediated double strand DNA break (DSB) near the active *VSG*, the repair of which yields a high percentage of trypanosomes (~10%) switching exactly once to another *VSG*[43].

Because of its extremely high frequency of switching (the highest we have ever seen *in vitro*), I reasoned that I could use the Δ70 cell line to visualize a large population of cells undergoing VSG coat replacement via flow cytometry (Fig. 1). In these experiments, Δ70 cultures were induced with Dox for a 6-hour period, after which the cells were washed and grown in Dox-free media. Samples were then taken at various time points for flow cytometry analysis. Cells were stained with antibodies recognizing two different VSGs: VSG2, the initial pre-switch VSG; and VSG3 (a.k.a. Lister 427-3, VSG224), one of many possible post-switch VSGs. VSG3 was chosen because this cell line switches to that particular VSG more frequently than others (~15% of the switched population expresses VSG3)[43].

In accordance with the previously observed results, Δ70 cells did not switch at high frequency in the absence of Dox, but Dox-induced cells switched at a rate of ~10^{-1} – 10^{-2} C/PD, (Fig. 2.1b). By analyzing the emergence of cells staining positive for VSG3 at early time points, I determined that switched cells could not be identified until ~12 h after the beginning of Dox induction (i.e. ~6 h after the end of Dox induction). At 12 h, these VSG3+ cells also stained highly positive for VSG2, indicating that they were simultaneously displaying both VSG2 and

VSG3 as they underwent VSG coat replacement (Fig 2.1c). From 12 h – 48 h, the large population of switched cells (both VSG3+ and VSG3-) could be seen decreasing in VSG2 staining level as the VSG2 was replaced with new VSG (Fig. 2.1c). Thus, all cells undergoing coat replacement could be distinguished from non-switched cells by the level of VSG2 antibody staining. Further, the rate of VSG coat replacement could be determined by the decrease in fluorescence intensity over time. However, this method alone would not allow direct comparison of the rate of VSG turnover in switching and non-switching cells. Non-switching cells still turn over VSG2, but they continue to express VSG2, and therefore VSG2 antibody staining levels do not change (Fig 2.1c, population in top left quadrants).

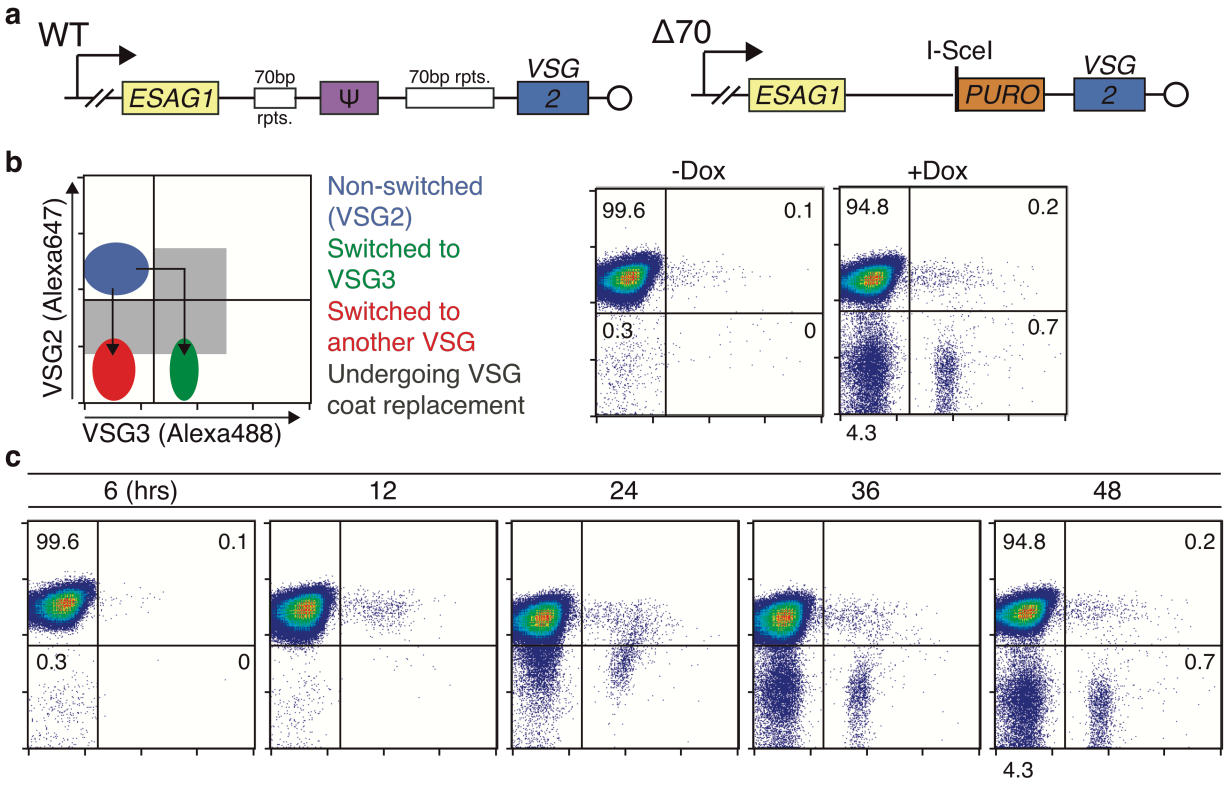

Figure 2.1. Visualization of switching cells by flow cytometry.

(a) Diagrams of the active VSG expression sites (BES1) of WT cells and the Δ70 line (adapted from[43]). WT diagram shows the promoter (bent arrow), *ESAG1*, the 70 bp repeats (rpts.), a *VSG* pseudogene (ψ), the active *VSG* (*VSG2*), and the telomere (circle). In the Δ70 line, the 70 bp rpts. and ψ are deleted and replaced with an I-SceI restriction site and a puromycin resistance gene (*PURO*). **(b)** VSG switching in induced (Dox+) and non-induced (Dox-) Δ70 cells at 48hrs. **(c)** Δ70 trypanosomes undergoing VSG coat replacement following a genetic *VSG* switch. Percentage of cells in each quadrant are shown at 6 hr and 48 hr. For both (a) and (b), cells were induced to switch at time t = 0 hr. VSG2 is the initial, pre-switch VSG, while VSG3 is one of many possible post-switch VSGs.

2.3 Development of a specific, high efficiency VSG labeling method using the enzyme Sortase A

To examine VSG turnover in switching cells as well as non-switched cells that maintain consistent VSG2 levels, I developed a method of fluorescently labeling surface VSGs on live trypanosomes. The goal was to label a pool of surface VSGs and calculate the rate of VSG

turnover in both switching and non-switching cells by measuring the loss of fluorescence intensity over time. The labeling method I designed was based on the transpeptidase enzyme Sortase A, derived from *Streptococcus pyogenes* (hereafter referred to as only "sortase"). Sortase recognizes the peptide "sorting motif" (LPXT[GG/AA]), cleaves the motif between the Thr and [GG/AA] residues, and mediates a covalent bond between the Thr residue and an additional peptide substrate containing an N-terminal $(Gly)_3$ or $(Ala)_2$ sequence in a process known as "sortagging"[164]. Thus, if the VSG and a fluorophore-peptide conjugate each contained either the sorting motif or N-terminal (Gly/Ala) residues in the correct combination, the sortase enzyme would covalently attach the fluorophore to the VSG. As opposed to other potential VSG-labeling strategies, sortagging would specifically label the VSG instead of other *T. brucei* proteins. It would also be a highly versatile labeling technique, allowing attachment of not only fluorophores, but also (theoretically) any molecule that could be conjugated to the proper peptide sequence.

To attempt to generate a recombinant "sortaggable" VSG2, I created several constructs based on a previous study in which 11 sites were identified in VSG2 that were conducive to peptide insertion[165]. I designed 3 peptide insertion sequences to introduce a sorting motif into the identified sites in VSG2: (1) GGG**LPETG**GS, (2) **LPETG**GSGLEVLFQGPG (Prescission Protease site underlined, included to make peptide more flexible by cleaving via protease treatment), and (3) **LPETG**GS**LPETG**GS**LPET** (3 sorting motifs). I also designed an insertion peptide (GGGENLYFQGGG; TEV protease site underlined) that would leave an N-terminal $(Gly)_3$ sequence in the VSG once treated with TEV protease (to serve as the N-terminal substrate for a sortagging reaction together with a fluorophore-peptide containing a sorting motif). I inserted these peptides into the 11 identified sites within the *VSG2* gene, and cloned the recombinant genes into a previously established vector, pUB39[166], making 44 constructs in total.

Based on the pUB39 backbone, the *VSG2* genes in the resulting constructs were targeted for insertion into the *T. brucei* rDNA spacer region and were preceded by a Tet operator, such that the recombinant VSG2 proteins would be expressed under Dox/Tet control. Upon transfecting these constructs into VSG3-expressing trypanosomes (from the "Single Marker" lineage[167]), only some of the recombinant VSGs were successfully expressed on the cell surface following Dox induction, as determined by flow cytometry using anti-VSG2 antibodies. Unfortunately, none of the recombinant VSG2 proteins containing sorting motifs could be labeled following incubation with purified sortase enzyme and the complementary fluorophore-peptide (see Methods for sortase expression and purification and source of synthesized peptides).

I ultimately succeeded in creating a sortaggable VSG2 because of two key insights: (1) the mature VSG2 naturally contains an $(Ala)_2$ sequence at the N-terminus following cleavage of an N-terminal signal peptide[163], and this could serve as a substrate for the sortagging reaction; and (2) this VSG2 N-terminus was likely inaccessible to sortase, because it is located too close to the body of the protein[50]. I therefore reasoned that I might be able to render the $(Ala)_2$ sequence accessible by extending the VSG2 N-terminus. Fortuitously, one of the peptide insertion constructs I had already designed contained such an extension. This construct (originally called "VSG2-1D") will henceforth be referred to as "$VSG2^{STa}$". The natural N-terminal sequence of VSG2 is AAEKGFKQAF, while the N-terminus of $VSG2^{STa}$ is AAGGGENLYFQGGGGGGFKQAF (peptide insertion underlined). A diagram of the sortagging reaction with $VSG2^{STa}$ and a sorting motif-containing peptide conjugate is shown in Fig. 2.2a. I first expressed the $VSG2^{STa}$ construct within a VSG3-expressing cell line (as described above). I found that live cells expressing $VSG2^{STa}$ were successfully sortagged with

fluorophore (FITC) when incubated with sortase and the peptide conjugate FITC-GGGSLPETGG, whereas cells expressing only wild type VSG2 or VSG3 were not (Fig 2.2b).

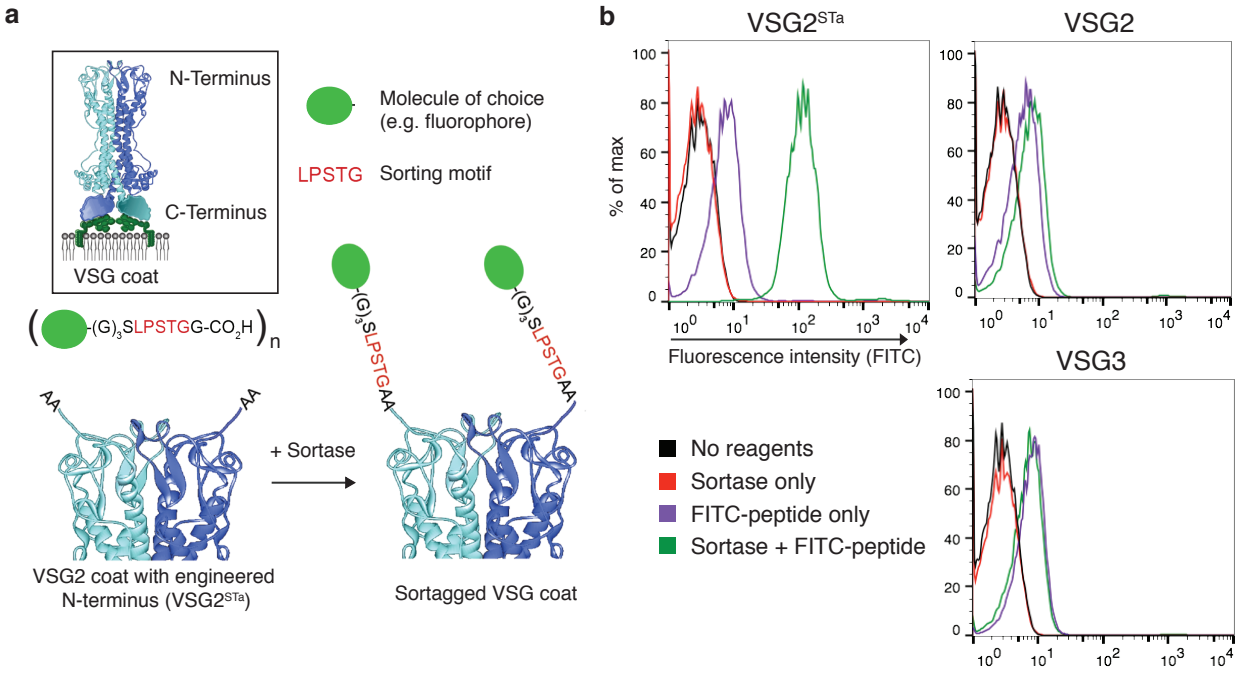

Figure 2.2. Sortagging live trypanosomes with engineered VSG2^{STa}.

(a) Illustration of VSG2^{STa} sortagging. **(b)** Flow cytometry analysis of live trypanosomes following incubation with sortagging reagents. VSG2^{STa} (expressed ectopically in a VSG3-expressing cell line) is sortagged only when incubated with both sortase and a FITC-peptide conjugate containing a sorting motif (FITC-GGGSLPETGG). Wild type VSG2- and VSG3-expressing cells are not sortaggable. VSG image in (a) was adapted from a previous publication[75] with permission from the author.

Having engineered a sortaggable VSG, I next developed a construct to insert the *VSG2*^{STa} gene into the active BES (BES1) of the VSG2-expressing single marker (SM) cell line[167], replacing the wild type *VSG2* gene (Fig. 2.3a). The construct, pSY37F1D-CTR, includes in order: the *VSG2* co-transposed region (CTR), which contains the 5' *VSG2* untranslated region (UTR); the *VSG2*^{STa} gene with its 3' UTR; a Hygromycin resistance gene (HYG); and a telomere-abutting sequence called the telomere seeds. Transfecting this construct into trypanosomes introduces *VSG2*^{STa} into BES1 via BIR through homology in the *VSG2* CTR, after which a new telomere grows from the telomere seeds. I transfected the construct into SM parasites, resulting in the clone KI-VSG2^{STa} (Fig. 2.3a). Proper insertion of the construct was verified by southern blot (Fig. 2.3b), confirming that KI-VSG2^{STa} exclusively expressed VSG2^{STa}.

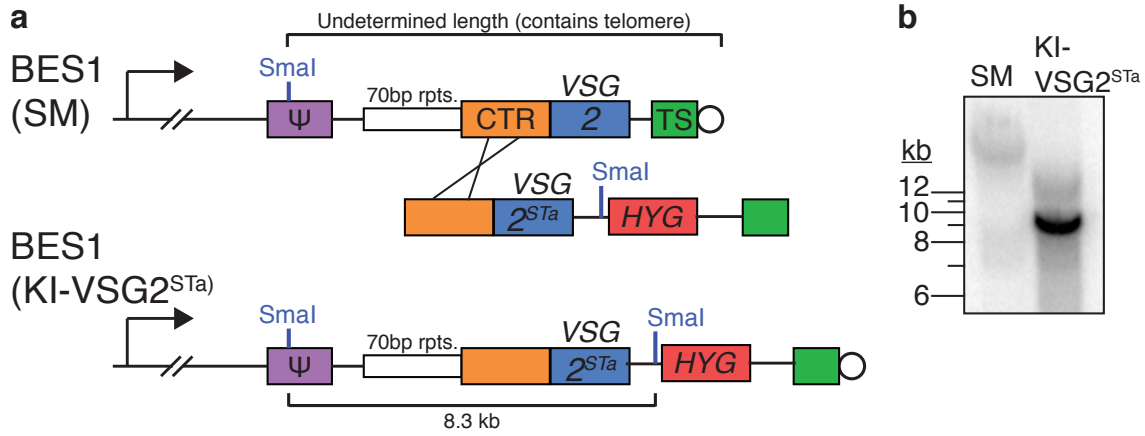

Figure 2.3. Creation of VSG2^{STa} knock-in clone KI-VSG2^{STa}.

(a) (Top) Diagram of the active BES (BES1) in VSG2-expressing single marker (SM) cells; shows the promoter (bent arrow), a *VSG* pseudogene (ψ), 70 bp repeats, the *VSG2* co-transposed region (CTR), *VSG2*, the telomere seed region (TS) and the telomere (circle). (Middle) The pSY37F1D-CTR construct containing *VSG2*^{STa} and a hygromycin resistance gene (HYG) is recombined into BES1 via break-induced replication (BIR) using the *VSG2* CTR for homology. (Bottom) Diagram of resulting BES1 in the VSG2^{STa} knock-in clone KI-VSG2^{STa}. **(b)** Southern blot of genomic DNA (gDNA) from SM and KI-VSG2^{STa} cells digested with SmaI and probed against *VSG2*. KI-VSG2^{STa} gDNA contains the appropriate 8.3 kb band as shown in (a).

I then used the KI-VSG2^{STa} clone in a series of experiments to test and optimize the VSG sortagging platform (Fig 4). I found that VSG sortagging was a versatile tool, as I was able to label cells with diverse "tag" molecules conjugated to or containing the peptide sorting motif. These tags included fluorophores (e.g. FITC), the small molecule hapten nitrophenol (NP), and GFP (with GGGS**LPETG**G added to the C-terminus) (Fig 2.4a). Secondly, I found that while the literature describes the "universal" sorting motif as LP**X**TG[168,169], the sortase enzyme I used (derived from *S. pyogenes*) functioned at greatest efficiency when the sorting motif was LP**S**TG (Fig. 2.4b), and I therefore used this motif for all subsequent sortagging. Unsurprisingly, LPSTG is also the motif typically used by the *S. pyogenes* bacteria[170].

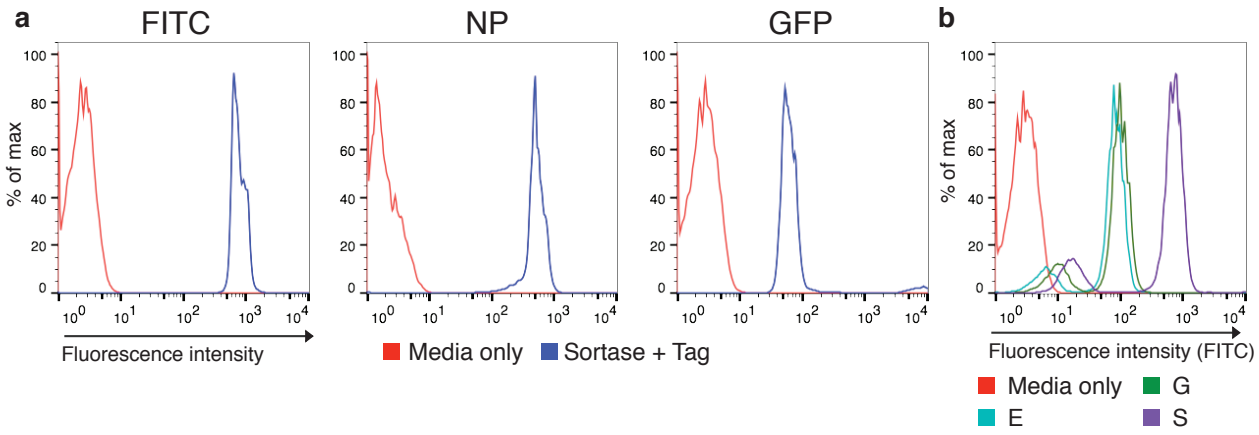

Figure 2.4. Sortagging versatility and sorting motif optimization.
(a) Sortagging live KI-VSG2^{STa} cells with different tags: FITC (FITC-GGGS**LPSTG**G), nitrophenol (NP) (NP-GGGS**LPSTG**G), and GFP (GFP-GGGS**LPETG**G). Cells were incubated in HMI-9 media with or without sortase and tag. NP-tagging of trypanosomes was visualized after staining with fluorophore-conjugated anti-NP antibody **(b)** Testing multiple sorting LPXTG motifs (tags are FITC conjugated to GGGS**LPXTG**G where X is E, G, or S as indicated). "Media only" represents cells incubated in HMI-9 without sortase or tag.

Finally, I performed additional control experiments to verify that VSG sortagging would be a viable method of measuring VSG turnover. First, to examine whether sortagging affected trypanosome growth rate, I developed a protocol to stain trypanosomes with CFSE (an intracellular fluorescent stain that dilutes as a result of cell proliferation, and is commonly used as a proliferation metric[171]). I compared the growth rates of tagged and non-tagged trypanosomes by measuring the decrease in CFSE mean fluorescence intensity (MFI) in each population over time, and found that sortagging had no effect on proliferation (Fig 2.5a). Second, fluorescence microscopy of trypanosomes 12 hours after sortagging showed that sortagged VSG was still evenly distributed across the cell surface (Fig. 2.5b). This even distribution suggests that sortagged VSGs are trafficked as normal VSGs and are not grouped or sequestered while on the cell surface, during cell division, or during VSG endocytosis and recycling. Finally, decrease in the fluorescence intensity of sortagged trypanosome populations cultured over time indicated turnover of these labeled VSGs (Fig. 2.5c). However, in order to use fluorescence intensity as an accurate metric of VSG turnover, I still needed to account for non-linearity in raw MFI measurements. To do this, I used a set of commercial calibration beads to convert the MFI of each trypanosome sample into Molecules of Equivalent Soluble Fluorochrome (MESF) units[172] (described in Methods). MESF units represent the mean absolute fluorophore amount per cell, and therefore the mean absolute number of tagged VSGs per cell (Fig. 2.5c).

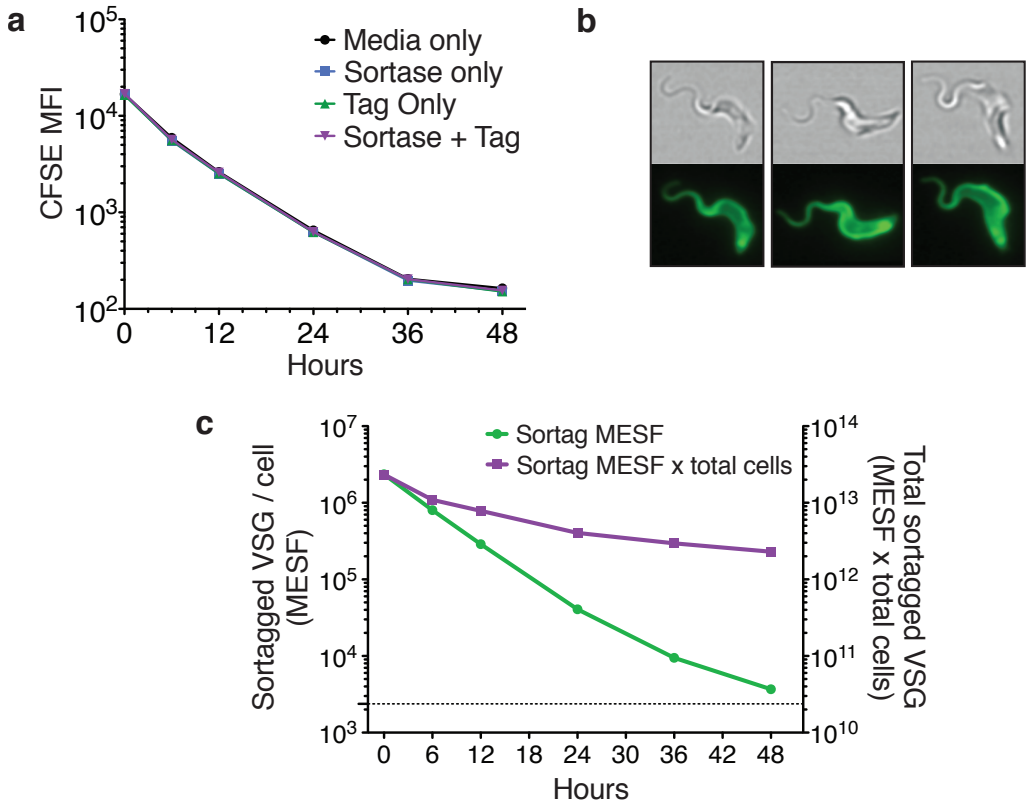

Figure 2.5. Validation of fluorescent sortagging as VSG turnover measurement strategy.

(a) Lack of effect of sortagging on cell growth rate. Data show flow cytometry measurements of population mean fluorescence intensity (MFI) of CFSE. Cells were treated with HMI-9 alone (Media only), or HMI-9 with sortase enzyme, fluorescent tag, or both sortase and tag; then with CFSE prior to culture. **(b)** Live KI-VSG2^{STa} trypanosomes 12 hours after sortagging with the fluorophore FITC. **(c)** Loss of FITC-sortagged VSGs over time in KI-VSG2^{STa} trypanosomes. Population mean fluorescence intensity (MFI) values were converted to absolute units (Molecules of Equivalent Soluble Fluorochrome, MESF)[172]. Sortag MESF (plotted on left Y axis) is the mean amount of sortagged VSG remaining per cell. Dotted line is associated with the left Y axis and represents background MESF of non-sortagged cells. Sortag MESF x total cells (plotted on right Y axis) is the total cell-associated, sortagged VSG remaining in the population. This value was calculated by subtracting background MESF from the sortag MESF value and multiplying by the total number of cells in the population

2.4 Calculation of VSG turnover rates in switching and non-switching cells

I then inserted the sortaggable *VSG2*^{STa} into the VSG expression site of the high switching Δ70 cell line, replacing the active *VSG2* gene (Δ70^{STa}). This allowed me to calculate the rate of VSG loss in both switched and non-switched cells by quantifying decreases in fluorescence intensity from antibody staining and sortagging over time (Fig. 2.6a-c). Because flow cytometry measures individual cells, VSG loss rates were calculated at the single-cell level, and therefore include contributions both from the dilution of VSGs during cell division (population doubling time, t_D) and from VSG shedding and degradation (VSG half-life, $t_{1/2}$). Evidence of the latter factor, (loss of VSGs from the entire trypanosome population by shedding and degradation) is shown by the negative slope of the "Sortag MESF x total cells" curve in Fig. 2.5c above. The combined VSG loss rate at the single-cell level is the rate most relevant to immune evasion, and I have termed this value the "effective VSG half-life" ($t_{E1/2}$). Calculated $t_{E1/2}$ values (~4.6 hrs on average, Fig. 2.6c) agreed between measurement methods, and were similar to previously published population-wide data (~5.9 hrs, see section 2.4.1 for calculation)[82,83]. Notably, $t_{E1/2}$ values were comparable for switched and non-switched cell populations, indicating that VSG turnover rates are identical in recently switched and non-switched cells. These results were not confounded by large differences in growth rate between cell populations (Fig. 2.6d). Based on this $t_{E1/2}$ of 4.6 hrs, trypanosomes with fully replaced VSG coats would not arise until approximately 107 hrs (~4.5 days) after a genetic *VSG* switch (See section 2.4.1 for calculation), suggesting that switched trypanosomes and their progeny may be susceptible to immune clearance for extended periods.

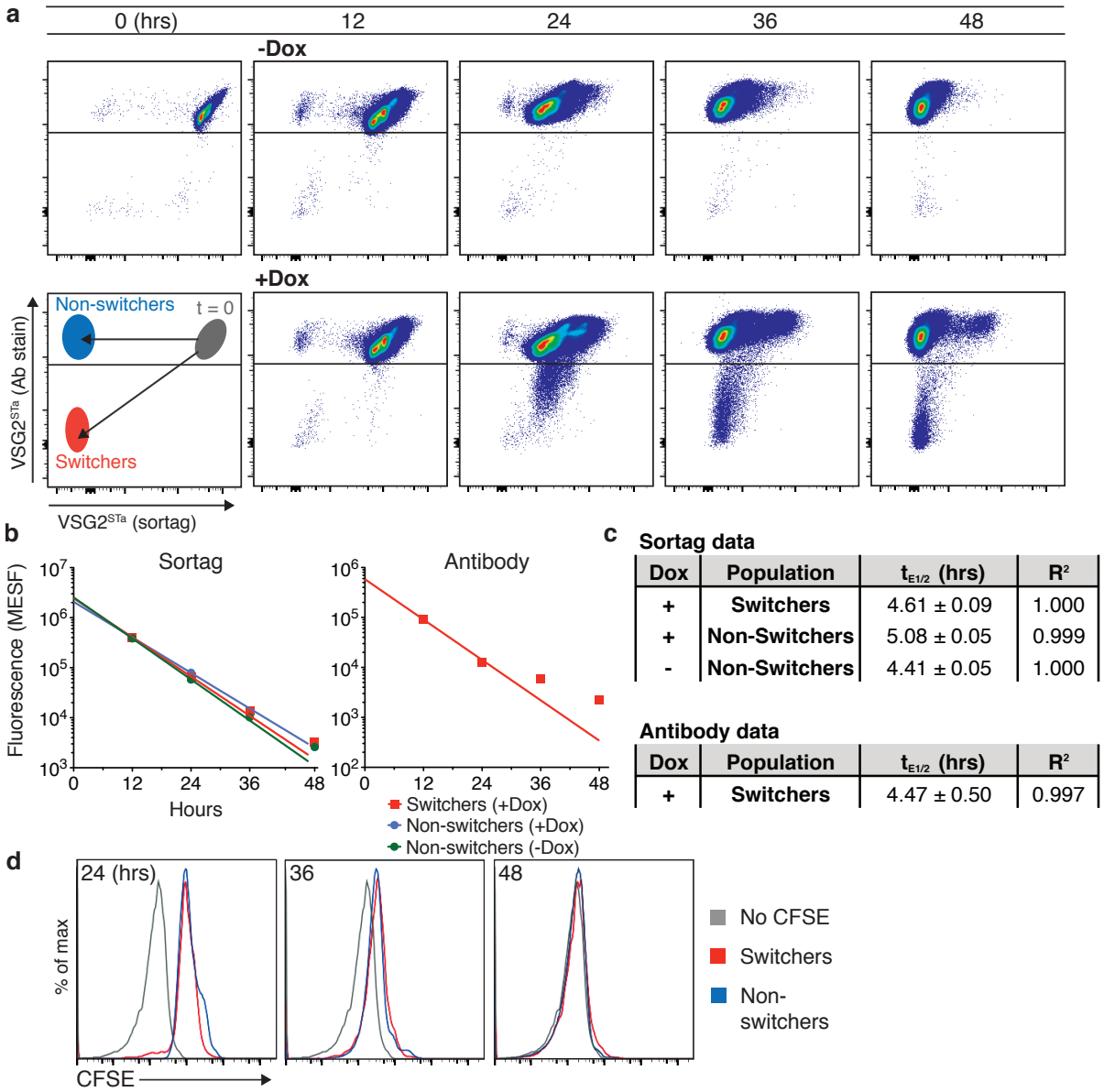

c

Sortag data

Dox	Population	$t_{E1/2}$ (hrs)	R^2
+	**Switchers**	4.61 ± 0.09	1.000
+	**Non-Switchers**	5.08 ± 0.05	0.999
-	**Non-Switchers**	4.41 ± 0.05	1.000

Antibody data

Dox	Population	$t_{E1/2}$ (hrs)	R^2
+	**Switchers**	4.47 ± 0.50	0.997

Figure 2.6. Calculation of VSG turnover rates in switching and non-switching cells.

(a) VSG2^{STa} loss over time in sortagged and induced (+Dox) or non-induced (-Dox) Δ70^{STa} cells. Line shows the gate between "Switcher" and "Non-switcher" populations. **(b)** and **(c)** Calculation of rates of VSG loss ($t_{E1/2}$) in Switcher and Non-switcher populations as gated in (a). For (**d**), Raw MFI values for Ab staining and sortag levels were converted to MESF units (see Methods). Lines on plots show non-linear regression analyses. **(e)** $t_{E1/2}$ calculated for indicated populations (Value ± SE) and goodness of non-linear regression fit (R^2). (**d**) Relative growth rates of Switcher and Non-switcher populations measured by CFSE staining.

2.4.1 Details of VSG turnover rate calculations

The estimated expected $t_{E1/2}$ value from previously published data can be calculated via the equation in Fig. 2.7a. Using the $\Delta 70^{STa}$ clone t_D (7.2 hrs, Fig 2.7b) and published $t_{1/2}$ of 32 hrs[82,83], the expected $t_{E1/2}$ value is ~5.9 hrs. The total duration of the VSG coat replacement process can be calculated via the equation in Fig. 2.7c. Using the values $N_0 = 10^7$ VSGs (a full coat prior to genetic VSG switch), and $t_{E1/2} = 4.6$ hr (Fig. 2.6c), the estimated time to reach N = 1 VSG remaining is 107 hrs (~4.5 days). Beyond this point, trypanosomes with fully switched coats will arise.

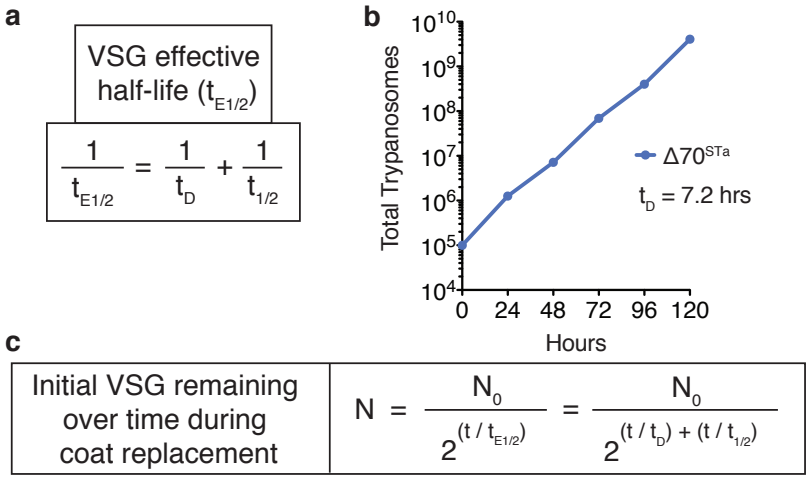

Figure 2.7. VSG turnover equations and $\Delta 70^{STa}$ growth rate.

(a) Equation relating $t_{E1/2}$, t_D, and $t_{1/2}$ ($t_{E1/2}$ = VSG effective half-life. t_D = trypanosome population doubling time. $t_{1/2}$ = VSG protein half life). Both VSG dilution through cell division and VSG loss through shedding and degradation contribute to the total rate of VSG loss from each individual trypanosome. The combined half-life value ($t_{E1/2}$) is mathematically equivalent to the sum of the inverses of these partial half-life values. **(b)** Growth rate of $\Delta 70^{STa}$. **(c)** Formula to calculate initial VSG remaining over time during coat replacement. N_0 = total initial VSG at time t = 0 (i.e. ~10^7 VSGs, or 100%). t = time since genetic VSG switch occurred. N = amount of initial VSG remaining after time t. These equations were adapted[83] for ease of interpretation in the context of this thesis.

2.5 Generation of dual expressor (DE) trypanosomes that co-express two VSGs at varied ratios

To understand the impact of VSG coat replacement dynamics on successful immune evasion during an infection, I sought to examine the vulnerability of trypanosomes with partially replaced coats to antibody-mediated clearance. I first needed to generate a set of dual-expressor (DE) trypanosome clones that simultaneously expressed two surface VSGs at varied ratios, representing switched cells at intermediate stages of coat replacement. The mechanisms that control gene expression levels in *T. brucei* are poorly characterized. However, studies have shown that alterations in the 5' and 3' UTR sequences flanking genes can affect mRNA and protein expression levels[173,174]. With this in mind, I designed a strategy to create a set of DE clones using varied UTR sequences to modulate *VSG* expression.

I developed a set of constructs to modify a parental cell line originally expressing VSG3 (WT-VSG3) by inserting *VSG2* into the *VSG3* expression site upstream of *VSG3* (Fig. 2.8a), following a strategy similar to that demonstrated in previous publications[175]. In this design, VSG2 and VSG3 represent pre-and post-switch VSGs, respectively. My constructs each contained a blasticidin (BSD) resistance gene and a *VSG2* gene flanked by a unique set of UTRs, and this entire cassette was targeted to a unique region in BES1 by flanking homologies (Fig. 2.8a). Lacking an obvious empirical reason to choose any particular UTRs, I experimented with combinations of UTRs from (1) *VSG2* itself, (2) *T. brucei* genes that are commonly used in lab vectors (*actin, aldolase*), and (3) a modified procyclin 5' UTR used in the study[173] that demonstrated 5' UTR-mediated modulation of gene expression. This strategy was successful in generating DE clones with varied VSG2 surface expression levels (Fig. 2.8b). VSG2 expression levels were stable over time in each clone (Fig. 2.8c), and reproducible between clones

transfected with the same construct. Previous studies have shown that co-expression of two VSGs does not perturb trypanosome growth or normal cellular function[175,176], and I also observed no growth defect in the DE clones (Fig. 2.8d). To ensure that my calculations of surface VSG2 expression ratios (Fig. 2.8b) were accurate, I performed the flow cytometry-based measurements underlying these data using a saturating concentration of anti-VSG2 antibody (Fig. 2.9a). Similar measurements of VSG3 expression levels in the DE clones indicated that VSG2 expression did not affect the amount of VSG3 present on the cell surface (Fig. 2.9b and c).

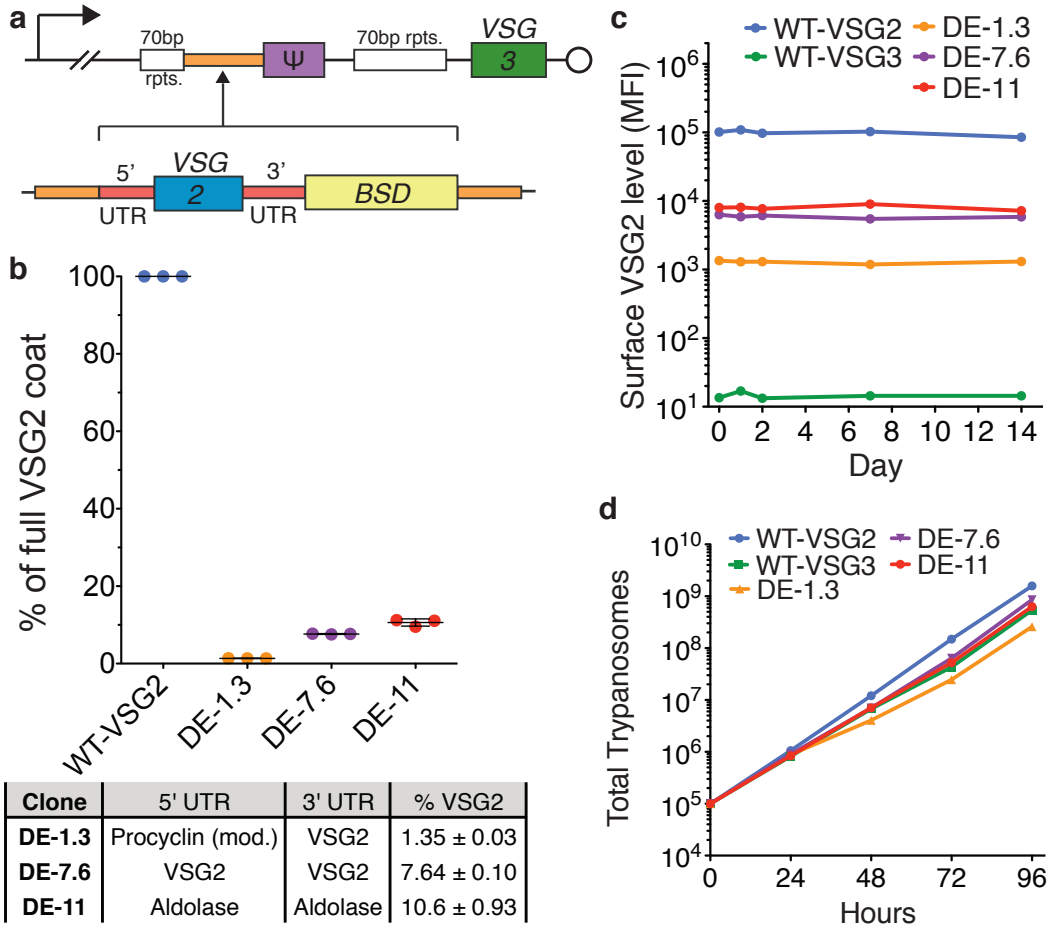

Clone	5' UTR	3' UTR	% VSG2
DE-1.3	Procyclin (mod.)	VSG2	1.35 ± 0.03
DE-7.6	VSG2	VSG2	7.64 ± 0.10
DE-11	Aldolase	Aldolase	10.6 ± 0.93

Figure 2.8. Dual-expressor clones stably express two VSGs at different ratios.

(a) Construction of dual-expressor (DE) clones. (Top) Diagram of the active VSG expression site (BES1) of the parental cell line shows the promoter (bent arrow), 70 bp repeats (rpts.), a *VSG* pseudogene (ψ), the telomere (circle), the active *VSG* (*VSG3*), and an intergenic region unique to BES1 (orange). (Bottom) The *VSG2* insertion constructs contain a Blasticidin resistance cassette (BSD) and a *VSG2* gene flanked by 5' and 3' UTRs that are unique to each construct. These insertions are targeted to BES1 by homology to the indicated intergenic region. **(b)** Analysis of the level of surface VSG2 present on DE clones. Raw fluorescence intensity values (population MFI via VSG2 Ab staining at saturating concentration, see Fig. 2.9a) were converted to absolute units (MESF). VSG2 level was calculated as a percentage of the MESF value of a full VSG2 coat (WT-VSG2). Table indicates 5' and 3' UTRs used and the resulting percentage of surface VSG2 expressed for each clone. Bars and % VSG2 values represent mean ± SD. **(c)** Stability of surface VSG2 levels expressed by DE clones (population MFI, VSG2 Ab staining) in culture. **(d)** Growth rate analysis of WT-VSG2, WT-VSG3, and DE clones.

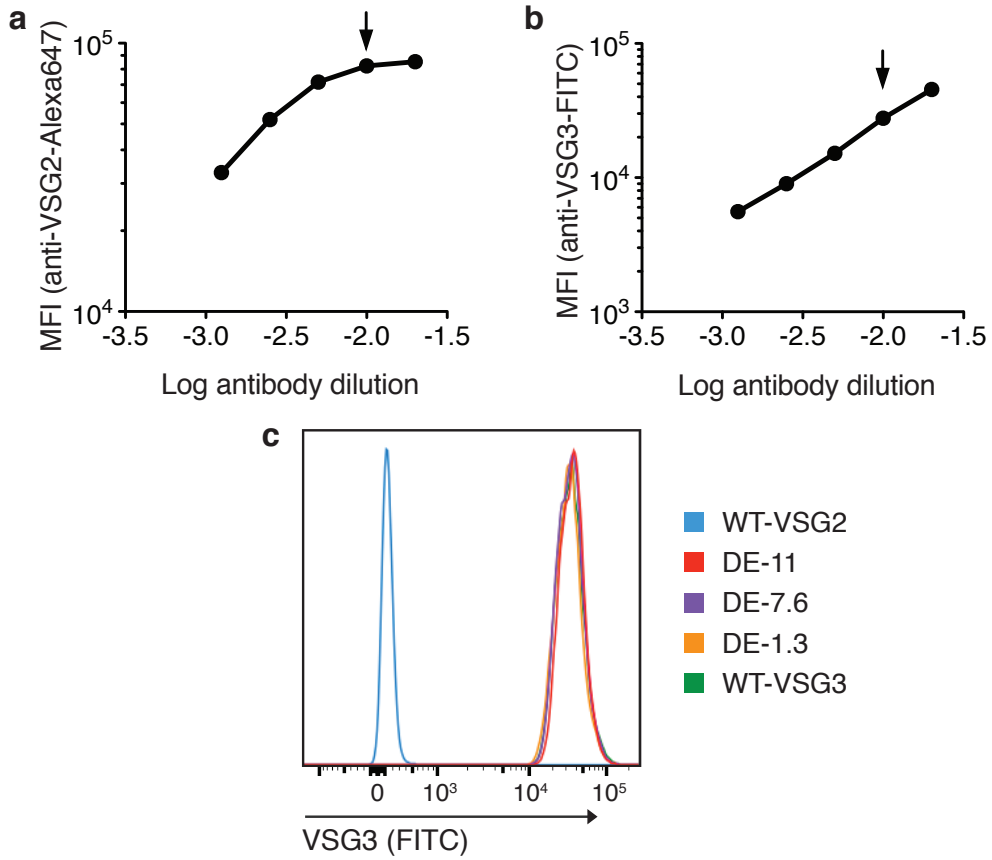

Figure 2.9. Flow cytometry-based measurements of VSG surface expression.

(a) Titration curve of monoclonal anti-VSG2-Alexa647 Ab staining of WT-VSG2 cells. Data are represented as population mean fluorescence intensity (MFI) measured via flow cytometry (see Methods for sample preparation). Saturating levels of VSG2 staining were reached with this Ab; arrow indicates the concentration used for calculation of relative surface VSG2 expression in DE clones (Fig. 2.8b). **(b)** Titration curve (as in (a)) of monoclonal anti-VSG3-FITC Ab staining of WT-VSG3 cells. After several fluorophore conjugation and Ab concentration attempts, I was unable to obtain a saturating concentration of this Ab. (**c)** Analysis of anti-VSG3-FITC staining at non-saturating levels (at concentration indicated by arrow in (b)), indicated that the amounts of surface VSG3 expressed by WT-VSG3 cells and each of the DE clones are approximately equal. Unlike the VSG2 ratio measurements (Fig. 2.8b), this result should be valid even without saturating conditions, as cells with equal VSG3 staining will not differentially affect the free anti-VSG3 Ab concentration present during staining.

2.6 Development of an immunization strategy to elicit a VSG-specific IgM response

During infection, T-cell independent VSG-specific IgM responses comprise the most rapid host defense against parasite proliferation[132], and non-switched trypanosomes have been shown to be cleared predominately via early arising IgM antibodies[40] (see section 1.8.1 for further discussion). Therefore, my goal was to develop a mouse immunization strategy to elicit VSG-specific IgM in order to best replicate the natural immune environment of cells undergoing VSG coat replacement. Using this strategy, I could raise IgM against VSG2 in mice, and then challenge the mice with the DE clones to determine each clone's susceptibility to VSG2-specific IgM-mediated clearance. To examine the kinetics of the antibody response to *T. brucei* infection, I infected mice with an injection of 50 SM (VSG2-expressing) trypanosomes, cleared the infection on day 4 using the drug berenil, and took blood samples on days 4-14 to monitor the development of the antibody response by ELISA. In agreement with previously published data[40,157], anti-VSG IgM reached peak titers on days 8–10 post-infection (Fig 2.10a). Class-switched IgG antibodies did not arise in most mice until day 12 or later, although IgG was detectable in the serum of one mouse on day 10. These IgM dynamics meant that common strategy of infecting mice with live trypanosomes and clearing with drugs prior to re-challenge was not suitable for my experiments. Berenil, the drug used to clear infection, produces a prophylactic effect lasting as long as 28 days[177], leaving the mice protected against challenge with parasites expressing any VSG well beyond the timeline of the early IgM response.

To solve this problem, I tested multiple strategies to prepare killed, non-infectious trypanosomes that could be used for immunization. Formalin fixation was an option, but studies have shown that very large quantities of fixed trypanosomes are needed to generate a strong immune response[132], and fixation would likely disrupt the protein coat. As alternative options, I

decided to try heat killing and UV-irradiation. Dead trypanosomes normally release their surface VSG due to an endogenouse lipase (GPI-PLC, see section 1.6), rendering them unusable for elicitation of VSG-specific responses. I therefore used a VSG2-expressing cell line that lacks GPI-PLC and retains an intact VSG coat following cell death[85]. Numerous attempts at heat killing resulted in trypanosome samples that were either denatured by overheating, or not fully killed (live trypanosomes would appear over time when the samples were cultured). In contrast, I was able to design a UV-irradiation protocol that reproducibly fully deactivated trypanosome samples while leaving the VSG coats intact. I then compared these immunizations using UV-irradiated trypanosomes to injection and clearance of live trypanosomes. For the UV-irradiated immunizations, I tried single injections (day 0 only), as well as double (days 0 and 3) and triple (days 0, 2, and 4) injections. Multiple injections were better than a single injection, but triple injections did not improve the IgM response over double injections (Figure 2.10b). Double injections of UV-irradiated trypanosomes elicited a VSG2-specific IgM response approximating that elicited by live trypanosomes, and significant production of class-switched (IgG) antibodies was not observed during the 14 days following immunization (Fig. 2.10c). The double UV-irradiated trypanosome injection strategy thus appeared to meet the requirements of generating a strong IgM response while not infecting the mice or introducing prophylactic drug treatment.

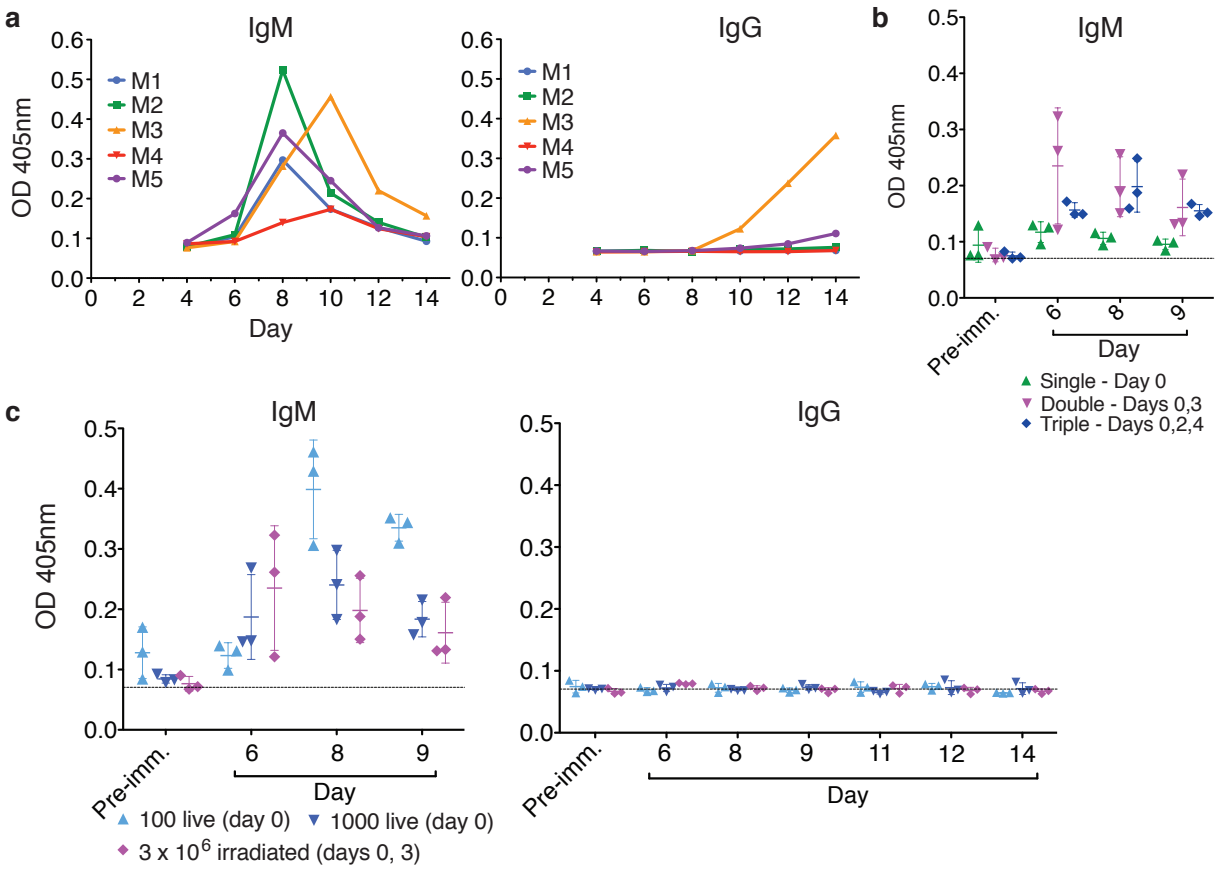

Figure 2.10. Dynamics of antibody response to live and UV-irradiated trypanosomes

VSG2-specific IgM and IgG titers elicited by live or UV-irradiated trypanosomes. Data show relative titers over time (days after initial injection) as measured by ELISA. **(a)** 50 VSG2-expressing (SM) trypanosomes were injected into mice (M1-5) on day 0 and cleared with berenil on day 4. **(b)** Mice received an injection of 3 x 10^6 UV-irradiated trypanosomes on each of the days indicated. ELISA data of mouse serum collected prior to immunization is labeled "Pre-imm." **(c)** Live or UV-irradiated trypanosomes were injected as indicated. Live trypanosomes were cleared with berenil on days 4 or 5. ELISA data of mouse serum collected prior to immunization is labeled "Pre-imm." For (a) and (c), error bars represent mean ± SD (n = 3 mice/group), and dotted lines indicate average background OD in wells incubated with no serum.

2.7 Only partial coat replacement is required for immune evasion

I then used the immunization protocol to assess whether my DE clones could evade a VSG2-specific IgM response *in vivo* (Fig. 2.11). Immunized and non-immunized control mice received challenge injections at day 8 post-immunization, at which point the immunized mice had high IgM titers, and low or undetectable IgG titers (Fig. 2.11a). Challenge injections contained 100 live WT-VSG2 (expressing VSG2 only), WT-VSG3 (expressing VSG3 only), DE-1.3, DE-7.6, or DE-11 trypanosomes. Starting at day 4 post-challenge, mice were monitored for survival, and blood smears were examined daily for the presence of trypanosomes. My results clearly demonstrated a threshold surface VSG2 level required for IgM-mediated trypanosome clearance. Clones with surface VSG2 levels ≥7.6% (DE-7.6, DE-11, and WT-VSG2) were either cleared entirely or exhibited delayed infection in immunized mice (Fig. 2.11b), and VSG2 levels ≥7.6% also correlated with a survival advantage for immunized mice (Fig. 2.11c). In contrast, WT-VSG3 and DE-1.3 clones were not affected by pre-immunization in terms of infection dynamics (Fig. 2.11b), survival of infected mice (Fig 2.11c), or parasitemia levels during the first peak of infection (Fig. 2.11d). The lack of evident pressure from VSG2-specific antibodies on DE-1.3 trypanosomes was striking, as VSG2 proteins are abundant on the surface of these cells (~1.3×10^5 VSG2 proteins/cell). These data suggest that switched trypanosomes escape the early IgM response once they have replaced only ~99% of their initial coat.

Figure 2.11. Immunization-challenge experiments with DE clones reveal a threshold of immune evasion.

(a) VSG2-specific IgM and IgG Ab titers in the immunized and non-immunized mice (n = 49 mice/group) used for experiments shown in (b) and (c) at day 8 post-immunization (combined results of three independent experiments). Data show relative titers as measured by ELISA. Dotted lines indicate average background OD in wells incubated with no serum. **(b)** and **(c)**, Non-immunized mice and mice immunized against VSG2 were challenged with the trypanosome clones indicated. **(b)** Percentage of mice with confirmed infection over time, and **(c)** survival curves for immunization-challenge experiments. X axes indicate day post-challenge. Grey shading indicates the period following clearance of the parasitemia peak resulting from outgrowth of input parasites. For (b) mice were permanently scored as infected when trypanosomes were first identified via blood smear. For (b) and (c), statistical analysis was performed using the log-rank (Mantel-Cox) test (n = 9 for DE-7.6 immunized and DE-11 non-immunized, 10 for other groups); *** $P < 0.001$, ** $0.001 < P < 0.01$, N.S., not significant ($P > 0.05$). Data include combined results of three independent experiments (with n = 4 or 5 mice per experimental group per experiment). One trypanosome clone of each type was used in these experiments. **(d)** Levels of parasitemia at day 5 post-challenge in immunized and non-immunized mice (mean ± SD, n = 5 mice/group). Immunized and non-immunized parasitemia levels are not significantly different ($P > 0.5$) in mice showing parasitemia with WT-224 and DE-1.3 clones, as determined by *t*-test (variances are similar between groups, as determined by *F*-test). These data were collected in one experiment. **(e)** Lack of VSG2 and VSG3 expression in late-arising (beyond day 8) DE-7.6 and DE-11 infections in pre-immunized mice. Data show flow cytometry analysis of trypanosomes isolated from the blood of infected mice on day 15 post-challenge, along with control VSG2 and VSG3-expressing trypanosomes (WT-VSG2 and WT-VSG3, respectively). The data shown are representative of late-infection trypanosome isolates from all DE-7.6 and DE-11 infections observed in pre-immunized mice (1 infection in DE-7.6 mice, 6 infections in DE-11 mice; one mouse from each group did not present parasitemia high enough for trypanosome isolation and analysis).

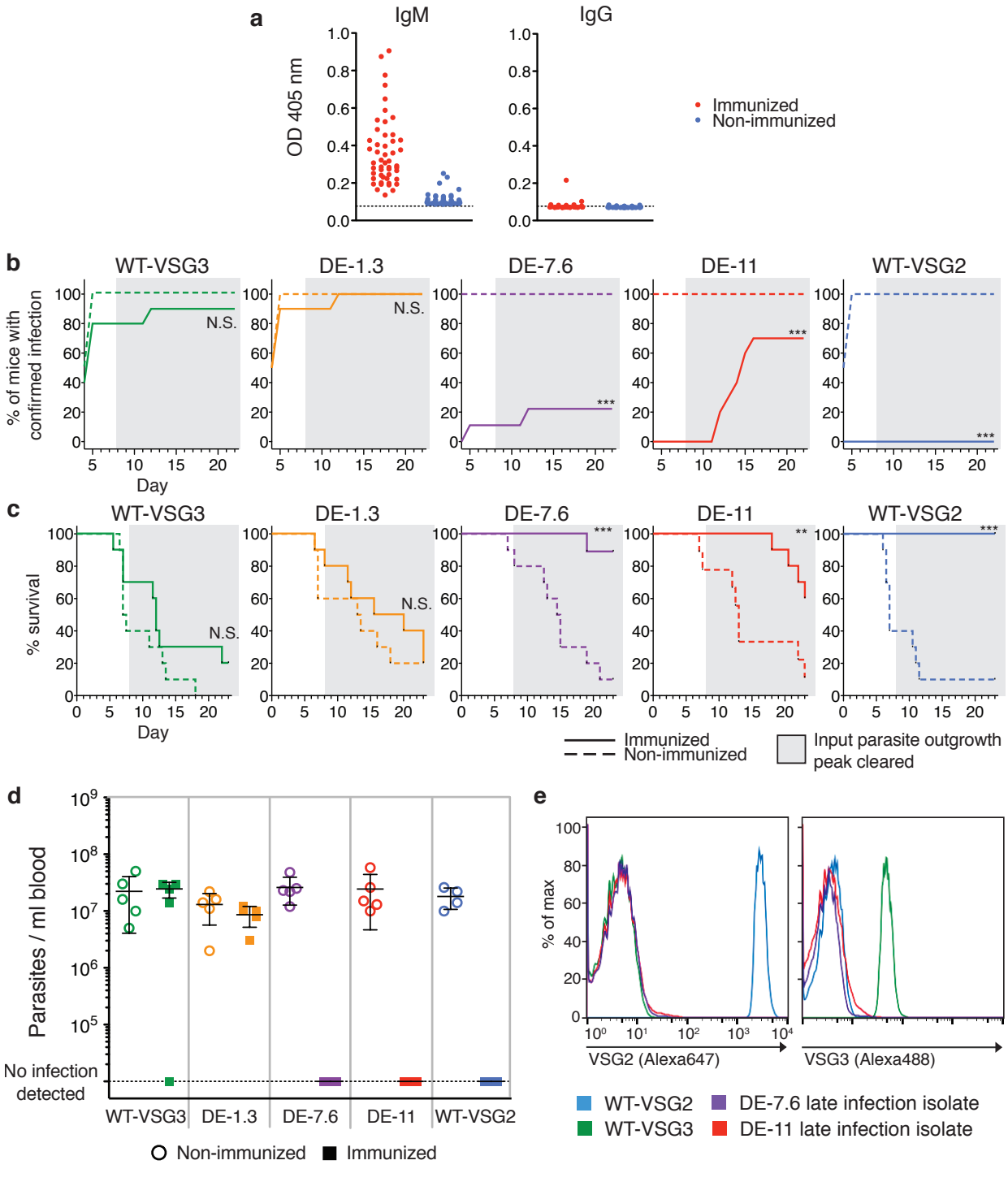
a
IgM
IgG
OD 405 nm
Immunized
Non-immunized
b
WT-VSG3
DE-1.3
DE-7.6
DE-11
WT-VSG2
% of mice with confirmed infection
N.S.
***
Day
c
% survival
**
Immunized
Non-immunized
Input parasite outgrowth peak cleared
d
Parasites / ml blood
No infection detected
Non-immunized
Immunized
e
% of max
VSG2 (Alexa647)
VSG3 (Alexa488)
WT-VSG2
WT-VSG3
DE-7.6 late infection isolate
DE-11 late infection isolate

A more detailed analysis of these results requires separation of the infections into two stages. Data from the first ~7 days post-challenge (Fig. 2.11b and c, unshaded regions) permits the most straightforward interpretation. The parasitemia peak representing immediate outgrowth of the input trypanosomes was uniformly detectable by day 4 or 5 post-challenge in non-immunized mice. Suppression of parasitemia in immunized mice at this time must be interpreted as a direct effect of pre-immunization on the survival of the input trypanosomes (Fig. 2.11b), which was the interaction I intended to examine. After this initial period, however, host-parasite interactions become more complex. If the input trypanosome peak occurred, mice either succumbed to infection immediately, or cleared the peak on days 6-8 by generating antibodies in response to the challenge injection. Mortalities occurring after day 8 thus resulted from expansion of switched parasite populations expressing VSGs not present in the input injections. Notably, trypanosomes isolated from several immunized mice that showed delayed infection with DE-7.6 and DE-11 clones had indeed lost expression of both VSG2 and VSG3 (Fig. 2.11e), suggesting that pre-immunization suppressed outgrowth of the input trypanosomes, but switched populations emerged following some level of early infection that had been undetectable by blood smear. Bearing these later complications in mind, the significant suppressive effects of pre-immunization on clones with surface VSG2 levels ≥7.6% are still most readily explained by the interactions of early IgM with the input trypanosomes during the first week of infection. Late interactions between maturing immune responses elicited against the input VSGs and emerging switched parasite populations may have some effect on the overall infection dynamics, but are unlikely to be the predominant factors influencing these data.

Combining these results with the VSG turnover rate measurements presented earlier permits a more complete analysis of the effect of coat replacement dynamics on successful

immune evasion. Full coat replacement takes ~4.5 days, but switched cells reach 7.6% and 1.3% initial VSG (levels on either side of the immune evasion threshold) after only 17.1 and 28.8 hrs, respectively (calculations performed as described in section 2.4.1). These data therefore suggest that although switched cells present initial VSG on their surface for extended periods, they are only vulnerable to immune clearance for a small fraction of that time.

2.8 IgM binding ability is dependent on VSG density

To examine the mechanism(s) underlying this immune evasion threshold, I assessed the ability of IgM to bind to the DE clones (Fig. 2.12). I raised VSG2-specific polyclonal IgM antibodies in two mice. Both IgM samples strongly stained DE-7.6, DE-11, and WT-VSG2 cells, but showed extremely weak or no binding to DE-1.3 and WT-VSG3 cells (Fig. 2.12a). To interpret this binding behavior, I developed a model predicting the number of contacts an individual IgM could make with surface VSGs present at varying densities. IgM is a pentameric, decavalent molecule whose binding capability is generally based on low-affinity, high-avidity interactions[178]. IgM is ~30-40 nm in diameter[179,180], while the VSG coat has been modeled as a hexagonal array of VSG homodimers with a spacing of ~5.8 nm[181] (Fig. 2.12b). Using these parameters, I predicted the number of initial VSGs within reach of a 40 nm-wide IgM at the coat replacement stages represented by the DE clones (Fig. 2.12c, calculations detailed in Methods). I estimate that a single IgM molecule can reach multiple initial VSGs at any given moment when initial VSG composes ≥7.6% of the total surface VSG, but this is no longer true when that value reaches 1.3%. I reached the same conclusion when I modeled this interaction assuming an IgM diameter of 30 nm. Thus, my model suggests that the observed *in vivo* immune evasion and *in vitro* IgM binding thresholds are driven by IgM's fundamental requirement for multiple antigen

contacts to allow successful binding and performance of effector functions. I therefore conclude that antigenic density, not abundance, is a key determinant of the efficacy of early IgM responses.

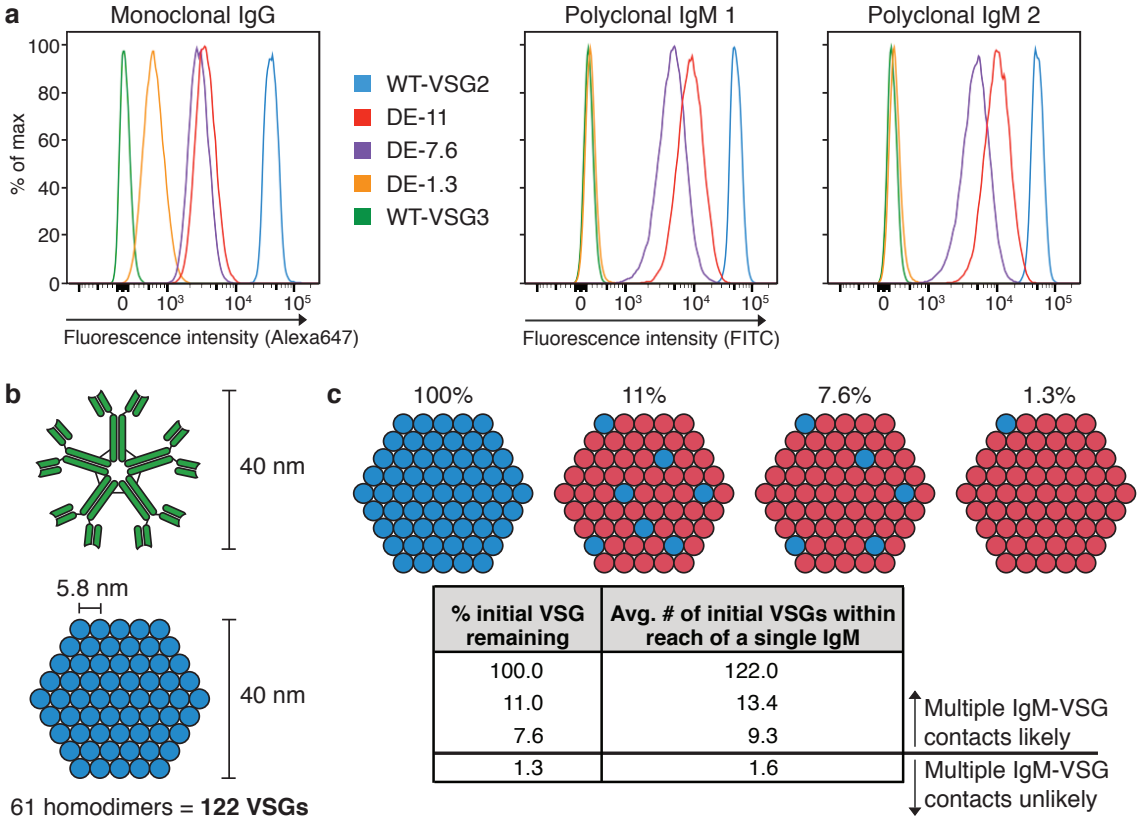

Figure 2.12. The effect of VSG density on IgM binding ability.

(a) VSG2-specific Ab binding to wild-type (WT) and dual expressor (DE) clones. Monoclonal anti-VSG2 IgG Ab was used as a control to demonstrate the presence of surface VSG2 in all DE clones (left). Binding ability of two polyclonal IgM antisera is shown on the right. Data are representative of three replications of this experiment. **(b)** and **(c)** A model detailing a proposed mechanism for the observed IgM binding threshold. **(b)** The binding footprint of IgM. Modeling the VSG coat (bottom) as a hexagonal array of VSG homodimers with a spacing of ~5.8 nm, an IgM molecule (top) with a diameter of 40 nm could contact a maximum of 61 homodimers (122 VSGs) at a single time. **(c)** The average number of initial VSGs within a given IgM binding footprint at varying stages of coat replacement.

2.9 Discussion

2.9.1 VSG coat fluidity affects IgM-VSG interactions

My mathematical model of the IgM-VSG coat interface (Fig. 2.12b and c) provides a framework for evaluating the impact of VSG density on IgM-VSG binding based on the two-dimensional scale of these interactions, but the dynamic nature of the system must also be considered. The VSG coat is highly fluid, and each monovalent IgM-VSG interaction has some discrete duration determined by the IgM's binding kinetics. Thus, the ability of a single IgM to make contacts with multiple cognate VSGs is actually based on the likelihood of a second cognate VSG coming into range of a given IgM during an initial monovalent interaction. This likelihood is highly influenced, but not fully determined, by average VSG spacing. Further, hydrodynamic flow generated by beating of the trypanosomal flagellum has been demonstrated to push surface VSG-Ig complexes towards the posterior end of the cell[75], which could produce a gradient of increasing VSG density on the trypanosome surface *in vivo*. This process may thereby increase the likelihood of polyvalent IgM-VSG interactions, and consequently decrease the expected threshold amount of cognate VSG necessary for IgM binding to a lower level than my model predicts. Conversely, the shear forces that hydrodynamic flow applies to IgM-VSG interactions could decrease the duration of each monovalent interaction, producing the opposite effect on the expected threshold amount. Overall, in cases where trypanosomes have ≥7.6% initial VSG remaining, a single IgM is likely to encounter multiple initial VSGs regardless of whether the VSG coat is in motion. For lower VSG percentages, the expected effect is more uncertain, though the empirical evidence presented here (Fig. 2.12a) suggests that the DE-1.3 clone is indeed below the IgM binding threshold. A deeper mechanistic evaluation would require

performing a similar analysis of IgM binding to trypanosomes in whole blood under flow conditions, but the technical capability to perform such experiments does not exist, at present.

2.9.2 The effect of VSG coat replacement on stimulation of a subsequent immune response

A prior study by Dubois et al.[182] examined the phenomenon of VSG coat replacement from another angle, demonstrating that trypanosomes simultaneously expressing two VSGs elicit a weaker antibody response than trypanosomes expressing only one VSG. This result informs the effect of VSG coat replacement on the development of new antibodies targeting subsequent waves of parasitemia, but does not address my focus, the effect of the previously stimulated antibody response on the switched (and partially coat-replaced) trypanosomes themselves. I did not examine the antibody response elicited by the DE clones in detail, as it was beyond the scope of this study. However, I do not see any conflict between my results and the results detailed in this prior publication, and suggest that these studies should be viewed as related but distinct bodies of work.

Chapter 3

An *O*-linked VSG glycan influences parasite virulence and interactions with host antibodies

3.1 Introduction and background data

This chapter details a collaborative body of work characterizing structural, biochemical, and functional attributes of VSG3 (a.k.a, Lister 427-3, MITat 1.3, VSG224). As a background to my contributions, this introductory section contains a summary of three data sets generated by collaborators: (1) the solving of the VSG3 crystal structure and the identification within the structure of an *O*-linked glycan (subsection 3.1.1) in the laboratory of Dr. Erec Stebbins (current address the German Cancer Research Center (DKFZ); Heidelberg, Germany); (2) mass spectrometry analyses of the VSG3 *O*-linked glycan (subsection 3.1.2) performed in the laboratory of Dr. Michael Ferguson (University of Dundee; Dundee, UK); and (3) identification of analogous glycans in other VSGs (subsection 3.1.3) via analyses from both collaborators. I was not involved in producing these data, and the associated techniques will not be included in the Methods section of this thesis. These presently unpublished results are included here because they form the basis of my contributions (and those of other Papavasiliou lab members) in evaluating the influence of the VSG3 *O*-glycan on parasite virulence and evasion of the host antibody response (described in the following sections of this chapter). Section 3.7 at the end of the chapter lists the specific contributions of each researcher involved in this study.

3.1.1 Identification of an O*-linked glycan on the membrane-distal surface of VSG3*

The diverse VSGs of *T. brucei* have been categorized into three distinct N-terminal classes (major classes A and B, and minor class C) based on patterns of analogous cysteine residues[123,163]. Although there are thousands of known *VSG* genes, only three crystal structures of VSG N-termini have been published to date, all belonging to class A[50-52]. Because of this lack of

depth and diversity in sampling, it seemed plausible that the published structures were an incomplete representation of the real structural variation between VSGs. Intriguingly, preliminary examinations of a common class B variant, VSG3, showed that it scored poorly against the class A VSG structures in structure-based prediction algorithms such as protein "threading"[183] (whereas the class A VSGs scored highly against one another). To examine whether VSG3 might contain unidentified conformational variability, our collaborators crystallized and solved the structure of this variant.

The VSG3 crystal structure did reveal several divergent structural features, but this thesis will focus on the most unexpected discovery: the identification of an *O*-linked α-glucose moiety attached to VSG3 residue S317 (Fig. 3.1). This *O*-glycan is located on the top (membrane-distal) surface of VSG3, and is therefore likely to be highly exposed to the immune system.

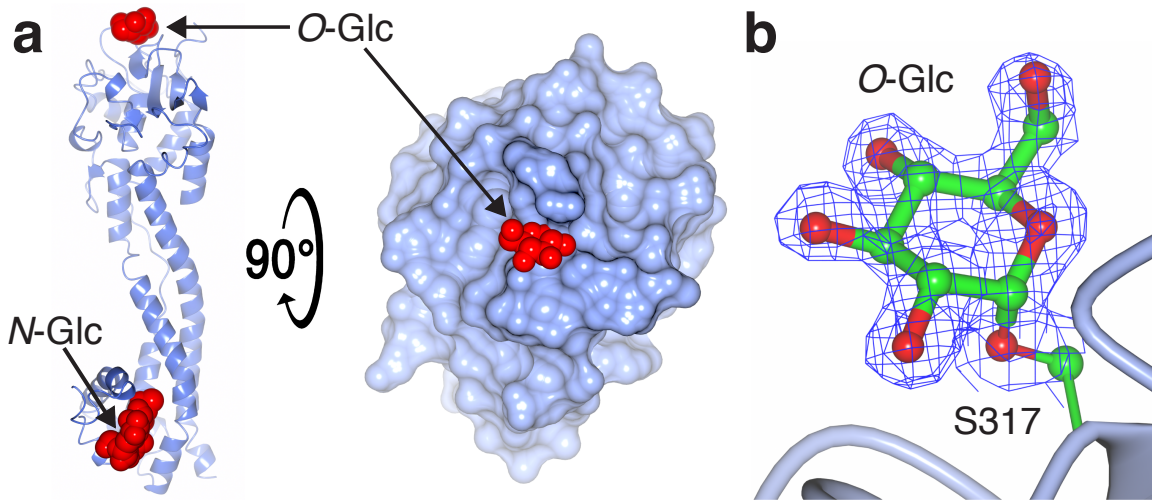

Figure 3.1. VSG3 structure reveals an *O*-linked glycan at residue S317.
(a) Structural diagram of VSG3. On the top surface of the upper lobe is a red space-filling representation of the α-glucose moiety attached to residue S317 (*O*-Glc). An N-linked glycan (*N*-Glc) is shown in the bottom lobe. A 90-degree rotation of the left model is rendered with molecular surfaces. **(b)** 1.4 angstrom resolution electron density map from the refined model of VSG3 clipped to the volume around the modeled glucose. S317 is shown connected to a ribbon diagram representation of the protein main chain.

3.1.2 Heterogeneity in VSG3 O-glycosylation

Mass spectrometric analysis of intact VSG3 by ES-MS before and after digestion with PNGaseF (which specifically removes N-glycans) validated the *O*-linked α-glucose moiety identified in the crystal structure, and additionally revealed heterogeneity in the number of *O*-linked glycans present (Fig. 3.2a and b). Subsequently, peptide mass analysis by LC-MS/MS confirmed that the peptide A311-K339 contained 0, 1, 2 or 3 hexose residues (Fig. 3.2c).

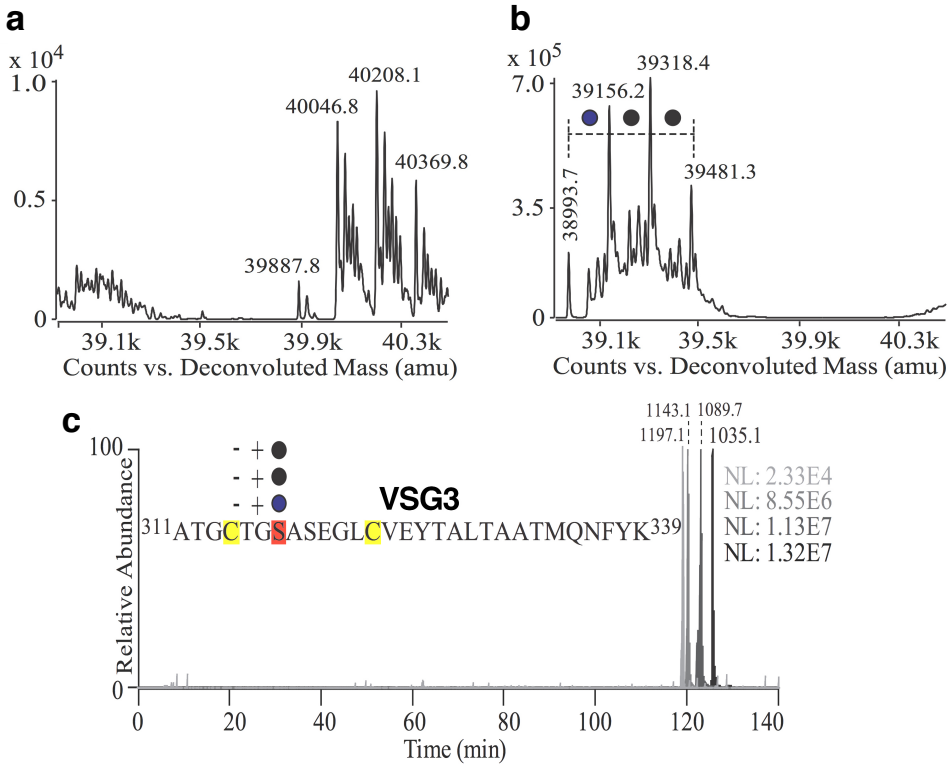

Figure 3.2. Mass spectrometry analysis reveals heterogeneity in VSG3 *O*-glycosylation. Deconvolved electrospray mass spectra of purified native VSG3 N-terminal domain before **(a)** and after **(b)** de-N-glycosylation with PNGaseF. The mass differences of ~162 Da between VSG3 species indicate *O*-glycosyl heterogeneity. The lowest mass in (b), 38993.7 Da, agrees with the theoretical mass for residues A20-G388 of VSG3 allowing for the conversion of N67 to D67 by PNGaseF and four disulfide bonds **(c)** Extracted ion chromatogram showing the elution profiles of $[M+3H]^{3+}$ ions (*m/z* 1035.1, 1089.1, 1143.1 and 1197.1) for the A311 to K339 peptide of VSG3 containing 0, 1, 2 and 3 hexose residues, respectively. These elute by reversed-phase HPLC from most to least hydrophilic with decreasing numbers of sugar residues attached.

The MS/MS product ion spectra of several peptide glycoforms further defined the *O*-glycosylation site as S317 (Fig. 3.3).

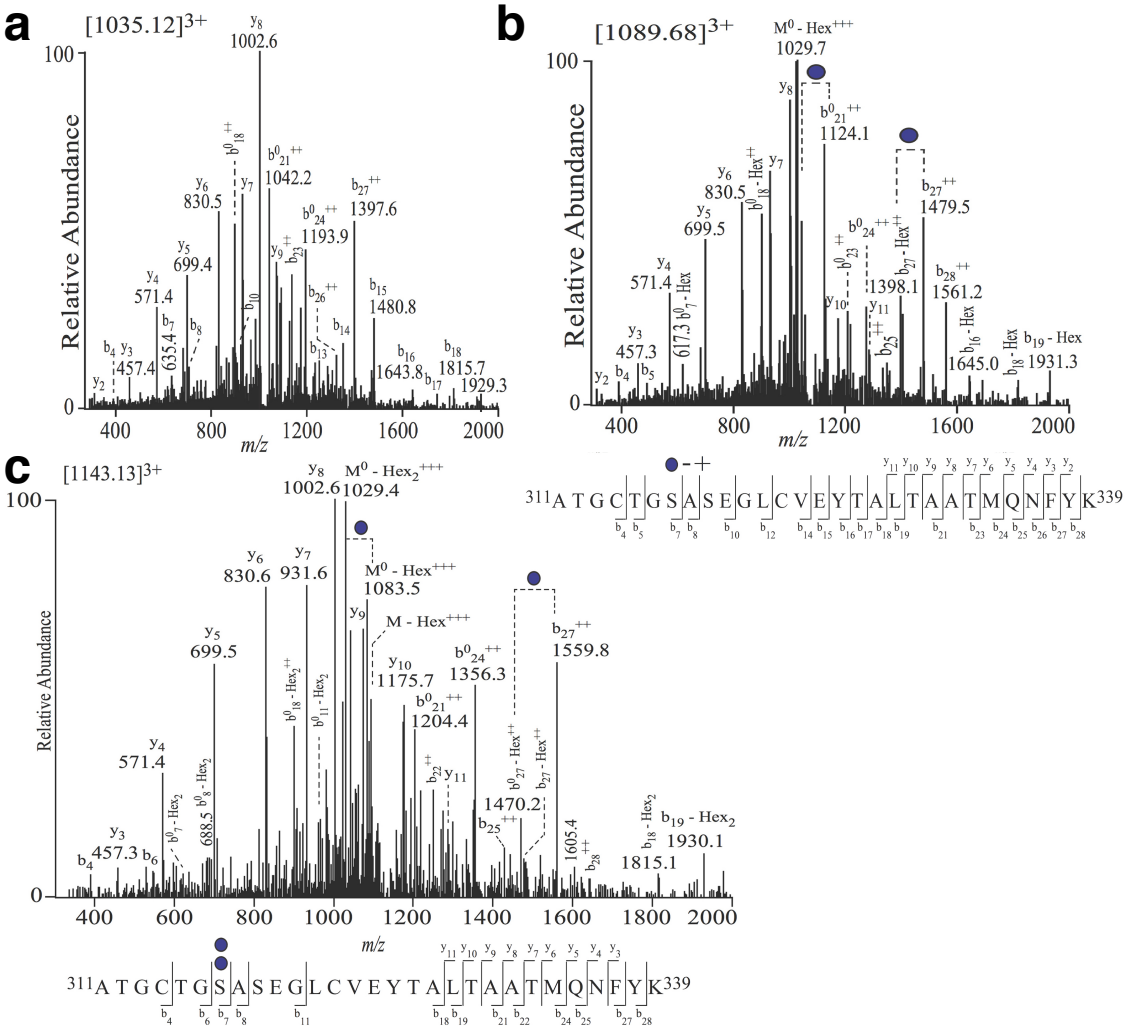

Figure 3.3. MS/MS characterization of heterogeneous *O*-linked VSG3 surface glycans. The product ion mass spectra of $[M+3H]^{3+}$ ions corresponding to the VSG3 peptide A311-K339 containing **(a)** zero, **(b)** one, and **(c)** two hexose residues. For (b), the diagnostic b7-Hex ion at *m/z* 617.3 suggests that S7 in the peptide was converted to dehydro-alanine through β-elimination, defining the *O*-glycosylation site in the original VSG3 sequence as S317. For (c), the b7 and b8 ions suggest that both hexoses are attached to S7 (S317 in the full VSG3 sequence) and not to any other hydroxyl-amino acids in the sequence.

Together, these data strongly indicate that there is a heterogeneous chain of 0-3 hexoses attached to VSG3 residue S317. No evidence of additional glycosylation of serines or threonines was observed. Based on the ES-MS spectra (Fig. 3.2a and b), the proportions of the 0, 1, 2 and 3 hexose glycoforms were estimated at 8%, 33%, 37%, and 22%, respectively. While *O*-linked carbohydrates are known in other kinetoplastids[184], such modifications have not been previously described in *T. brucei*. Further, no carbohydrates of any kind have been previously been identified on the top surface of a VSG.

3.1.3 Analogous O*-glycans in other VSGs*

The *O*-glycan in VSG3 is located in an exposed loop stabilized in the upper lobe by flanking cysteines involved in a disulfide bridge (the peptide CTG**S**ASEGLC, residues 314-323, Fig. 3.4a). To assess the prevalence of surface *O*-linked glycosylation, our structural biologist collaborator compiled a list of VSGs from diverse genomic locations[34] with N-terminal domains that threaded to VSG3 and contained cysteine-flanked, serine- or threonine-containing loops analogous to the glycosylated loop in VSG3. A subset of this list is shown in Fig 3.4b. Two of these (VSG11 and VSG615) and an additional VSG that did not thread to VSG3 (VSG21) were analyzed by mass spectrometry. The results showed that both VSG11 and VSG615 possessed heterogeneous *O*-linked hexose modifications analogous to those found in VSG3 (Fig. 3.4c and d), while VSG21 did not. These data suggest that surface *O*-linked glycosylation could be a widespread VSG modification present throughout trypanosome infections.

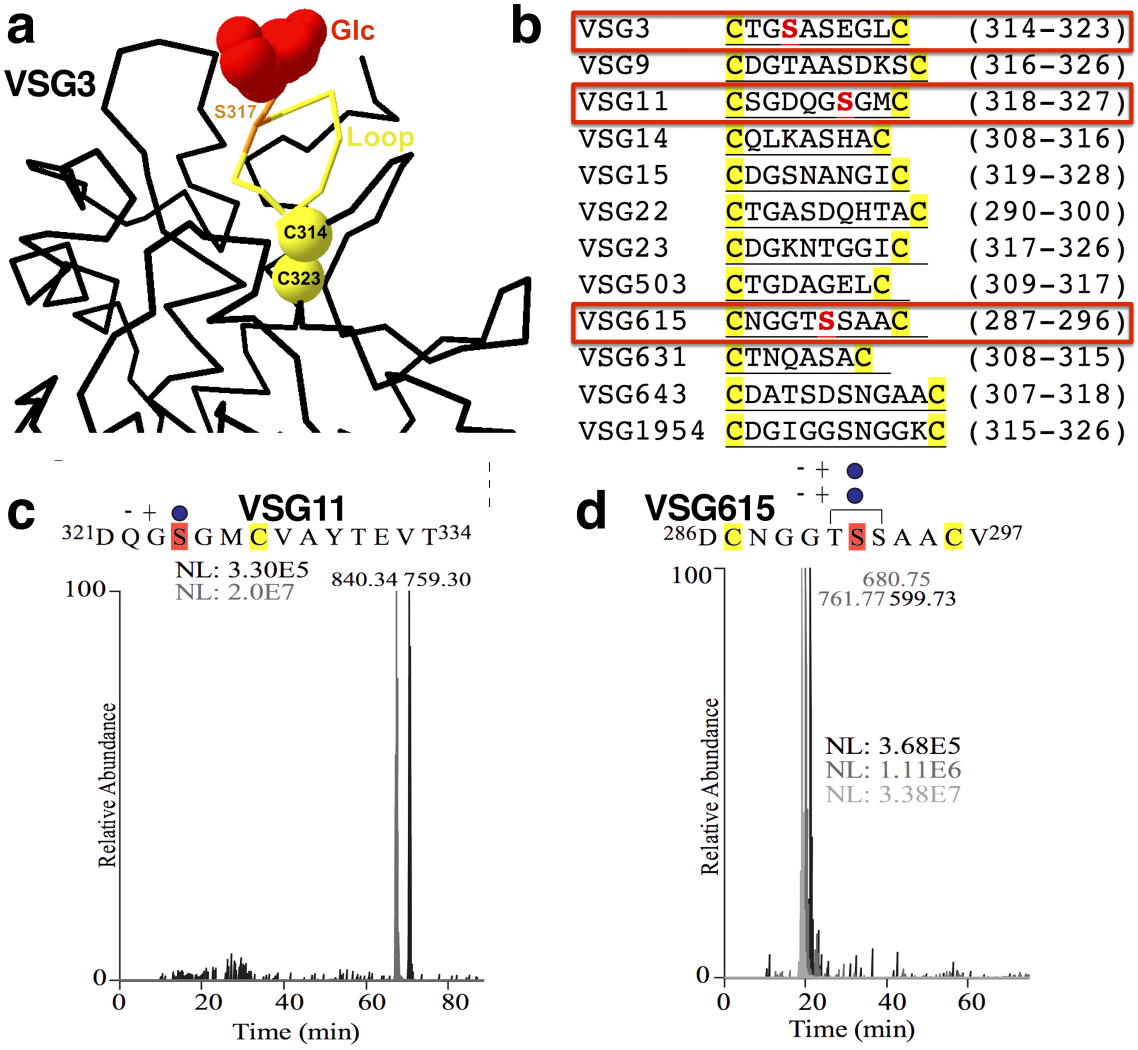

Figure 3.4. Identification of heterogeneous *O*-linked glycans in additional VSGs.

(a) Cysteine-flanked glycan loop of VSG3 with the loop in yellow and the disulfide-bridged cysteines shown as yellow spheres and labeled, S317 shown as a stick model in orange, and the glucose atoms in red. **(b)** Comparison of hypothesized "*O*-linked glycan" loops in additional VSGs. *O*-glycosylation was examined and confirmed for three VSGs (boxed in red): VSG3, VSG11, and VSG615. **(c)** and **(d)** Extracted ion chromatograms showing glycan heterogeneity in the elution profiles of $[M+3H]^{3+}$ ions for the indicated peptides of VSG11 and VSG615, respectively (similar to Fig. 3.2c for VSG3). The determined (VSG11) and the proposed (VSG615) modified serine residues are indicated within the relevant peptide (the MS/MS data of the VSG615 glycopeptides did not allow unambiguous assignment of S292 as the unique *O*-glycosylation site, and thus T291 and S297 could also potentially be sites of modification).

3.2 Cloning isogenic trypanosome strains expressing wild type VSG3 ($VSG3_{WT}$) or non-*O*-glycosylated mutant VSG3 ($VSG3_{S317A}$)

Because of its central placement on the top surface of VSG3, we wondered whether the *O*-linked glycan might affect interactions with the host immune response. To examine this, we genetically engineered isogenic trypanosome strains that expressed either a wild type VSG3 ($VSG3_{WT}$) coat or a VSG3 coat with a S317A point mutation ($VSG3_{S317A}$, which cannot be *O*-glycosylated). First, VSG3 was cloned into the pUB39[166] vector, and the S317A mutation was introduced by quick-change PCR. The pUB39 vector inserts included genes into the *T. brucei* rDNA spacer, where they are expressed under control of a Tet operator. The $VSG3_{S317A}$ mutant construct was transfected into VSG2-expressing (SM) trypanosomes to test that the mutant protein could be expressed and presented on the cell surface (alongside the endogenous VSG2) and recognized by our anti-VSG3 antibody. This test was successful, and the $VSG3_{WT}$ and $VSG3_{S317A}$ genes were then cloned into the pSY37F1D-CTR-BSD vector (described in section 2.3), creating plasmids pKI224-WT and pKI224-S317A, respectively. These plasmids were then used to transfect VSG2-expressing SM and GPI-$PLC^{-/-}$ trypanosomes, resulting in four clones: KI.$VSG3_{WT/S317A}$-1 (SM background) and KI.$VSG3_{WT/S317A}$-2 (GPI-$PLC^{-/-}$ background). A diagram of wild type BES1, the pKI224-WT/S317A constructs, and BES1 in the KI.$VSG3_{WT/S317A}$ clones is shown in Fig 3.5.

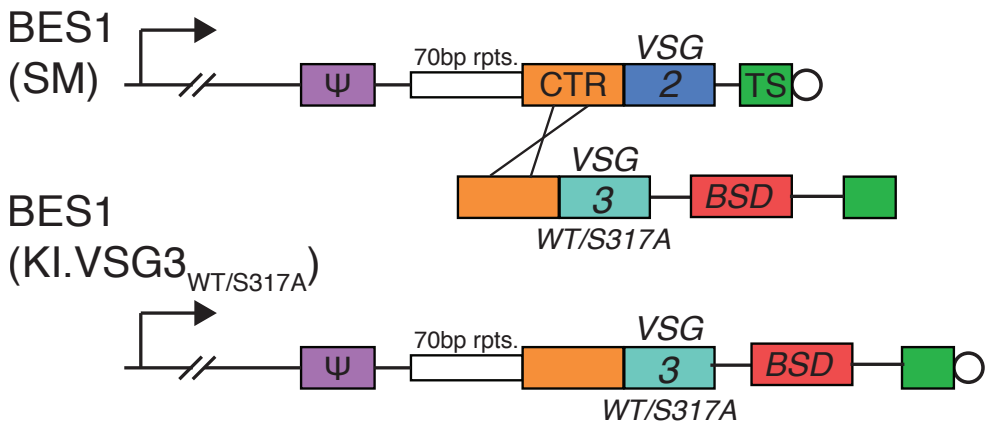

Figure 3.5. Generation of $VSG3_{WT}$ and $VSG3_{S317A}$ knock-in clones.
(a) (Top) Diagram of the active BES (BES1) in VSG2-expressing SM and GPI-$PLC^{-/-}$ cells; shows the promoter (bent arrow), a *VSG* pseudogene (ψ), 70 bp repeats (rpts.), the *VSG2* co-transposed region (CTR), *VSG*2, the telomere seed region (TS) and the telomere (circle). (Middle) The pKI224-WT/S317A constructs containing $VSG3_{WT}$ or $VSG3_{S317A}$ and a blasticidin resistance gene (BSD) are recombined into BES1 via break-induced replication (BIR) using the *VSG2* CTR for homology. (Bottom) Diagram of resulting BES1 in the $VSG3_{WT/S317A}$ knock-in clones.

3.3 VSG3-expressing trypanosomes lacking the *O*-glycan show decreased virulence

We then used these strains to infect naïve C57BL/6J mice. We observed that whereas all $VSG3_{WT}$-infected animals succumbed to infection during the first peak of parasitemia (days 6-9 post infection), all but one $VSG3_{S317A}$-infected animal survived the first peak (Fig. 3.6a). Late mortality events (after day 10) in this latter mouse group resulted from outgrowth of parasites that had switched expression to other VSGs. The data in Fig. 3.6a are combined results of two experiments with independent sets of clones: KI.$VSG3_{WT/S317A}$-1 and KI.$VSG3_{WT/S317A}$-2. Both clone sets individually produced the same result (Fig. 3.6b and c), suggesting that the observed decrease in parasite virulence resulting from the S317A mutation is not a clone-dependent artifact. C57BL/6J is an inbred mouse strain, and different mouse strains can display immune responses with distinct characteristics. To assess whether the observed virulence differential was

dependent on the host genetic background, I also repeated the infections in an outbred mouse strain (CD-1). While more mice infected with $VSG3_{S317A}$ trypanosomes succumbed to infection during the first peak of parasitemia in these infections, the virulence differential was still readily apparent (Fig. 3.6d).

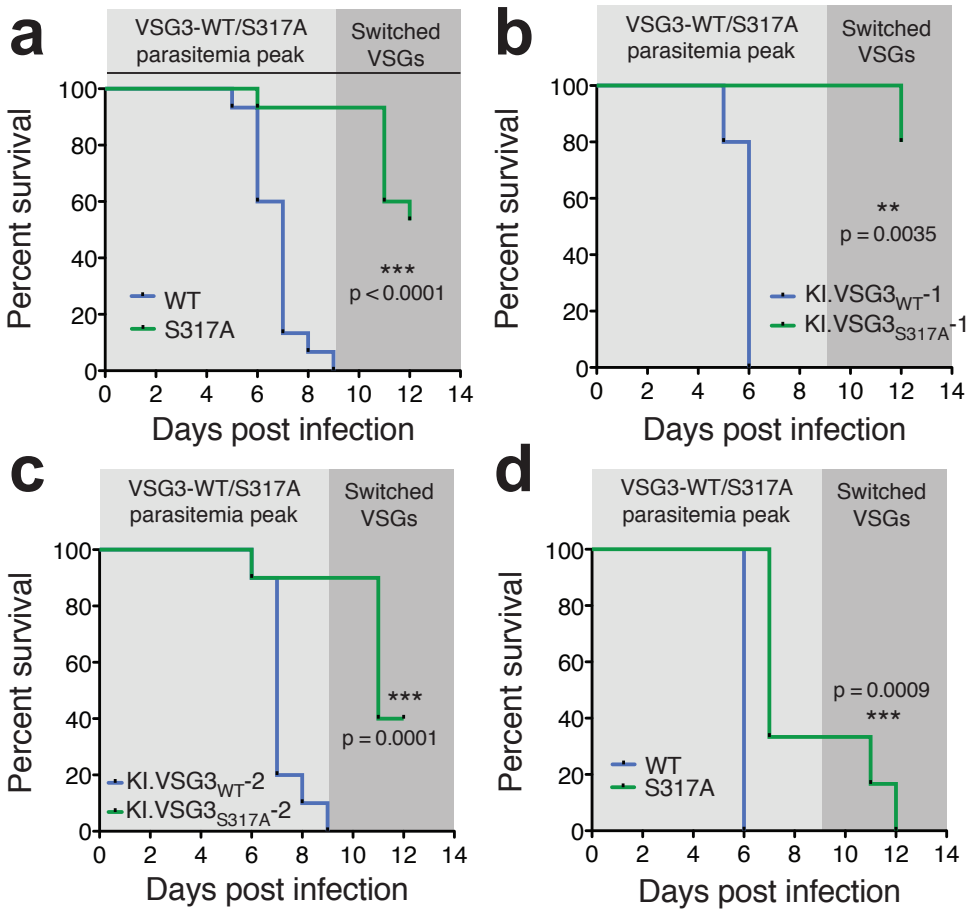

Figure 3.6. VSG3-expressing parasites lacking the *O*-glycan show decreased virulence. Survival of mice infected with trypanosomes expressing $VSG3_{WT}$ or non-*O*-glycoslyated mutant $VSG3_{S317A}$. Shaded regions represent sequential "peaks" of parasitemia. **(a)** Combined results from two experiments with independent trypanosome clone sets (n = 15 mice/group, data from individual clone sets are shown separately in (b) and (c)). **(b** and **c)** Results from infections with clones **(b)** KI.$VSG3_{WT/S317A}$-1 (n = 5 mice/group), and **(c)** KI.$VSG3_{WT/S317A}$-2 (n = 10 mice/group). Mice in (a-c) are C57BL/6J. **(d)** Results from infections in CD1 mice (n = 6 mice/group; clones KI.$VSG3_{WT/S317A}$-1 were used). All statistical analyses were performed using the log-rank (Mantel-Cox) test.

We also observed slightly lower peak parasitemia levels in the $VSG3_{S317A}$ infections compared to the $VSG3_{WT}$ infections (Fig. 3.7a-d). However, growth curves between the wild type and mutant VSG3 trypanosomes were similar *in vitro* (Fig. 3.7e and f), suggesting that the differences observed *in vivo* were due to host factors rather than clone-intrinsic. We therefore reasoned that our collective mouse infection data likely reflected a role for the *O*-linked sugar in evasion of the host immune response.

O-glycan-mediated impairment of the host's ability to generate protective antibodies would make parasites expressing *O*-glycosylated VSG3 more virulent within the first peak of infection. Further, VSG-specific IgM can be present at low titers by day 5 post infection[40], and *O*-glycan-dependent disparity in the efficiency of antibody-mediated clearance at this stage could account for the observed differences in day 5 parasitemia levels. Another interesting observation in the day 5 parasitemia data was that parasitemia levels of both wild type and mutant VSG3 trypanosomes were higher in CD-1 mice than in the C57BL/6J mice (Fig. 3.7d compared to a-c). This apparent mouse strain-dependent effect on trypanosome proliferation could explain why the CD-1 mice generally succumbed to infection more rapidly than C57BL/6J mice (Fig. 3.6d compared to a-c).

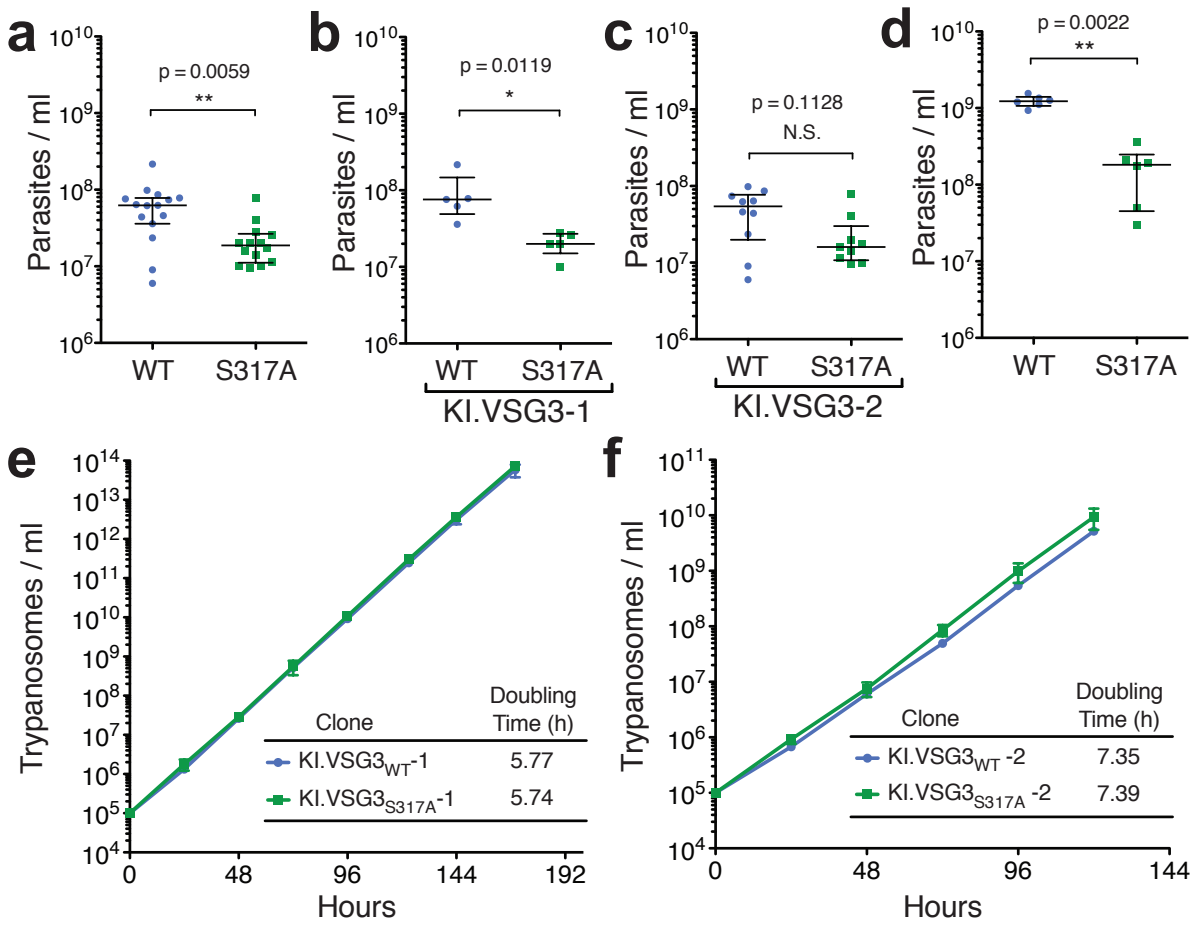

Figure 3.7. Day 5 parasitemia and *in vitro* growth rates of VSG3$_{WT}$ and VSG3$_{S317A}$ clones. **(a-d)** Parasitemia levels at day 5 post infection. **(a)** Combined results from two experiments with independent trypanosome clone sets (n = 15 mice/group, data from individual clone sets are shown separately in (b) and (c)). **(b** and **c)** Results from infections with clones **(b)** KI.VSG3$_{WT/S317A}$-1 (n = 5 mice/group), and **(c)** KI.VSG3$_{WT/S317A}$-2 (n = 10 mice/group). Mice in (a-c) are C57BL/6J **(d)** Results from infections in CD1 mice (n = 6 mice/group; clones KI.VSG3$_{WT/S317A}$-1 were used). Statistical values were calculated by two-sided Mann-Whitney test; bars represent median and interquartile range. **(e)** and **(f)** comparisons of *in vitro* growth rates for **(e)** the KI.VSG3-1 clone set, and **(f)** the KI.VSG3-2 clone set.

3.4 $VSG3_{WT}$- and $VSG3_{S317A}$-elicited antibody responses differ in their ability to protect against cognate parasites

To address the hypothesis that the *O*-glycan chains impede the host's ability to generate a protective antibody response, we performed additional infection experiments in which mice were pre-immunized prior to parasite challenge. We inoculated mice with UV-irradiated parasites expressing either $VSG3_{WT}$ or $VSG3_{S317A}$ (clones KI.$VSG3_{WT}$-2 and KI.$VSG3_{S317A}$-2, which are GPI-$PLC^{-/-}$ and therefore retain their VSG coats following irradiation). I had shown previously that this protocol yields an immune response that mimics the response to the infective parasite (discussed in section 2.5). We then challenged these mice via injection of live cognate parasites at day 8 post immunization and monitored mouse blood smears for the presence of trypanosomes on days 5-8 post-challenge. As shown in Fig. 3.8a, non-immunized mice (the same mice from Figs. 3.6a and 3.7a above) uniformly presented parasitemia by day 5. We found that pre-immunization with $VSG3_{S317A}$ was highly protective, suppressing detectable outgrowth of cognate $VSG3_{S317A}$ trypanosomes in 83.3% (10/12) of mice (Fig. 3.8a). In contrast, pre-immunization with $VSG3_{WT}$ was only marginally protective against cognate $VSG3_{WT}$ trypanosomes, suppressing outgrowth in 25% (3/12) of mice. All mice that presented parasitemia either succumbed to infection or cleared the parasites by day 8. The discrepancy in the protective effect of pre-immunization was also evident in survival differences between the two mouse groups (Fig. 3.8b). These results provide evidence that the *O*-linked glycan chains displayed by VSG3 inhibit the ability of the host antibody response to mediate parasite clearance.

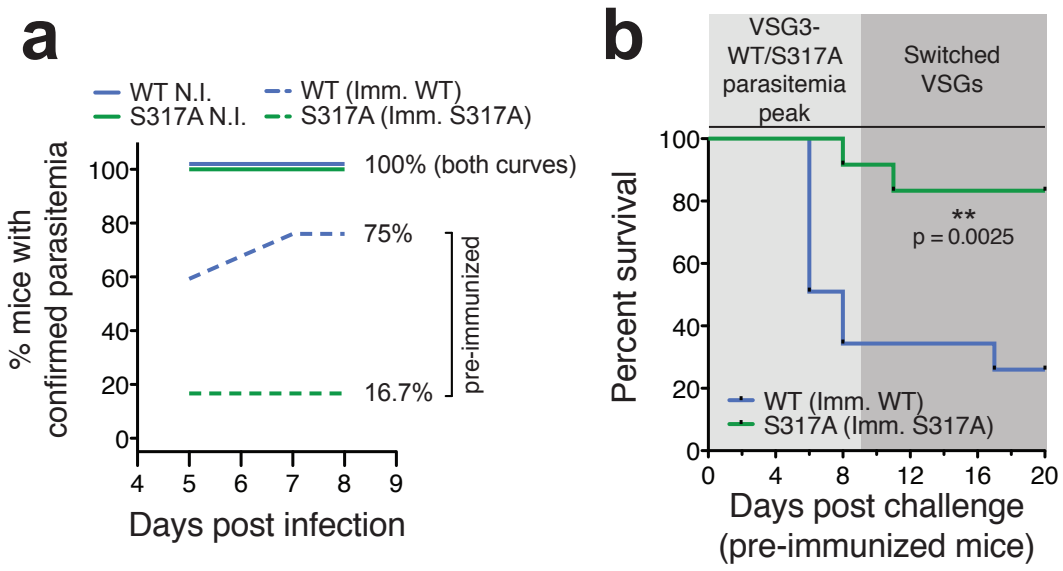

Figure 3.8. The VSG3 *O*-glycan limits the protective effects of pre-immunization

(a) Emergence of parasitemia in non-immunized (N.I.) and pre-immunized mice. N.I. data are from infections shown in Fig 3.6a and Fig. 3.7a (n = 15 mice/group). Pre-immunized mice (n = 12 mice/group) were inoculated with UV-irradiated trypanosomes expressing $VSG3_{WT}$ or $VSG3_{S317A}$ (Imm. WT or S317A, respectively) on days -8 and -5 relative to challenge. Challenge injection contained live parasites expressing the same VSG to which the mice were immunized. Mice were permanently scored as "parasitemia confirmed" when parasites were first detected via blood smear. **(b)** Survival of the pre-immunized mice following challenge. Shaded areas represent sequential peaks of parasitemia.

3.5 The VSG3 *O*-glycan affects the binding of antibodies to the trypanosome surface

To directly examine the effect of the *O*-glycan chains on the properties of the host antibody response, we collected antisera elicited by $VSG3_{WT}$ or $VSG3_{S317A}$-coated parasites at day 8 post-infection, when the early IgM antibodies responsible for parasite clearance reach peak titers. We then performed flow cytometry analysis to assess antisera binding in the context of the intact parasite surface coat. In accordance with our *in vivo* results (Fig. 3.8), we found that $VSG3_{WT}$- elicited antisera exhibited markedly lower binding against cognate $VSG3_{WT}$ trypanosomes, as compared to $VSG3_{S317A}$-elicited antisera binding cognate $VSG3_{S317A}$

trypanosomes (Fig. 3.9a and b; additional statistical analyses of these data are described in section 3.5.1). These antibody binding data thus further support an immunomodulatory role for the VSG3 *O*-glycan chains.

Analyses of the cross-reactivities of these polyclonal antisera (Fig. 3.9a and b) did not suggest a simple mechanistic explanation as to how the heterogeneous VSG3 *O*-glycan chains cause elicitation of IgM responses that are poorly functional against cognate $VSG3_{WT}$ coats. Notably, however, the unusual pattern of $VSG3_{WT}$-elicited antisera binding $VSG3_{S317A}$ parasites better than cognate $VSG3_{WT}$ parasites was also recapitulated by our VSG3-specific monoclonal antibody. This IgG1 class antibody was also raised against $VSG3_{WT}$ but shows higher binding against $VSG3_{S317A}$ trypanosomes (Fig. 3.9c). Thus, the effect was reproducible among our three polyclonal antisera and can also be identified at the level of individual antibodies. Ultimately, the binding patterns as a whole must be dependent on the properties of individual antibodies comprising the polyclonal antisera, which cannot be predicted *a priori* (discussed in greater detail in section 4.5).

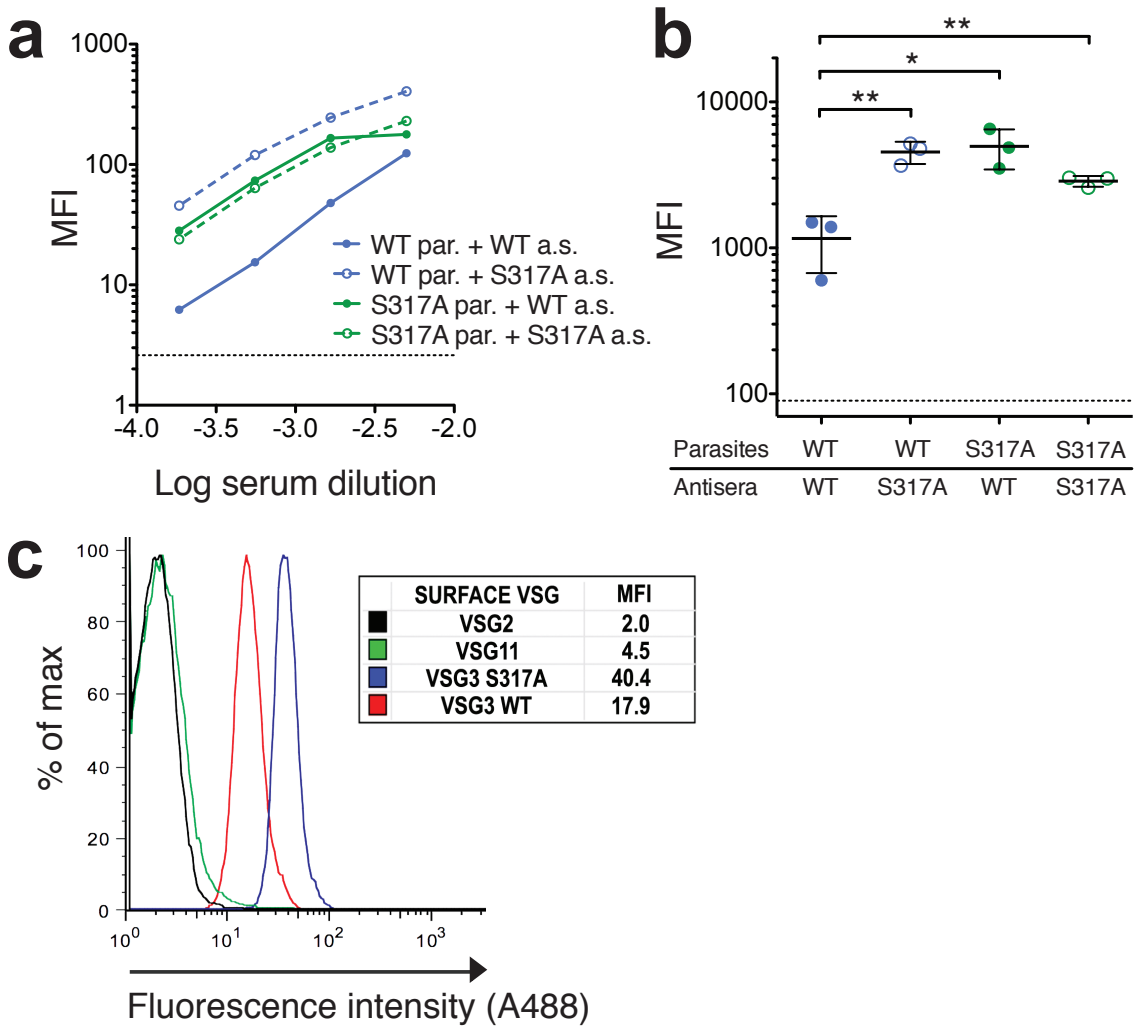

Figure 3.9. $VSG3_{WT}$-elicited antibodies bind cognate $VSG3_{WT}$ trypanosomes poorly.

(a) Comparison of $VSG3_{WT}$ or $VSG3_{S317A}$-elicited IgM antisera (a.s.) binding to live $VSG3_{WT}$ or $VSG3_{S317A}$-expressing parasites (par.). Binding was measured by the mean fluorescence intensity (MFI) of parasite samples stained with (1) dilutions of primary antisera and (2) FITC-labeled anti-mouse-IgM. Data are shown for one antiserum sample per VSG type. **(b)** Similar to (c) but with a single dilution (1:2000) of distinct antisera, elicited by infection of multiple mice (n = 3 independent antisera/VSG type). Statistical values were calculated by two-sided *t*-tests comparing the sets of three sample MFIs, assuming normal distribution (* $0.01 < p < 0.05$, ** $0.001 < p < 0.01$; bars show mean and SD). For (a) and (b), dotted lines represent background MFI. **(c)** Binding of an Alexa488-labeled monoclonal antibody raised against $VSG3_{WT}$ to trypanosomes expressing different VSGs. VSG2 is an unrelated class A VSG and VSG11 is a class B VSG that is also *O*-glycosylated (see Fig. 3.4)

3.5.1 Statistical analyses of VSG3$_{WT/S317A}$-elicited antisera binding data

The statistical analyses reported in Fig. 3.9b were performed by two-sided *t*-tests assuming normal distribution of MFI data. To deepen this analysis and account for possible deviation from normal distribution, I performed additional analyses of the underlying flow cytometry data using R and Prism software. Fig. 3.10a shows the means (MFI) and standard deviations (SD) of the flow cytometry data presented in Fig. 3.9b, as well as the MFI and SD of the same flow cytometry data combined by sample type (i.e. independent antiserum samples grouped). Because flow cytometry sample Ns are so large, a two-tailed *t*-test or non-parametric (Mann-Whitney) test of each individual sample compared to each other sample (and each group compared to each other group) yields a p value < 0.001 for every comparison. These p values signify real variation between samples, but do not inform the magnitude or relevance of these variations. Two comparisons offer a more meaningful interpretation: (1) The mean of each individual WT parasites + WT antiserum sample is at least one SD below the mean of each individual sample from all other groups, and (2) The mean of the combined WT parasites + WT antisera group is two SDs below the mean of each other group (calculated using the larger of the two SDs in each comparison). Therefore, the differences are not only statistically significant (p values), but the WT cells + WT antisera combination shows meaningfully lower IgM binding than all other combinations, based on the magnitude of the differences in sample means compared to the degree of variation within the data.

Fig. 1.10b shows the same data examined differently by regrouping sample MFIs and performing a nonparametric, two-tailed Mann-Whitney test of each group of 3 samples of the same type compared to the other 9 samples combined. Through this analysis, the WT cells + WT antisera combination is the only group that is significantly different from all of the others.

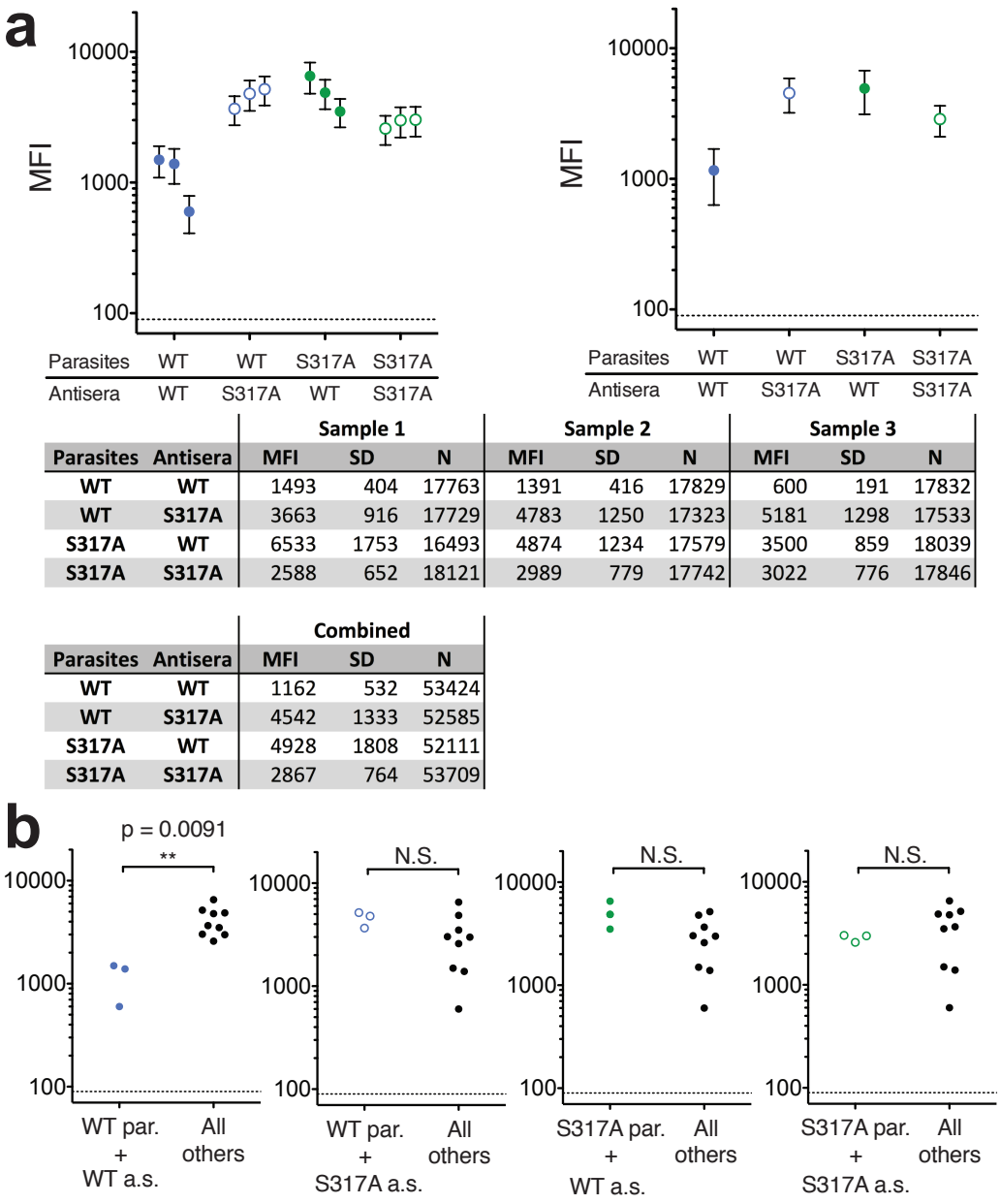

		Sample 1			Sample 2			Sample 3		
Parasites	**Antisera**	**MFI**	**SD**	**N**	**MFI**	**SD**	**N**	**MFI**	**SD**	**N**
WT	**WT**	1493	404	17763	1391	416	17829	600	191	17832
WT	**S317A**	3663	916	17729	4783	1250	17323	5181	1298	17533
S317A	**WT**	6533	1753	16493	4874	1234	17579	3500	859	18039
S317A	**S317A**	2588	652	18121	2989	779	17742	3022	776	17846

		Combined		
Parasites	**Antisera**	**MFI**	**SD**	**N**
WT	**WT**	1162	532	53424
WT	**S317A**	4542	1333	52585
S317A	**WT**	4928	1808	52111
S317A	**S317A**	2867	764	53709

Figure 3.10. Statistical analyses of VSG3 antibody binding data.

(Left) The mean (MFI) and standard deviation (SD; error bars) of the flow cytometry data shown in Fig. 4e (three independent antiserum samples per VSG type; one dilution (1:2000) of each). (Right) MFI and SD of the same flow cytometry data combined by sample type (i.e. independent antiserum samples grouped). These data are also shown below in tables, which include the number of cells analyzed (N) in each sample/group. **(f)** Two-tailed Mann-Whitney test of each group of 3 samples of the same type compared to the other 9 samples combined (par. = parasites, a.s. = antisera).

3.6 Discussion

Altogether, the glycan-dependent discrepancies observed in (1) parasite clearance following infection (Fig. 3.6), (2) generation of protective immunity from pre-immunization (Fig. 3.8), and (3) cognate antibody binding (Figs. 3.9 and 3.10) strongly indicate that the heterogeneous VSG3 *O*-glycan chains aid the parasite in evasion of the host's humoral immune response. VSG glycosylation thus appears to represent an additional *T. brucei* immune evasion strategy that overlaps with the broader strategy of antigenic variation. Further, the identification of analogous *O*-glycans in other VSGs provides evidence that this may be a widespread VSG modification, but additional research will be required to verify whether the *O*-glycans in these VSGs are also immunomodulatory.

Our data suggest that the greater virulence and heightened day 5 parasitemia levels of the $VSG3_{WT}$ trypanosomes in naïve mouse infections (Figs. 3.6 and 3.7) can be sufficiently accounted for by glycan-mediated impairment of the host antibody response. In particular, the marginal protection provided by $VSG3_{WT}$ pre-immunization (Fig 3.8) shows that $VSG3_{WT}$ trypanosome outgrowth is often poorly inhibited by host antibodies, and it follows that these parasites would be more capable of overwhelming the host. However, we have not disproven the possibility that the VSG3 *O*-glycan chains could also alter trypanosome-host interactions in other ways, such as affecting parasite localization or interactions with carbohydrate receptors on host cells. Thus, inhibition of antibody recognition might be the only role of the *O*-glycan in affecting parasite virulence, or it could be one of multiple roles.

Finally, the immune inhibitory effect of the VSG3 *O*-glycan is not entirely unexpected, as antigen glycosylation has been shown to inhibit immune recognition of other pathogens as well. Surface antigen glycosylation is a common immune evasion strategy in viruses, and studies have

demonstrated that these surface glycans can specifically inhibit antibody recognition and the development of protective antibody responses[185,186]. Such strategies are also used by bacterial pathogens. For example, *Neisseria meningitidis* glycosylates invariant peptidic regions of its type IV pili in order to avoid immune recognition[187].

3.7 Researcher contributions

VSG3 crystallization and structural analyses (section 3.1.1): Dragana Nešić and C. Erec Stebbins. Mass spectrometry analyses (sections 3.1.2 and 3.1.3): Liaqat Ali and Michael A. J. Ferguson. Structural prediction analyses (section 1.3.3): Francisco Aresta-Branco and C. Erec Stebbins. VSG purification (section 3.1): Jason Pinger, Dragana Nešić, Francisco Aresta-Branco, and F. Nina Papavasiliou. $VSG3_{WT/S317A}$ knock-in vector cloning and transfections (section 3.2): Jason Pinger, Hee-Sook Kim, and Shanin Chowdhury. Naïve mouse infections (section 3.3): Jason Pinger, Shanin Chowdhury, and F. Nina Papavasiliou. Trypanosome growth assays (section 3.3): Jason Pinger and Francisco Aresta-Branco. Pre-immunized mouse infections (section 3.4): Jason Pinger, Francisco Aresta-Branco, and Shanin Chowdhury. Antibody binding analyses (section 3.5): Jason Pinger, Shanin Chowdhury, and F. Nina Papavasiliou. Antibody binding statistical analyses (section 3.5.1): Jason Pinger. Conceived and designed the experiments (all sections): Jason Pinger, Dragana Nešić, C. Erec Stebbins, Liaqat Ali, Michael A. J. Ferguson, and F. Nina Papavasiliou.

Chapter 4

Discussion

4.1 The influence of the VSG coat replacement immune evasion threshold on parasitemia dynamics and VSG diversity during infection

In Chapter 2, I demonstrate that trypanosomes require ~4.5 days to fully replace their VSG coats following a genetic *VSG* switch, and that these cells are only vulnerable to clearance by early IgM antibodies for, at most, the initial ~29 hours of that period. To fully evaluate the impact of these results in the context of an infection, we must also consider the timing of the genetic switch in relation to the establishment of the immune response. It remains unclear whether regulation of *VSG* switching is purely stochastic or whether environmental stimuli affect switching frequency, but the fact that switching occurs *in vitro* suggests that there is at least some host-independent, stochastic element to the process[118,119]. Analyses of infection dynamics indicate that early VSG-specific IgMs only reach titers capable of clearing non-switched trypanosomes 5-6 days after the initial stimulus[40]. Trypanosomes switching very early in infection or near the beginning of waves of parasitemia may therefore fully replace their VSG coats before the IgM response becomes effective, so it is possible that infections could persist even if trypanosomes remained vulnerable for longer portions of the coat replacement process.

However, the limited vulnerability window I have described certainly does impact the character of each successive wave of parasitemia. The total number of trypanosomes present within an infected host exponentially increases as a wave of parasitemia reaches its peak. Whether or not *VSG* switching is purely stochastic, the absolute number of independent switch events must also accumulate accordingly nearer to the peak. If all of the parasites that switch up to 29 hours before a parasitemia peak are able to survive (as opposed to only those that switch

several days before the peak), this would imply a significantly greater number of switched cells forming the subsequent wave of parasitemia.

A larger population of surviving switched cells would affect more than just the initial level of parasitemia in the subsequent peak. The likelihood that any particular new *VSG* gene will be expressed following a genetic switch is probabilistically determined[41] (section 1.7.6). Consequently, a greater number of switched cells would also produce a greater diversity of VSGs expressed amongst those cells. A recent study conducted by our group demonstrated that VSG expression is highly diverse within individual waves of parasitemia, and that some major variants comprise large portions of the population, while some minor variants appear only transiently[37]. It is possible that high VSG diversity is necessary for selection of the few variants that will be successful in a given host environment or a given immune environment, particularly for sustaining long-term infection. The narrow post-switch vulnerability window I describe in Chapter 2 is not the only mechanism affecting VSG diversity, but it may prove to be an important contributing factor. Ultimately, the question of whether a more stringent immune evasion threshold would permit (or disallow) sustained infections cannot be answered with certainty.

4.2 Antigen density and IgM functionality

In addition to addressing a gap in our understanding of *T. brucei* pathogenesis, the work presented in Chapter 2 may hold broader relevance to the basic biology of IgM. It has been known for many years that IgM binding is generally dependent on polyvalent interactions (i.e. avidity) and is therefore sensitive to antigen density[178]. However this is the first study, to my knowledge, in which antigen has been titrated on the surface of a pathogen, and a relatively sharp, density-dependent cutoff of IgM functionality has been established *in vivo*. It is striking that IgM

can shift from providing strong protection to providing no discernible protection against a pathogen following only a ~6-fold reduction in cognate antigen density (7.6%/1.3%; clones DE-7.6 and DE-1.3; Fig. 2.11), particularly when the antigen is still highly abundant on the cell surface at the lower density (~130,000 copies/cell). Further examination of intermediate DE-clones between DE-7.6 and DE-1.3 could help in determining more precisely where the IgM functionality threshold lies, and how sharp of a cutoff it is.

IgM plays an important protective role in a number of other immune interactions as well. Both induced IgM responses and natural IgMs (non-mutated IgMs constitutively produced in the absence of immune stimulation) form a crucial first line of defense against many pathogens in addition to *T. brucei*[188-190]. Further, although IgM responses are commonly considered to offer only transient, early immunity against pathogens, they have also been shown to provide long-term protection in the form of persistent antibody titers[191], or rapid antibody production following restimulation of IgM memory B cells[190,192]. In cancer immunology, circulating natural IgM antibodies are known to constitute an innate-like surveillance mechanism. These antibodies can recognize tumor-specific carbohydrate epitopes on aberrantly glycosylated cell surface antigens and mediate tumor cell death[193,194]. Lastly, IgM antibodies that recognize autoantigens have been shown to actually promote tolerance and protect against inflammatory and autoimmune disease, although the mechanisms underlying these effects are not completely understood[195]. Remyelination-promoting self-reactive IgM antibodies have even entered clinical trials for multiple sclerosis treatment[196]. I propose that each of these IgM interactions is likely to be sensitive to antigen density (potentially excepting occasions where an IgM has undergone affinity maturation or a germline IgM has unusually high affinity for its cognate antigen). My results in Chapter 2 suggest that a critical antigen density threshold exists for *in vivo* IgM

functionality, at least in some cases. The possibility of such an effect should be considered for other IgM-related studies, particularly in cases where IgM might be used as a therapeutic, or where relevant antigens might vary in density (e.g. between patients; between cell types; or on a pathogen surface, as in *T. brucei*).

4.3 The functional attributes of individual VSGs

In Chapter 3, I describe our discovery of a new form of VSG post-translational modification (PTM), *O*-linked glycosylation, which can impair the host's ability to generate a protective antibody response against the modified VSG. The identification of analogous glycans in other VSGs suggests that this may be a shared trait among many VSGs, and may therefore have a significant impact during *T. brucei* infections. Perhaps more intriguingly, this discovery highlights a gap in our current knowledge of the diverse functional attributes of individual VSGs. While *O*-glycosylation appears to be somewhat widespread among VSGs, it is still worth noting that the first distinct type of VSG we chose to characterize contained a novel feature. We may have been fortunate in our choice, but it is also possible that many VSGs include biochemical features that have yet to be discovered. There are a wide array of possible PTMs, any of which could affect the antigenicity of individual VSGs displaying them. Indeed, additional types of PTMs are known to affect antibody recognition of antigens displayed by other pathogens. Methylation of the *Leptospira interrogans* antigen LipL32 has been shown to potently reduce the reactivity of antisera derived from *L. interrogans*-infected patients[197], and variable phosphocholine and phosphoethanolamine modifications can alter the antigenicity of the *Neisseria gonorrhoeae* type IV pilus structure[198]. For *T. brucei*, it is worth considering that some VSG PTMs could also have the opposite effect of reducing antigenic variability. Antibodies raised against a PTM on one VSG could recognize the same PTM on a different VSG, although

such antibodies may or may not provide protective immunity. In any case, the results of our analyses of the VSG3 *O*-glycan demonstrate that VSG PTMs can constitute critical antigenic determinants, and are worthy of further study.

Individual VSGs may also display distinct functional qualities unrelated to their antigenicity. It has been known for decades that *SRA*, the *T. brucei rhodesiense* gene that enables parasite evasion of the primate innate immune factors TLF1 and TLF2, encodes a VSG-like protein[199]. Much more recently, a VSG was identified that is able to confer resistance to the trypanocidal drug suramin, but only while the trypanosomes are actively expressing the VSG[200]. VSGs are not generally assumed to have a function beyond shielding the parasite from antibody pressure. However, with such a vast range of *VSG* genes that are constantly recombining by mosaic formation[120], it is perhaps probable that individual VSGs may on occasion develop functional attributes that are then selected for and improved by evolution. The different advantageous functions these VSGs could serve are innumerable: they could affect nutrient uptake, interactions with host cells (immune or otherwise) or other trypanosomes, parasite propensity to cross the blood brain barrier, parasite localization within host tissues, etc. Some other pathogens also display variant surface antigens that serve functional roles in addition to aiding immune evasion. In malaria, members of the PfEMP1 variant antigen family (proteins exported to the membrane of erythrocytes infected with *Plasmodium falciparum*) are known to mediate adhesion to the endothelial lining of blood vessels and direct tropism to different vascular regions[201]. Bacteria of the genus *Borrelia* (including the causative agents of Lyme disease and tick-borne relapsing fever) also express variant antigens that influence tissue tropism and patterns of pathogenesis[202]. In *T. brucei,* the discovery and characterization of specialized

functions of individual VSGs represents a virtually unexplored, and potentially fruitful research avenue.

It is unclear to what extent VSG proteins might display unique biochemical properties or perform specialized functions. The number of VSGs with solved, high-resolution N-terminal crystal structures remains very small (four in total, counting VSG3 described here). Increasing efforts to biochemically characterize or solve the structures of additional VSGs would help in determining the full diversities of VSG structural features and PTMs. One screening method to identify VSGs of interest could be to incubate diverse trypanosome populations with antibodies, lectins, or other agents that specifically recognize known PTMs, and isolate trypanosomes expressing these modifications via flow cytometry sorting (FACS) or immunoprecipitation. Of course, this method would only be feasible for those modifications for which such reagents were available. With regard to discovering novel VSG functions, specific traits would likely have to be screened individually. For example, sequencing the VSGs present in trypanosomes extracted from different mouse tissues could indicate whether any VSGs are enriched in a certain area, potentially providing evidence of VSG-based parasite tropism. Altogether, determining the true extent of functional and biochemical variability between VSGs would be a worthwhile endeavor to improve our understanding of *T. brucei* antigenic diversity and disease pathogenesis, with potential implications for other pathogens as well.

4.4 VSG cross-reactivity and antigenic diversity in sustained infections

While high diversity in VSG expression may be advantageous for ensuring selection of a VSG appropriate for a given environment, it also exposes the VSG repertoire to the host immune system more rapidly, which could exhaust the total antigenic diversity available to the parasite. However, several pieces of evidence suggest that exhaustion of the VSG repertoire may not pose

a significant constraint on long-term trypanosome infections. First, the basic fact that VSG expression *is* highly diverse during infection[37] indicates that infections can persist with a high rate of exposure of distinct VSGs. Secondly, *T. brucei gambiense* infections in humans and other African trypanosome infections in animals can persist up to several years before death of the host[1,2]. This suggests that (1) trypanosomes are capable of continually developing sufficient antigenic diversity over extremely long periods (via mosaic VSG formation), or (2) the immunosuppressive methods trypanosomes employ make sustained antigenic diversity less important, or even unnecessary. The full long-term immune evasion mechanism almost certainly relies on both of these factors, but the relative importance of each factor at different stages of infection remains unclear.

Examination of antisera cross-reactivity patterns between VSGs may provide insight into the extent of VSG diversity required to continually evade the host antibody response. One way to explore this (similar to my proposal for identifying PTMs above) would be to (1) raise polyclonal antisera against multiple VSGs, (2) incubate the individual antisera with trypanosome populations expressing many VSGs, (3) isolate the bound trypanosomes by FACS or immunoprecipitation, and (4) sequence the isolated parasites to determine what features were shared between cross-reactive VSGs. Such analyses should take into account the possibility that homologous VSG regions could be antigenically distinct due to variable PTMs, and shared PTMs could lead to cross-reactivity between otherwise dissimilar VSGs. Mosaic VSGs are particularly intriguing with regard to cross-reactivity. These VSGs are created by segmental gene conversion events that accumulate donor VSG segments over time, and some related mosaic VSGs containing homologous regions are antigenically distinct[120] (see section 1.7.4). Cross-reactivity between related mosaic VSGs could also be examined by the method described above

or by similar methods. If these types of analyses were combined with structural information, they could also provide direct insight into which VSG regions were accessible to or commonly targeted by host antibodies.

A number of observations suggest that *T. brucei* interactions with host immunity change significantly in late stages of infection. As infection progresses, depletion of various B cell populations occurs[156,158,160], and after several weeks, infected mice display poor stimulation of secondary (memory) antibody responses and poor control of infectious agents that they have previously developed immunity against[159,160] (discussed in section 1.8.4). Further, while periodic waves of parasitemia are hallmarks of early *T. brucei* infection (due to cycles of successive antibody responses and parasite clearance), this distinct periodicity often breaks down at late stages, suggesting that parasite-antibody interactions are qualitatively different at these time points[37,41]. Examination of VSG expression in late stages of infection has shown that although populations expressing a given VSGs can persist for longer periods, they are often still cleared at some point[37]. This pattern indicates that VSG-specific antibody responses can still be generated late in infection, albeit less rapidly and perhaps less comprehensively. Thus, immune suppression alone may not be sufficient to ensure escape from antibody pressure, and the parasite may require continuous antigenic variation even at late stages. One way to examine this could be to challenge mice late in infection with pleomorphic trypanosome strains that are incapable of switching their VSG coat (e.g. by expressing a VSG at an ectopic location). If these parasites were able to persist for long periods, it would provide evidence that antigenic variation is not required at late infection stages. However, the tools to perform the necessary genetic manipulations of pleomorphic strains do not exist at present, and the high virulence of genetically tractable monomorphic strains would limit their utility for this purpose.

4.5 Mechanism of VSG3 *O*-glycan-mediated impairment of the antibody response

The binding properties of $VSG3_{WT}$- and $VSG3_{S317A}$-elicited antisera (referred to in this section as WT and S317A antisera, respectively) against $VSG3_{WT}$- and $VSG3_{S317A}$-expressing trypanosomes (WT and S317A parasites, respectively) suggest a complicated mechanism for the immunomodulatory effect of the *O*-glycan chains. The fact that WT antisera bind S317A parasites well weakens the explanation that the *O*-glycan simply causes elicitation of antibodies that are poorly functional. In the reverse combination, the strong binding of S317A antisera against WT parasites indicates that the *O*-glycan is not broadly able to inhibit antibody binding. These data therefore suggest that the poor binding of the WT/WT parasite/antisera combination may result from a combined effect of the *O*-glycan at both the antibody elicitation stage and in the subsequent antibody-parasite interactions.

It is important to discuss the potential effects of *O*-glycosylation on the epitope repertoire of VSG3. The most intuitive scenario is one where the glycan simply occludes an epitope in $VSG3_{WT}$ that is then exposed when the glycan is removed in $VSG3_{S317A}$. However, the full effects of the glycan may vary considerably depending the precise binding specificity of a given antibody as well as the interactions of the glycan with surrounding peptidic regions of VSG3 itself. This is succinctly summarized in an excerpt from a review by Lisowska (2002):

> *"Glycoproteins may elicit antibodies against defined carbohydrate structures, which are recognized irrespective of their carrier protein or in the context of their location in the antigen polypeptide chain. Moreover, N- and O-glycans frequently modulate the activity of adjacent peptidic epitopes due to intramolecular carbohydrate-protein interactions [...] The presence of glycan(s) may not only enhance or decrease the reactivity of the peptidic epitope (quantitative change),*

but may also form a neoepitope or abolish the reaction (qualitative effect). There are no distinct rules as to which monosaccharide components of N- or O-glycans are most important for these effects… various components or fragments of the oligosaccharide chain may exert different (sometimes opposite) effects."[203]

In other words, glycans can create a set of epitopes that are distinct from those presented by the aglycosylated protein, and these altered epitopes may not necessarily contain the glycan itself. Subsequently, a given antibody raised against a glycoprotein may have unaffected, increased, or decreased binding affinity based on (1) the presence or absence of the glycan, (2) the length and composition of the glycan chain, and (3) the allosteric effect of the glycan on the structural conformation of the surrounding peptide regions (which may also vary based on the length and composition of the glycan chain). The impact of differential glycosylation can vary dramatically and unpredictably for individual antibodies. One recent study, which examined the binding patterns of a set of monoclonal antibodies against variably glycosylated peptides of the protein MUC1, provides examples of such effects[204].

In the case of VSG3, our data suggest that *O*-linked glycosylation produces, minimally, four antigenically variable entities on the trypanosome surface: VSG3 can be decorated with 0, 1, 2 or 3 hexose units linked to S317 (at an estimated ratio of 8%, 33%, 37%, and 22%, respectively). We have also found that these hexoses, though anchored to the VSG by an *O*-linked glucose, may contain both glucose and mannose moieties (with the exact percentages of each and linkages still under investigation). Such alternative stereochemistries of glycans have also been shown to alter their protein binding properties[205]. Additionally, IgM antibodies (the Ig class of relevance to these studies), are particularly sensitive to epitope density (see Chapter 2). The presence of various glycoforms on a $VSG3_{WT}$ coat could reduce the effective densities of

any epitopes altered by glycosylation, while a $VSG3_{S317A}$ coat would be comparatively homogenous and potentially more amenable to binding for IgMs with certain specificities.

Overall, the effects of glycosylation make $VSG3_{WT}$ more antigenically diverse than $VSG3_{S317A}$. Non-O-glycosylated VSG3 possesses only one set of epitopes. Mono-, di-, and tri-glycosylated VSG3 each possess a partially altered set, with each additional sugar group varying the peptide and glycan epitopes presented to an unknown degree. This variability could affect both the comparative immunodominance of epitopes in antibody elicitation and individual antibody binding patterns against the varied epitopes (i.e. antibodies may effectively bind some glycoforms but not others). Bearing these uncertainties in mind, there may be highly antigenic peptidic epitopes presented in the WT parasites that are still presented to a lesser degree in the WT (e.g. only in certain glycoforms) than in the S317A parasites. The properties of our VSG3-specific monoclonal antibody provide evidence for such a scenario, as this antibody was raised against WT parasites and appears to recognize a peptidic epitope common to $VSG3_{WT}$ and $VSG3_{S317A}$, but binds S317A parasites more strongly (Fig. 3.9c).

Ultimately, it is not possible to predict, *a priori*, the prevalence of elicited antibodies in our antisera with given binding epitopes, glycoform specificities, and affinities, but these are the factors that underlie our binding results in aggregate. The determination of a detailed mechanism for the data we observe would therefore require additional research, most likely including the cloning of individual IgM antibodies elicited against $VSG3_{WT}$ and $VSG3_{S317A}$ and comparing their binding patterns against individual intact VSG3 glycoforms, or possibly VSG3 peptide glycoforms.

Chapter 5

Methods

5.1 Trypanosome cell lines

All trypanosome cell lines were bloodstream-form trypanosomes ultimately derived from the *Lister427* "single marker" (SM) cell line[167]. Trypanosomes were cultivated in HMI-9 medium with 10% fetal bovine serum (Sigma F4135) at 37°C and 5% CO_2. "WT-VSG2" trypanosomes are unaltered SM cells. Derivation of the Δ70 clone has been described previously[43]. The WT-VSG3 clone used in Chapter 2 was isolated from a group of switched cells from the 70.II line published by Hovel-Miner et al.[43]. In this clone, *VSG3* is the active *VSG* gene expressed from Bloodstream Expression Site 1 (BES1). The Δ70 and WT-VSG3 clones were provided by Dr. Galadriel Hovel-Miner (current address: George Washington University). VSG2-expressing trypanosomes lacking GPI-PLC (*GPI-PLC*$^{-/-}$)[84] were provided by Dr. George Cross (Rockefeller University). Methods of generating the additional transgenic cell lines used in this thesis are described in individual sections below.

5.2 Monoclonal anti-VSG antibodies

The monoclonal anti-VSG antibodies used in these studies were produced by the Antibody and Bioresource Core Facility of the Memorial Sloan Kettering Cancer Center. The anti-VSG2 antibody is clone VSG221-31G9, while the anti-VSG3 antibody is clone VSG224-11D6 (both publicly available [http://macfwebext.mskcc.org/EstablishedMAb/SearchEstablishedMAbs.aspx]). Only these two clones were used, but experiments were performed using individually prepared antibody-fluorophore conjugates (the fluorophore conjugates used in each experiment are indicated in

methods and figure legends). These antibody-fluorophore conjugates were generated using purified antibody and Invitrogen protein labeling kits, following manufacturer instructions (Alexa647 A20173; Alexa488 A10235; Pacific Blue P30012; FITC F10240).

5.3 Engineering sortaggable VSG2 (VSG2^{STa}) and VSG2^{STa} knock-in clones

The amino acid sequence GGGENLYFQGGGGGG was cloned into VSG2 (GenBank X56762) replacing residues E29-G31[165]. This segment immediately follows two Ala residues which form the N terminus of the mature VSG2 protein after the preceding leader peptide sequence is removed[163] (thus the mature VSG2^{STa} protein begins AAGGGENLYFQGGGGGGFKQAFWQPLCQVS-, insertion underlined). The original plasmid construct for VSG2^{STa} knock-in, pSY37F1D-CTR (derived from pSY37[206], a gift of Dr. Hee-sook Kim; current address: Cleveland State University), contains in order: 1156bp of the "cotransposed region" (CTR) preceding the VSG2 open reading frame in BES1 of the *Lister427* genome, immediately followed by the previously described *VSG2^{STa}* gene, then a Hygromycin resistance gene (HYG), and finally a 200bp telomere seed region. A BglII restriction site was used to linearize the plasmid, leaving the CTR and telomere seed on opposing ends of the resulting DNA fragment. This fragment was then used for transfection of WT-VSG2 (SM) cells via the Amaxa nucleofector protocol as previously described[207], resulting in clone KI-VSG2^{STa}. To knock *VSG2^{STa}* into Δ70 cells (which are already hygromycin resistant), a new plasmid construct (pSY37F1D-CTR-BSD) was created by introducing a blasticidin resistance gene (BSD) in place of HYG. Plasmid linearization and transfection were performed as above, resulting in clone Δ70^{STa}. In both cases, the transfection replaces the previously active *VSG2* gene, such that KI-VSG2^{STa} and Δ70^{STa} express only VSG2^{STa}.

5.4 Sortase A purification

Plasmid containing the *S. pyogenes*-derived sortase A expression construct (pSpSortA-pET28a[208], a gift of Dr. Assaf Raz, Rockefeller University) was transformed into BL21 DE3 cells (Life Technologies C6000-03). Colonies from this transformation were used to inoculate large cultures of LB media (VWR 1.10285.0500) and grown shaking at 37°C to an optical density (OD_{600}) of 0.4 - 0.8. Cultures were then induced with 1mm IPTG, grown an additional 3-4hr, and harvested by centrifugation. Cell pellets were resuspended in TBS/imidazole (20mM Tris, 150mM NaCl, 20mM imidazole), and lysed using an EmulsiFlex-C5 homogenizer (Avestin). DNAse-A powder (Sigma D5025) and 5mM BME were added to the lysate, and it was centrifuged to remove particulate. The supernatant was poured over a column of Ni chelating beads (Qiagen D-40724) which had been equilibrated with wash buffer (20mM Tris, 300mM Nacl, 20mM imidazole, 5mM BME). The column was washed with 100ml wash buffer and eluted with 30-35ml elution buffer (20mM Tris, 300mM NaCl, 200mM imidazole, 5mM BME). Samples containing protein were pooled and dialyzed in (20mM Tris, 150mM NaCl, 1mM DTT). The resulting sample was concentrated using a centrifugal filter unit (Amicon Ultra – 10,000 NMWL, Millipore), aliquoted, and frozen for future use.

5.5 Sortagging reaction

FITC (5-FAM; 5-carboxyfluorescein), nitrophenol (NP) and TAMRA-peptide conjugates ([FITC]/[NP]/[TAMRA]-GGGS<u>LPSTG</u>G**,** sortase recognition motif underlined) were synthesized by Elim Biopharmaceuticals. Sortagging solutions containing 100uM purified Sortase A and 300-600uM peptide conjugate [Concentration varied between experiments of different types, but was consistent for replicates of the same experiment] in HMI-9 media were incubated on ice for 30-60min. Trypanosomes expressing $VSG2^{STa}$ were pelleted, resuspended in

the sortagging solution, and incubated for 1 hr at 4°C on an inversion rotator. Cells were then pelleted, washed once with HMI-9 media, and pelleted again before final resuspension in HMI-9. These cells were then analyzed immediately or returned to normal culture conditions. For Fig. 2.2, ectopic expression of $VSG2^{STa}$ was induced by adding 100 ng/ml Dox to culture media 24 hrs before isolating cells for sortagging reaction. For Fig. 2.4a, NP-tagging of trypanosomes was visualized after staining with Alexa647-labeled anti-NP antibody (Genway Biotech GWB-4C4D87). For Fig. 2.5b, Sortagged KI-$VSG2^{STa}$ cells were cultured for 12 hrs prior to imaging. Imaging was performed using an ImageStream-X flow cytometer (Amnis). For Fig. 2.5c, sortagged KI-$VSG2^{STa}$ cells were isolated from culture at indicated time points and analyzed via BD-FACSCalibur flow cytometer.

5.6 Southern blot

Trypanosome Genomic DNA was isolated using DNAzol (Invitrogen 10503-027) following manufacturer protocol, and 10 ug of this DNA was digested overnight with 200 U SmaI restriction enzyme. Digested DNA was extracted by phenol/chloroform using MaXtract Low Density columns (Qiagen). This DNA was then run on a 0.8% TAE agarose gel for 12 h at 50V. DNA was denatured and transferred to Amersham Hybond-N+ membrane (GE Scientific) by capillary blotting according to manufacturer instructions, and UV-crosslinked using a FB-UVXL-1000 UV crosslinker (Fisher Scientific). *VSG2* ^{32}P-radiolabeled probe was produced by PCR amplification using the Prime-It II Random Labeling Kit (Stratagene). Blot was hybridized, washed, and visualized using a phosphoroimaging apparatus and Typhoon Scanner (GE Healthcare).

5.7 Trypanosome clone growth rate analyses

Trypanosomes were diluted to 10^5 cells/ml in culture. Cell concentration was analyzed every 24 hours, and cultures were diluted back to 10^5 cells/ml immediately after measuring concentration. Total cell number was calculated by multiplying the concentration each day by the dilution factors of each previous day.

5.8 Conversion of MFI values to MESF values

Quantum FITC and Alexa647 MESF bead kits (Bangs Laboratories cat. 555 and 647) were used to convert sortag (FITC) or anti-VSG2-antibody stain (Alexa647 conjugate,1:2000 dilution) raw mean fluorescence intensity (MFI) values to absolute Molecules of Equivalent Soluble Fluorochrome (MESF) units[172] per manufacturer instructions. For each fluorophore, a set of Quantum beads were run on the flow cytometer immediately prior to trypanosome sample acquisition, using identical settings. These bead sets consisted of 5 or 6 samples of beads, each of which were conjugated to a known amount of fluorophore. Bead MFI values were then entered into Bangs Laboratories software provided with the kits, which generated a calibration curve for converting MFI of other samples to MESF units. MFI values from trypanosome samples were then entered into this same software to obtain absolute MESF values.

5.9 VSG coat replacement: visualization and rate calculation

5.9.1 Switch induction for Δ70 and $\Delta 70^{STa}$ cell lines

$\Delta 70$ or $\Delta 70^{STa}$ trypanosomes were diluted to 10^5 cells/ml in culture flasks containing HMI-9 with 1ug/ml Doxycycline (Dox), then incubated in normal culture conditions for 6 hrs. At 6 hrs, cells were pelleted, washed with Dox-free HMI-9, then resuspended in Dox-free HMI-9 and incubated again in normal culture conditions. Non-induced cells were treated identically, except without

Dox in the initial 6 hr incubation. For sortagging/switching experiments (Fig. 2.6), $\Delta 70^{STa}$ cells were sortagged as described in section 5.5 (using 600uM 5-FAM-peptide) immediately prior to switch induction.

5.9.2 Flow cytometry sample preparation

All of the following samples, solutions, and incubation steps were at 4°C or on ice to prohibit antibody internalization during sample preparation. Samples of 2 x 10^6 trypanosomes were isolated from induced or non-induced cultures, pelleted, and resuspended in HMI-9 containing monoclonal antibodies recognizing VSG2 (the pre-switch VSG, antibody was anti-VSG2-Alexa647 [1:2000 dilution]) and VSG3 (one of many post-switch VSGs, antibodies were anti-VSG3-Alexa488 [1:400 dilution] or anti-VSG3-Pacific Blue [1:100 dilution]). Samples were incubated on an inversion rotator for 10 min, then pelleted and washed once with HMI-9. Samples were then pelleted again, resuspended in HMI-9 containing 500ng/ml Propidium Iodide (BD 556463), and analyzed using a BD-FACSCalibur (Fig. 2.1) or BD-LSRII (Fig. 2.6) flow cytometer. Single-stain samples for flow cytometry compensation were prepared identically using the same antibody and Propidium Iodide concentrations, CFSE staining, or sortagging procedures.

5.9.3 VSG $t_{EI/2}$ calculations

Flow cytometry data was analyzed using FlowJo software. Trypanosome populations were gated via forward and side scatter, then dead cells were excluded by gating cells negative for Propidium Iodide staining. $t_{E1/2}$ values were calculated from data from the 12 hr post-induction time point onward, because the presence of cells expressing switched VSGs (see VSG3-positive cells in Fig. 2.1c) indicated that the genetic VSG switch had occurred by this point, and thus

VSG coat replacement was actively taking place. “Switcher” populations were gated from “non-switcher” populations by anti-VSG2 antibody staining (Alexa647 conjugate,1:2000 dilution; see Fig. 2.6a) for 24 hr – 48 hr time points. For the 12 hr time point, the switcher and non-switcher populations were not gated separately, because at this early stage the switchers had not lost enough VSG221 to be identified as distinct from the non-switchers. MFI values from switcher and non-switcher populations were converted into MESF units as described in section 5.8, and $t_{E1/2}$ values were calculated via non-linear regression analysis using Prism software.

5.10 CFSE cell proliferation analysis

Immediately following sortagging reaction (section 5.5), trypanosomes were pelleted and resuspended in CFSE buffer (PBS, 0.1% BSA, 154mM Glucose), then added to solutions containing CFSE buffer with 800nM (final concentration) CFSE (Invitrogen C34554). Samples were incubated for 15 min at 37°C, then the reaction was quenched by adding the entire volume to 5x volume of HMI-9 and incubating for 5 min at room temperature. Cells were pelleted and washed once with HMI-9, then induced to switch (section 5.9.1) or returned to normal culture conditions. Sample collection and preparation, and flow cytometry gating were performed as described above.

5.11 Generation and characterization of DE clones

5.11.1 Construct cloning and transfection

Simultaneous expression of two *VSGs* from the active Bloodstream Expression Site (BES) has been described previously[175]. For my constructs, a ~1kb stretch of unique intergenic region (UIR) from *Lister427* BES1 was amplified from WT-VSG2 genomic DNA (gDNA) using primers JPC1_UniqueFor and JPC2_UniqueRev, while a pUC19 backbone was amplified using

primers JPC3_pUC19For and JPC4_pUC19Rev (see section 5.20 for primer sequences). These PCR fragments were digested with XhoI and BglII and ligated to create plasmid pJP01. The UIR contains a BsaAI blunt end restriction site near the center of the region that was used for subsequent cloning steps. pJP01 also contains NotI restriction sites flanking the UIR, which allow release of this fragment.

For each DE clone construct, the *VSG2* gene, its flanking UTRs, and a BSD resistance cassette were cloned into the pJP01 vector (cut at the BsaAI site in the center of the UIR) by Gibson assembly (cloning kit: NEB E5510S) using PCR fragments with 30bp of overlapping homology at the junctions. The resulting plasmids were digested with NotI and transfected into parental clone WT-VSG3 via the Amaxa nucleofector protocol as previously described[207]. Cloning details for each specific clone are described in the next section, and primer sequences are shown in section 5.20.

5.11.2 Cloning details

1) Clone DE-1.3 (plasmid pJP04):

The modified procyclin (Procyclin (mod)) 5'UTR was based on the pNS10/54 5'UTR published by Siegel et al.[173]. It was created by assembly PCR using overlapping oligos, followed by insertion into a pGEM backbone. The full Procyclin (mod) sequence is shown below. This 5'UTR was amplified with primers JPC18_GibsonP2For and JPC19_GibsonP2Rev. The VSG2 sequence was amplified from pSY37*[206] with primers JP09_VSG221_For and JPC24_GibsonP3221UTR_Rev. The BSD cassette (*BSD* gene with surrounding actin 5' and 3'UTRs) was amplified from pHJ37-BSD (derivative of pHJ37*, unpublished) with primers JP11_ACT5UTRStart_For and JPC22_GibsonP5Rev.

2) Clone DE-7.6 (plasmid pJP05):

VSG2 with its 5' and 3' UTRs was amplified from pSY37* with primers JPC26_GibsonP3221UTR_For and JPC24_GibsonP3221UTR_Rev. The BSD cassette was amplified as in clone DE-1.3.

3) Clone DE-11 (plasmid pJP07):

The Aldolase 5'UTR was amplified from pSY37* with primers JPC31_JP07P2_For and JPC32_JP07P2_Rev. VSG2 was also amplified from pSY37 with primers JP09_VSG221_For and JPC20_GibsonP3Rev. The Aldolase 3'UTR was amplified from pLEW100*[167] with primers JP10_Ald3UTR_For and JPC21_GibsonP4Rev. The BSD cassete was amplified as in clones DE-1.3 and DE-7.6.

*These plasmids were provided by Dr. Hee-sook Kim (current address: Cleveland State University)

5.11.3 Analysis of VSG surface expression levels

VSG2 and VSG3 surface expression were measured by quantitative flow cytometry analysis. Flow cytometry samples were prepared as described in section 5.9.2, with the following exceptions: Samples for Fig. 2.9b and c were prepared using single anti-VSG3 antibody solutions diluted as indicated. For Fig. 2.8b and Fig. 2.9a, samples contained 3 x 10^4 cells of the indicated clone, pelleted along with 10^6 WT-VSG3 cells. This permitted use of a saturating anti-VSG2-Alexa647 antibody concentration (1:100 dilution, see Supplementary Fig. 2a), because fewer VSG2-expressing cells were present to draw antibody out of solution. The additional WT-VSG3 cells allowed effective pelleting of such small samples of the VSG2-expressing clones.

Saturating levels of anti-VSG2-Alexa647 antibody were necessary to ensure that limiting antibody concentration did not skew relative surface VSG2 expression measurements.

For Fig. 2.9b, Conversion to MESF units was performed as described in section 5.8 to convert raw fluorescence intensity data to absolute values. The background MESF value (from cells with no antibody staining) was subtracted from the sample MESF values to generate "$MESF_{-BG}$" values. VSG percentages were calculated as the DE clone $MESF_{-BG}$ divided by the WT-VSG2 $MESF_{-BG}$. MESF calculation was not performed for Fig. 2c, because relative staining levels were sufficient to assess VSG2 expression stability over time. All samples for Figs. 2.8 and 2.9 were analyzed using a BD-LSRII flow cytometer. For data analysis (using FlowJo software), trypanosome populations were gated via forward and side scatter, then dead cells were excluded by gating cells negative for Propidium Iodide staining.

5.12 Generation of isogenic $VSG3_{WT}$ and $VSG3_{S317A}$-expressing clone sets

The wild type *VSG3* and *VSG3-S371A* point mutant genes were transfected into trypanosomes by means of the pSY37F1D-CTR-BSD vector[209] described in Chapter 2. This vector contains a blasticidin-resistance gene (BSD) cassette and allows a "knock-in" transfection in which the *VSG* gene included in the vector replaces the endogenous *VSG2* gene in the telomeric Bloodstream-form Expression Site 1 (BES1) of the *Lister427* genome (see diagram, Fig. 3.5).

5.12.1 Plasmid cloning

Plasmid cloning was performed as follows: first, the wild type *VSG3* gene was amplified from trypanosomal genomic DNA (*Lister 427*) into a pGEM subcloning vector (Promega A1360), and the S317A mutation was introduced by QuickChange PCR. Wild type and mutant *VSG3* genes were then cloned into the vector pUB39[166] (replacing *VSG117* in the original vector via HindIII

and BamHI sites) to create pSUN7 and pSUN8. *VSG3* and *VSG3-S317A* were amplified from pSUN7 and pSUN8, respectively, using primers 224_BsiWI_For (GCGACACGTACGCGGCATGCAAGCGGCAGCA) and 224_AvrII_Rev (AATTAACCTAGGGGGCAATTCCAGCTGTC) (these PCR fragments contained the WT/S317A *VSG3* coding regions along with the surrounding *VSG117* 5' and 3' UTRs from the pUB39 vector). The backbone vector pSY37F1D-CTR-BSD was digested with BsiWI and SpeI, and the larger fragment was isolated by gel purification. *VSG3* and *VSG3-S317A* PCR fragments were digested with BsiWI and AvrII and ligated into the pSY37F1D-CTR-BSD backbone fragment, resulting in final plasmids pKI224 and pKI224-S317A, respectively.

5.12.2 Transfections and resultant clones

These plasmids were then linearized with XhoI and transfected into a parental clone expressing VSG2 via the Amaxa nucleofector protocol as previously described[207]. BSD resistant clones were selected based on expression of VSG3 (by FACS) and counterselected for dual expressors (which co-expressed VSG2; also by FACS), using monoclonal antibodies to VSG2 and VSG3. VSG2 counterselection was used to eliminate a subset of clones which integrated the VSG3 cassette ectopically. Two sets of clones were generated. Transfection of *VSG3* and *VSG3-S317A* into the *Lister 427* "single marker" cell line[167] produced clones KI.VSG3$_{WT}$-1 and KI.VSG3$_{S317A}$-1, respectively. Transfection of *VSG3* and *VSG3-S317A* into a different VSG2-expressing *Lister 427* cell line (GPIPLC null,[84]) produced clones KI.VSG3$_{WT}$-2 and KI.VSG3$_{S317A}$-2, respectively. KI.VSG3$_{WT}$-2 and KI.VSG3$_{S317A}$-2 were thus generated on a GPIPLC-/- background. The lack of a GPI-PLC gene does not affect parasite virulence or the course of parasitemia[84], and consequently should not affect interpretation of the mouse infection results shown. The presence

of the single point mutation within $VSG3_{S317A}$ was verified in the KI.$VSG3_{S317A}$ clones through RT-PCR amplification and sequencing.

5.13 Immunization of mice with UV-irradiated *GPI-PLC*$^{-/-}$ trypanosomes

VSG2, $VSG3_{WT}$, or $VSG3_{S317A}$-expressing *GPI-PLC*$^{-/-}$ trypanosomes were pelleted from culture, washed with irradiation buffer (PBS, 154mM Glucose), and resuspended in irradiation buffer to a density of 10^7 cells/ml. 1ml of this resuspension was aliquoted into each well of a 6 well tissue culture plate (Falcon 353046). Plates were UV-irradiated for 10 min in 1 min intervals using a FB-UVXL-1000 UV crosslinker (Fisher Scientific). Plates were swirled between 1 min intervals to ensure equal irradiation of trypanosomes. Irradiated cells were pelleted and resuspended in HMI-9 at desired concentration, and 100ul of this solution was injected i.p. into mice. This immunization procedure was performed twice on each mouse on day 0 and day 3 (except while initially testing immunization methods; shown in Fig.2.10b). For experiments shown in chapter 2, immunization injections contained 3 x 10^6 UV-irradiated trypanosomes. For experiments shown in chapter 3, immunization injections contained 2-3 x 10^6 UV-irradiated trypanosomes. For live trypanosome comparison immunizations (Fig. 2.10c), mice were infected on day 0 with 100 or 1000 live WT-VSG2 trypanosomes via i.p. injection. Infections were cleared with 250ng berenil/mouse injected i.p. on the day trypanosomes were identified by blood smear (day 4 for 1000 injected, day 5 for 100 injected). Berenil treatment was repeated 24 hours after initial treatment. Serum samples for ELISA analysis were obtained via submandibular bleed, and serum was separated from whole blood using Microtainer serum collection tubes (BD 365967).

5.14 Mouse infection and immunization-challenge experiments

5.14.1 Chapter 2

All mice were female, wild type C57BL/6J, aged 6-9 weeks at experiment start (Jackson Laboratory). Mice were immunized with UV-irradiated VSG2-expressing GPI-PLC$^{-/-}$ trypanosomes, and serum samples were obtained for ELISA analysis (from immunized and non-immunized control mice) on day 8 post-immunization as described above. Later that same day, mouse groups were challenged via i.p. injection of 100 live WT-VSG2, WT-VSG3, DE-11, DE-7.6, or DE-1.3 trypanosomes in HMI-9. Mice were monitored for survival twice daily on days 4 – 16 post-challenge, then once daily until day 23. Mice were also monitored for trypanosome infection by blood smear (blood from mouse tail clippings was examined by eye under a microscope for the presence of trypanosomes), and permanently scored as "confirmed infected" once trypanosomes were identified, regardless of whether parasitemia subsequently fell to undetectable levels. Blood smear monitoring occurred daily from days 4 – 8 post-challenge (i.e. through the first peak on infection) for all mice. After day 8, all mice that had not yet exhibited parasitemia were monitored daily until the mouse died or the experiment ended. At all times, if blood smears indicated a quantifiable level of parasitemia, parasitemia was measured using a hemocytometer. One mouse in the non-immunized DE-11 group was excluded from analysis because ELISA results showed high anti-VSG2 IgM titers despite lack of immunization, and one mouse in the immunized DE-7.6 group was excluded because it died during the course of the experiment from a cause unrelated to trypanosomiasis. All animal experiments were approved by Rockefeller University's institutional animal care and use committee under protocol #16894.

5.14.2 Chapter 3

All mice were wild type males or females, aged 6-9 weeks at experiment start (Jackson Laboratory). For Figs. 3.6 and 3.7a-d, groups of C57BL/6J or CD-1 mice were infected via i.p. injection of 100 live trypanosomes expressing either $VSG3_{WT}$ or $VSG3_{S317A}$. For Fig. 3.8, C57BL/6J mice were immunized with UV-irradiated trypanosomes as described in section 5.13 (using clones KI.$VSG3_{WT}$-2 or KI.$VSG3_{S317A}$-2). The subsequent challenge injection was administered 8 days after the initial immunization, and consisted of 100 live trypanosomes (as in the naïve mouse experiments). For all infection experiments, mouse survival was assessed daily, and parasitemia was monitored starting on day 4 or 5 by blood smear (blood from mouse tail clippings was examined by eye under a microscope for the presence of trypanosomes) or by counting parasite numbers using a hemocytometer. For Fig 3.8a, mice were permanently scored as "confirmed parasitemia" when parasites were first identified by blood smear, regardless of whether parasitemia subsequently fell to undetectable levels. All animal experiments were approved by Rockefeller University's institutional animal care and use committee under protocol #16894.

5.15 Analysis of VSG expression in infection isolates

Trypanosomes were isolated from mouse blood during some infections for flow cytometry-based VSG expression analysis. For these analyses, 100 ul infected mouse blood was collected and incubated twice with 1 ml Red Blood Cell Lysing Buffer (Sigma R7757) for 4 minutes at room temperature. Samples were then resuspended in 100 ul HMI-9 with a 1:50 dilution of Mouse FC Block (BD 553142) and incubated on an inversion rotator for 10 minutes at 4°C (all subsequent steps were on ice or at 4°C). 10 ul of each sample was then added to 100 ul of HMI-9 containing

anti-VSG2-Alexa647 (1:1000 dilution) and anti-VSG3-Alexa488 (1:200 dilution) antibodies. These solutions were incubated on an inversion rotator for 10 minutes, pelleted, and washed once with 1 ml HMI-9. Samples were then pelleted again, resuspended in 200 ul HMI-9, and analyzed using a BD-FACSCalibur flow cytometer. Control WT-VSG2 and WT-VSG3 samples were pelleted from culture and stained identically with the same anti-VSG2 and anti-VSG3 antibody dilutions.

5.16 ELISA assays

ELISA assays were performed using established methods. ELISA plates (Corning 9018) were coated with 2.3 ug/ml purified VSG2 in borate buffer (100mM Boric Acid, 25mM Sodium Borate, 75mM Sodium Chloride), then blocked with blocking buffer (1% BSA in borate buffer). Primary antibody solutions contained 1:30 (Fig. 3a) or 1:100 (Supplementary Fig. 3a) dilutions of mouse antisera in blocking buffer. Secondary antibody solutions contained 1:1000 dilutions of Goat Anti-Mouse IgM-AP (SouthernBiotech 1021-04) or Goat Anti-Mouse IgG1-AP (SouthernBiotech 1070-04). Washes were performed using PBS with 0.05% Tween 20. Wells were developed in developing buffer (0.1M Glycine, 1mM Zinc Chloride, 1 mM Magnesium Chloride) with 1 mg/ml PNPP substrate (ThermoFisher 34047) and OD 405nm was read using a Spectramax M3 plate reader (Molecular Devices).

5.17 Elicitation of VSG-specific polyclonal IgM antisera

Female C57BL/6J mice were injected i.p. with live trypanosomes in 100-200ul HMI-9. For Chapter 2, injections contained 1-2 x 10^4 WT-VSG2 trypanosomes. For Chapter 3, injections contained 1 x 10^3 $VSG3_{WT}$ or $VSG3_{S317A}$-expressing trypanosomes. After 4 days, infections were cleared with 250ng berenil/mouse injected i.p., and berenil treatment was repeated after 24

hours. Clearance was necessary to prevent animals from succumbing to infection prior to developing significant antibody titers. On day 8 post-injection, blood was collected via cardiac puncture, and serum was separated from whole blood using Microtainer serum collection tubes (BD 365967).

5.18 Flow cytometry-based IgM binding assays

5.18.1 Chapter 2

Flow cytometry samples were prepared as described in section 5.9.2, except antibody binding was done in two steps: (1) VSG2-specific polyclonal IgM antisera, diluted 1:100 in mouse serum (Mouse Reference Serum, Bethyl Laboratories, RS10-101). (2) 1:500 dilution of Goat Anti-Mouse IgM-FITC (Southern Biotech 1021-02) in HMI-9. Samples were incubated for 10 min in each antibody solution and washed once with HMI-9 after each binding step. Control samples labeled with monoclonal anti-VSG2-Alexa647 were prepared using a single antibody incubation step. For data analysis (using FlowJo software), trypanosome populations were gated via forward and side scatter, then dead cells were excluded by gating cells negative for Propidium Iodide staining.

5.18.2 Chapter 3

Same as above except: (1) Primary staining was performed with $VSG3_{WT}$ or $VSG3_{S317A}$-elicited polyclonal IgM antisera diluted in HMI-9 (dilutions indicated in figure legends), and (2) secondary staining was performed with a 1:1000 dilution of goat anti-mouse IgM-FITC (SouthernBiotech 1021-02) in HMI-9.

5.19 Development of mathematical IgM-VSG coat binding interface model

To approximate the binding "footprint" of a pentameric IgM molecule on the VSG coat, the VSG coat was first modeled as a regularly spaced hexagonal grid, as has been shown in previous studies[181]. A regular hexagon of height h has 6 sides of length equal to ($h / 3^{1/2}$). A hexagon with a height of 40 nm (the upper estimate of the diameter of an IgM molecule) thus has sides of length ~23.1 nm. If such a hexagon has 5 VSG homodimers on each side, they will be equally spaced at ~5.8 nm (23.1 nm / 4 inter-homodimer spaces), a value extremely close to previously estimated homodimer spacing (5.7 nm spacing with a random displacement up to 0.5 nm)[181]. Filling this hexagon with additional VSG homodimers at the same spacing, we estimated that 61 VSG homodimers (or 122 VSG monomers) would be within reach of a single IgM with a 40 nm diameter (Fig 2.12b and c). The same calculations were performed for IgM with a 30 nm diameter: 30 nm / $3^{1/2}$ gives a side length of ~17.3 nm. Assuming 4 VSG homodimers on each side, they will again be equally spaced at ~5.8 nm (17.3 nm / 3 inter-homodimer spaces). Filling this hexagon results in 37 VSG homodimers (or 74 VSG monomers) within reach of a single IgM with a 30 nm diameter.

5.20 Primer and UTR sequences

Primers (Sequences 5'->3')

JPC1_UniqueFor: TATAAGATCTGCGGCCGCGAGTAAGTAAGTTGGAGCGCAC
JPC2_UniqueRev: ATATCTCGAGGCGGCCGCCATGCTGTCGGTTGTCGGACTTGG
JPC3_pUC19For: TATACTCGAGCCGGGAGCTGCATGTGTCAGAGG
JPC4_pUC19Rev: ATATAGATCTTCGTTCGGCTGCGGCGAGCGG
JPC18_GibsonP2For:
GGGAGGACTAACACAATGAATACGGTTTACACCGGTGGGCTGCACGCGCCTTCGAG
TTTT
JPC19_GibsonP2Rev:
TGACATTACCATTCCGGTACTGTTGGTAAAATGCCTTCCAATCAGGAGGCCCGGCTT
TTC
JP09_VSG221_For: ATGCCTTCCAATCAGGAGGCC
JPC24_GibsonP3221UTR_Rev:
GACTGTCTGATTGTCTAGAAATATTTTCTGGCAGGGCACAGCAAGGTCTTCTGAAAT
TCATGT
JP11_ACT5UTRStart_For: GGGCACAGCAAGGTCTTCTGA
JPC22_GibsonP5Rev:
CGTTTGTTATCTATGCAGTATTCTGCAGGCGTGATGAAGATGCAGATAGATGGCATA
GAT
JPC26_GibsonP3221UTR_For:
GGGAGGACTAACACAATGAATACGGTTTACATTGCATTTGGACACCGCTATACATAT
GTT
JPC31_JP07P2_For:
GGGAGGACTAACACAATGAATACGGTTTACGTGCTCAAGCTGTGTAGCGCACGCGT
TTCC
JPC32_JP07P2_Rev:
AGCCCGAAAACATAAACTCAACTGCAACGAATGCCTTCCAATCAGGAGGCCCGGCT
TTTC
JPC20_GibsonP3Rev:
CCTCTTTGGCTTGCAGTTTTGCTTTTTTAAGATCCTGCCCATTTAGTTGGCTTTTCCCT
T
JP10_Ald3UTR_For: GATCCTGCCCATTTAGTTGGC
JPC21_GibsonP4Rev:
GCCACTACAAGTTGGTTTCCTTCCCCTGCAGGGCACAGCAAGGTCTTCTGAAATTCA
TGT

Procyclin UTR (mod) sequence

ACCGGTGGGCTGCACGCGCCTTCGAGTTTTTTTTCCTTTTCCCCATTTTTTTCAACTTG
AAGGGTACCCTTCAATTACACCAAAAAATAAAATTCACAAACTTGGAATTCCTTTGT
GTTACATTCTTGATCGCTCGCACTGACATTACCATTCCGGTACTGTTGGTAAA

Chapter 6

References

1. Büscher, P., Cecchi, G., Jamonneau, V. & Priotto, G. Human African trypanosomiasis. *Lancet* **390,** 2397–2409 (2017).

2. Giordani, F., Morrison, L. J., Rowan, T. G., DE Koning, H. P. & Barrett, M. P. The animal trypanosomiases and their chemotherapy: a review. *Parasitology* **143,** 1862–1889 (2016).

3. Trindade, S. *et al*. Trypanosoma brucei Parasites Occupy and Functionally Adapt to the Adipose Tissue in Mice. *Cell Host and Microbe* **19,** 837–848 (2016).

4. World Health Organization. Working to overcome the global impact of neglected tropical diseases: first WHO report on neglected tropical diseases: update 2011. (2011).

5. Simarro, P. P., Jannin, J. & Cattand, P. Eliminating Human African Trypanosomiasis: Where Do We Stand and What Comes Next? *PLoS Med* **5,** e55–7 (2008).

6. Franco, J. R. *et al*. Monitoring the elimination of human African trypanosomiasis: Update to 2014. *PLoS Negl Trop Dis* **11,** e0005585–26 (2017).

7. Franco, J. R., Simarro, P. P., Diarra, A. & Jannin, J. G. Epidemiology of human African trypanosomiasis. *Clin Epidemiol* **6,** 257–275 (2014).

8. Alsford, S. *et al*. High-throughput decoding of antitrypanosomal drug efficacy and resistance. *Nature Publishing Group* **482,** 232–236 (2012).

9. Carnes, J. *et al*. Genome and phylogenetic analyses of Trypanosoma evansi reveal extensive similarity to T. brucei and multiple independent origins for dyskinetoplasty. *PLoS Negl Trop Dis* **9,** e3404 (2015).

10. Shaw, A. P. M., Cecchi, G., Wint, G. R. W., Mattioli, R. C. & Robinson, T. P. Mapping the economic benefits to livestock keepers from intervening against bovine trypanosomosis in Eastern Africa. *Prev. Vet. Med.* **113,** 197–210 (2014).

11. Büscher, P. *et al*. Do Cryptic Reservoirs Threaten Gambiense-Sleeping Sickness Elimination? *Trends in Parasitology* (2018). doi:10.1016/j.pt.2017.11.008

12. Hajduk, S. L. *et al*. Lysis of Trypanosoma brucei by a toxic subspecies of human high density lipoprotein. *J. Biol. Chem.* **264,** 5210–5217 (1989).

13. Raper, J., Fung, R., Ghiso, J., Nussenzweig, V. & Tomlinson, S. Characterization of a novel trypanosome lytic factor from human serum. *Infect. Immun.* **67,** 1910–1916 (1999).

14. Stephens, N. A., Kieft, R., MacLeod, A. & Hajduk, S. L. Trypanosome resistance to human innate immunity: targeting Achilles' heel. *Trends in Parasitology* **28,** 539–545

(2012).

15. Truc, P. *et al*. Atypical Human Infections by Animal Trypanosomes. *PLoS Negl Trop Dis* **7,** e2256–7 (2013).

16. Vanhollebeke, B. *et al*. Human Trypanosoma evansi infection linked to a lack of apolipoprotein L-I. *N. Engl. J. Med.* **355,** 2752–2756 (2006).

17. Van Vinh Chau, N. *et al*. A Clinical and Epidemiological Investigation of the First Reported Human Infection With the Zoonotic Parasite Trypanosoma evansi in Southeast Asia. *CLIN INFECT DIS* **62,** 1002–1008 (2016).

18. De Greef, C., Imberechts, H., Matthyssens, G., Van Meirvenne, N. & Hamers, R. A gene expressed only in serum-resistant variants of Trypanosoma brucei rhodesiense. *Mol. Biochem. Parasitol.* **36,** 169–176 (1989).

19. Xong, H. V. *et al*. A VSG expression site-associated gene confers resistance to human serum in Trypanosoma rhodesiense. *Cell* **95,** 839–846 (1998).

20. Uzureau, P. *et al*. Mechanism of Trypanosoma brucei gambiense resistance to human serum. *Nature Publishing Group* **501,** 430–434 (2013).

21. Capewell, P. *et al*. Differences between Trypanosoma brucei gambiense groups 1 and 2 in their resistance to killing by trypanolytic factor 1. *PLoS Negl Trop Dis* **5,** e1287 (2011).

22. Capewell, P. *et al*. The TgsGP gene is essential for resistance to human serum in Trypanosoma brucei gambiense. *PLoS Pathog* **9,** e1003686 (2013).

23. Vassella, E., Reuner, B., Yutzy, B. & Boshart, M. Differentiation of African trypanosomes is controlled by a density sensing mechanism which signals cell cycle arrest via the cAMP pathway. *Journal of Cell Science* **110 (Pt 21),** 2661–2671 (1997).

24. Reuner, B., Vassella, E., Yutzy, B. & Boshart, M. Cell density triggers slender to stumpy differentiation of Trypanosoma brucei bloodstream forms in culture. *Mol. Biochem. Parasitol.* **90,** 269–280 (1997).

25. Gray, G. D., Jennings, F. W. & Hajduk, S. L. Relapse of monomorphic and pleomorphic Trypanosoma brucei infections in the mouse after chemotherapy. *Z Parasitenkd* **67,** 137–145 (1982).

26. Fenn, K. & Matthews, K. R. The cell biology of Trypanosoma brucei differentiation. *Current Opinion in Microbiology* **10,** 539–546 (2007).

27. Tyler, K. M., Higgs, P. G., Matthews, K. R. & Gull, K. Limitation of Trypanosoma brucei parasitaemia results from density-dependent parasite differentiation and parasite killing by the host immune response. *Proceedings of the Royal Society B: Biological Sciences* **268,** 2235–2243 (2001).

28. Nolan, D. P., Rolin, S., Rodriguez, J. R., Van Den Abbeele, J. & Pays, E. Slender and stumpy bloodstream forms of Trypanosoma brucei display a differential response to extracellular acidic and proteolytic stress. *Eur. J. Biochem.* **267,** 18–27 (2000).

29. Dean, S., Marchetti, R., Kirk, K. & Matthews, K. R. A surface transporter family conveys the trypanosome differentiation signal. *Nature Publishing Group* **459,** 213–217 (2009).

30. Matthews, K. R. & Gull, K. Evidence for an interplay between cell cycle progression and the initiation of differentiation between life cycle forms of African trypanosomes. *J. Cell Biol.* **125,** 1147–1156 (1994).

31. Acosta-Serrano, A. *et al.* The surface coat of procyclic Trypanosoma brucei: programmed expression and proteolytic cleavage of procyclin in the tsetse fly. *Proc. Natl. Acad. Sci. U.S.A.* **98,** 1513–1518 (2001).

32. Gibson, W., Peacock, L., Ferris, V., Williams, K. & Bailey, M. Analysis of a cross between green and red fluorescent trypanosomes. *Biochem. Soc. Trans.* **34,** 557–559 (2006).

33. Peacock, L. *et al.* Identification of the meiotic life cycle stage of Trypanosoma brucei in the tsetse fly. *Proc. Natl. Acad. Sci. U.S.A.* **108,** 3671–3676 (2011).

34. Cross, G. A. M., Kim, H.-S. & Wickstead, B. Capturing the variant surface glycoprotein repertoire (the VSGnome) of Trypanosoma brucei Lister 427. *Mol. Biochem. Parasitol.* **195,** 59–73 (2014).

35. Cross, G. A. M. Identification, purification and properties of clone-specific glycoprotein antigens constituting the surface coat of Trypanosoma brucei. *Parasitology* **71,** 393 (1975).

36. Jackson, D. G., Owen, M. J. & Voorheis, H. P. A new method for the rapid purification of both the membrane-bound and released forms of the variant surface glycoprotein from Trypanosoma brucei. *Biochem. J.* **230,** 195–202 (1985).

37. Mugnier, M. R., Cross, G. A. M. & Papavasiliou, F. N. The in vivo dynamics of antigenic variation in Trypanosoma brucei. *Science* **347,** 1470–1473 (2015).

38. Ross, R. & Thomson, D. A case of sleeping sickness studied by precise enumerative methods: regular periodical increase of the parasites disclosed. … *Society of London Series B* (1910). doi:10.2307/80242

39. Gray, A. R. Precipitating antibody in trypanosomiasis of cattle and other animals. *Nature* **186,** 1058–1059 (1960).

40. Dempsey, W. L. & Mansfield, J. M. Lymphocyte function in experimental African trypanosomiasis. V. Role of antibody and the mononuclear phagocyte system in variant-specific immunity. *J. Immunol.* **130,** 405–411 (1983).

41. Morrison, L. J., Majiwa, P., Read, A. F. & Barry, J. D. Probabilistic order in antigenic variation of Trypanosoma brucei. *Int. J. Parasitol.* **35,** 961–972 (2005).

42. Jackson, A. P. *et al.* Antigenic diversity is generated by distinct evolutionary mechanisms in African trypanosome species. *Proc. Natl. Acad. Sci. U.S.A.* **109,** 3416–3421 (2012).

43. Hovel-Miner, G., Mugnier, M. R., Goldwater, B., Cross, G. A. M. & Papavasiliou, F. N. A Conserved DNA Repeat Promotes Selection of a Diverse Repertoire of Trypanosoma brucei Surface Antigens from the Genomic Archive. *PLoS Genet* **12,** e1005994–19 (2016).

44. Morrison, L. J., Marcello, L. & McCulloch, R. Antigenic variation in the African trypanosome: molecular mechanisms and phenotypic complexity. *Cell. Microbiol.* **11,** 1724–1734 (2009).

45. Deitsch, K. W., Moxon, E. R. & Wellems, T. E. Shared themes of antigenic variation and virulence in bacterial, protozoal, and fungal infections. *Microbiol. Mol. Biol. Rev.* **61,** 281–293 (1997).

46. Overath, P. & Engstler, M. Endocytosis, membrane recycling and sorting of GPI-anchored proteins: Trypanosoma brucei as a model system. *Mol. Microbiol.* **53,** 735–744 (2004).

47. Ziegelbauer, K. & Overath, P. Identification of invariant surface glycoproteins in the bloodstream stage of Trypanosoma brucei. *J. Biol. Chem.* **267,** 10791–10796 (1992).

48. Grünfelder, C. G. *et al.* Accumulation of a GPI-anchored protein at the cell surface requires sorting at multiple intracellular levels. *Traffic* **3,** 547–559 (2002).

49. Schwede, A., Macleod, O. J. S., MacGregor, P. & Carrington, M. How Does the VSG Coat of Bloodstream Form African Trypanosomes Interact with External Proteins? *PLoS Pathog* **11,** e1005259–18 (2015).

50. Blum, M. L. *et al.* A structural motif in the variant surface glycoproteins of Trypanosoma brucei. *Nature* **362,** 603–609 (1993).

51. Bartossek, T. *et al.* Structural basis for the shielding function of the dynamic trypanosome variant surface glycoprotein coat. *Nat Microbiol* **2,** 1523–1532 (2017).

52. Metcalf, P., Blum, M., Freymann, D., Turner, M. & Wiley, D. C. Two variant surface glycoproteins of Trypanosoma brucei of different sequence classes have similar 6 A resolution X-ray structures. *Nature* **325,** 84–86 (1987).

53. Mehlert, A., Zitzmann, N., Richardson, J. M., Treumann, A. & Ferguson, M. A. The glycosylation of the variant surface glycoproteins and procyclic acidic repetitive proteins of Trypanosoma brucei. *Mol. Biochem. Parasitol.* **91,** 145–152 (1998).

54. Vickerman, K. On the surface coat and flagellar adhesion in trypanosomes. *Journal of Cell Science* **5,** 163–193 (1969).

55. Freymann, D. *et al*. 2.9 A resolution structure of the N-terminal domain of a variant surface glycoprotein from Trypanosoma brucei. *J. Mol. Biol.* **216,** 141–160 (1990).

56. Chattopadhyay, A. *et al*. Structure of the C-terminal domain from Trypanosoma brucei variant surface glycoprotein MITat1.2. *J. Biol. Chem.* **280,** 7228–7235 (2005).

57. Barry, J. D. Capping of variable antigen on Trypanosoma brucei, and its immunological and biological significance. *Journal of Cell Science* **37,** 287–302 (1979).

58. Masterson, W. J., Taylor, D. & Turner, M. J. Topologic analysis of the epitopes of a variant surface glycoprotein of Trypanosoma brucei. *J. Immunol.* **140,** 3194–3199 (1988).

59. Hall, T. & Esser, K. Topologic mapping of protective and nonprotective epitopes on the variant surface glycoprotein of the WRATat 1 clone of Trypanosoma brucei rhodesiense. *J. Immunol.* **132,** 2059–2063 (1984).

60. Bütikofer, P., Malherbe, T., Boschung, M. & Roditi, I. GPI-anchored proteins: now you see 'em, now you don't. *FASEB J.* **15,** 545–548 (2001).

61. Hsia, R. C., Beals, T. & Boothroyd, J. C. Use of chimeric recombinant polypeptides to analyse conformational, surface epitopes on trypanosome variant surface glycoproteins. *Mol. Microbiol.* **19,** 53–63 (1996).

62. Schwede, A., Jones, N., Engstler, M. & Carrington, M. The VSG C-terminal domain is inaccessible to antibodies on live trypanosomes. *Mol. Biochem. Parasitol.* **175,** 201–204 (2011).

63. Ziegelbauer, K. & Overath, P. Organization of two invariant surface glycoproteins in the surface coat of Trypanosoma brucei. *Infect. Immun.* **61,** 4540–4545 (1993).

64. Sullivan, L., Wall, S. J., Carrington, M. & Ferguson, M. A. J. Proteomic selection of immunodiagnostic antigens for human African trypanosomiasis and generation of a prototype lateral flow immunodiagnostic device. *PLoS Negl Trop Dis* **7,** e2087 (2013).

65. Devine, D. V., Falk, R. J. & Balber, A. E. Restriction of the alternative pathway of human complement by intact Trypanosoma brucei subsp. gambiense. *Infect. Immun.* **52,** 223–229 (1986).

66. Ferrante, A. & Allison, A. C. Alternative pathway activation of complement by African trypanosomes lacking a glycoprotein coat. *Parasite Immunol.* **5,** 491–498 (1983).

67. McLintock, L. M., Turner, C. M. & Vickerman, K. Comparison of the effects of immune killing mechanisms on Trypanosoma brucei parasites of slender and stumpy morphology. *Parasite Immunol.* **15,** 475–480 (1993).

68. Bülow, R., Overath, P. & Davoust, J. Rapid lateral diffusion of the variant surface glycoprotein in the coat of Trypanosoma brucei. *Biochemistry* **27,** 2384–2388 (1988).

69. Allen, C. L., Goulding, D. & Field, M. C. Clathrin-mediated endocytosis is essential in Trypanosoma brucei. *EMBO J.* **22,** 4991–5002 (2003).

70. Manna, P. T., Boehm, C., Leung, K. F., Natesan, S. K. & Field, M. C. Life and times: synthesis, trafficking, and evolution of VSG. *Trends in Parasitology* **30,** 251–258 (2014).

71. Pal, A., Hall, B. S., Jeffries, T. R. & Field, M. C. Rab5 and Rab11 mediate transferrin and anti-variant surface glycoprotein antibody recycling in Trypanosoma brucei. *Biochem. J.* **374,** 443–451 (2003).

72. Grünfelder, C. G. *et al*. Endocytosis of a glycosylphosphatidylinositol-anchored protein via clathrin-coated vesicles, sorting by default in endosomes, and exocytosis via RAB11-positive carriers. *Mol. Biol. Cell* **14,** 2029–2040 (2003).

73. Engstler, M. Kinetics of endocytosis and recycling of the GPI-anchored variant surface glycoprotein in Trypanosoma brucei. *Journal of Cell Science* **117,** 1105–1115 (2004).

74. O'Beirne, C., Lowry, C. M. & Voorheis, H. P. Both IgM and IgG anti-VSG antibodies initiate a cycle of aggregation-disaggregation of bloodstream forms of Trypanosoma brucei without damage to the parasite. *Mol. Biochem. Parasitol.* **91,** 165–193 (1998).

75. Engstler, M. *et al*. Hydrodynamic Flow-Mediated Protein Sorting on the Cell Surface of Trypanosomes. *Cell* **131,** 505–515 (2007).

76. Natesan, S. K. A., Peacock, L., Matthews, K., Gibson, W. & Field, M. C. Activation of endocytosis as an adaptation to the mammalian host by trypanosomes. *Eukaryotic Cell* **6,** 2029–2037 (2007).

77. Kisalu, N. K., Langousis, G., Bentolila, L. A., Ralston, K. S. & Hill, K. L. Mouse infection and pathogenesis by Trypanosoma bruceimotility mutants. *Cell. Microbiol.* **16,** 912–924 (2014).

78. Fox, J. A., Duszenko, M., Ferguson, M. A., Low, M. G. & Cross, G. A. Purification and characterization of a novel glycan-phosphatidylinositol-specific phospholipase C from Trypanosoma brucei. *J. Biol. Chem.* **261,** 15767–15771 (1986).

79. Voorheis, H. P., Bowles, D. J. & Smith, G. A. Characteristics of the release of the surface coat protein from bloodstream forms of Trypanosoma brucei. *J. Biol. Chem.* **257,** 2300–2304 (1982).

80. Rolin, S. *et al*. Simultaneous but independent activation of adenylate cyclase and glycosylphosphatidylinositol-phospholipase C under stress conditions in Trypanosoma brucei. *J. Biol. Chem.* **271,** 10844–10852 (1996).

81. Hanrahan, O. *et al*. The glycosylphosphatidylinositol-PLC in Trypanosoma brucei forms

a linear array on the exterior of the flagellar membrane before and after activation. *PLoS Pathog* **5,** e1000468 (2009).

82. Bülow, R., Nonnengässer, C. & Overath, P. Release of the variant surface glycoprotein during differentiation of bloodstream to procyclic forms of Trypanosoma brucei. *Mol. Biochem. Parasitol.* **32,** 85–92 (1989).

83. Seyfang, A., Mecke, D. & Duszenko, M. Degradation, recycling, and shedding of Trypanosoma brucei variant surface glycoprotein. *J. Protozool.* **37,** 546–552 (1990).

84. Leal, S. *et al.* Virulence of Trypanosoma brucei strain 427 is not affected by the absence of glycosylphosphatidylinositol phospholipase C. *Mol. Biochem. Parasitol.* **114,** 245–247 (2001).

85. Webb, H. *et al.* The GPI-phospholipase C of Trypanosoma brucei is nonessential but influences parasitemia in mice. *J. Cell Biol.* **139,** 103–114 (1997).

86. Young, R. *et al.* Isolation and analysis of the genetic diversity of repertoires of VSG expression site containing telomeres from Trypanosoma brucei gambiense, T. b. brucei and T. equiperdum. *BMC Genomics* **9,** 385 (2008).

87. Hertz-Fowler, C. *et al.* Telomeric Expression Sites Are Highly Conserved in Trypanosoma brucei. *PLoS ONE* **3,** e3527–12 (2008).

88. Ullu, E., Matthews, K. R. & Tschudi, C. Temporal order of RNA-processing reactions in trypanosomes: rapid trans splicing precedes polyadenylation of newly synthesized tubulin transcripts. *Molecular and Cellular Biology* **13,** 720–725 (1993).

89. Cully, D. F., Ip, H. S. & Cross, G. A. Coordinate transcription of variant surface glycoprotein genes and an expression site associated gene family in Trypanosoma brucei. *Cell* **42,** 173–182 (1985).

90. Kooter, J. M. *et al.* The anatomy and transcription of a telomeric expression site for variant-specific surface antigens in T. brucei. *Cell* **51,** 261–272 (1987).

91. Zomerdijk, J. C., Kieft, R. & Borst, P. Efficient production of functional mRNA mediated by RNA polymerase I in Trypanosoma brucei. *Nature* **353,** 772–775 (1991).

92. Günzl, A. *et al.* RNA polymerase I transcribes procyclin genes and variant surface glycoprotein gene expression sites in Trypanosoma brucei. *Eukaryotic Cell* **2,** 542–551 (2003).

93. Navarro, M. & Gull, K. A pol I transcriptional body associated with VSG mono-allelic expression in Trypanosoma brucei. *Nature* **414,** 759–763 (2001).

94. Figueiredo, L. M. & Cross, G. A. M. Nucleosomes are depleted at the VSG expression site transcribed by RNA polymerase I in African trypanosomes. *Eukaryotic Cell* **9,** 148–154 (2010).

95. Stanne, T. M. & Rudenko, G. Active VSG expression sites in Trypanosoma brucei are depleted of nucleosomes. *Eukaryotic Cell* **9,** 136–147 (2010).

96. Glover, L., Hutchinson, S., Alsford, S. & Horn, D. VEX1 controls the allelic exclusion required for antigenic variation in trypanosomes. *Proc. Natl. Acad. Sci. U.S.A.* **113,** 7225–7230 (2016).

97. Horn, D. & McCulloch, R. Molecular mechanisms underlying the control of antigenic variation in African trypanosomes. *Current Opinion in Microbiology* **13,** 700–705 (2010).

98. Yang, X., Figueiredo, L. M., Espinal, A., Okubo, E. & Li, B. RAP1 is essential for silencing telomeric variant surface glycoprotein genes in Trypanosoma brucei. *Cell* **137,** 99–109 (2009).

99. Wickstead, B., Ersfeld, K. & Gull, K. The small chromosomes of Trypanosoma brucei involved in antigenic variation are constructed around repetitive palindromes. *Genome Res.* **14,** 1014–1024 (2004).

100. Myler, P. J., Allison, J., Agabian, N. & Stuart, K. Antigenic variation in African trypanosomes by gene replacement or activation of alternate telomeres. *Cell* **39,** 203–211 (1984).

101. Kim, H.-S. & Cross, G. A. M. TOPO3α Influences Antigenic Variation by Monitoring Expression-Site-Associated VSG Switching in Trypanosoma brucei. *PLoS Pathog* **6,** e1000992–14 (2010).

102. Robinson, N. P., Burman, N., Melville, S. E. & Barry, J. D. Predominance of duplicative VSG gene conversion in antigenic variation in African trypanosomes. *Molecular and Cellular Biology* **19,** 5839–5846 (1999).

103. Hovel-Miner, G. A. *et al.* Telomere Length Affects the Frequency and Mechanism of Antigenic Variation in Trypanosoma brucei. *PLoS Pathog* **8,** e1002900–10 (2012).

104. Myler, P., Nelson, R. G., Agabian, N. & Stuart, K. Two mechanisms of expression of a predominant variant antigen gene of Trypanosoma brucei. *Nature* **309,** 282–284 (1984).

105. Glover, L., Alsford, S., Beattie, C. & Horn, D. Deletion of a trypanosome telomere leads to loss of silencing and progressive loss of terminal DNA in the absence of cell cycle arrest. *Nucleic Acids Research* **35,** 872–880 (2007).

106. Rudenko, G., McCulloch, R., Dirks-Mulder, A. & Borst, P. Telomere exchange can be an important mechanism of variant surface glycoprotein gene switching in Trypanosoma brucei. *Mol. Biochem. Parasitol.* **80,** 65–75 (1996).

107. McCulloch, R. & Barry, J. D. A role for RAD51 and homologous recombination in Trypanosoma brucei antigenic variation. *Genes Dev.* **13,** 2875–2888 (1999).

108. Hartley, C. L. & McCulloch, R. Trypanosoma brucei BRCA2 acts in antigenic variation and has undergone a recent expansion in BRC repeat number that is important during homologous recombination. *Mol. Microbiol.* **68,** 1237–1251 (2008).

109. Dobson, R., Stockdale, C., Lapsley, C., Wilkes, J. & McCulloch, R. Interactions among Trypanosoma brucei RAD51 paralogues in DNA repair and antigenic variation. *Mol. Microbiol.* **81,** 434–456 (2011).

110. Proudfoot, C. & McCulloch, R. Distinct roles for two RAD51-related genes in Trypanosoma brucei antigenic variation. *Nucleic Acids Research* **33,** 6906–6919 (2005).

111. Glover, L., McCulloch, R. & Horn, D. Sequence homology and microhomology dominate chromosomal double-strand break repair in African trypanosomes. *Nucleic Acids Research* **36,** 2608–2618 (2008).

112. Glover, L., Alsford, S. & Horn, D. DNA Break Site at Fragile Subtelomeres Determines Probability and Mechanism of Antigenic Variation in African Trypanosomes. *PLoS Pathog* **9,** e1003260 (2013).

113. Boothroyd, C. E. *et al.* A yeast-endonuclease-generated DNA break induces antigenic switching in Trypanosoma brucei. *Nature* **459,** 278–281 (2009).

114. Berriman, M. *et al.* The genome of the African trypanosome Trypanosoma brucei. *Science* **309,** 416–422 (2005).

115. McCulloch, R., Rudenko, G. & Borst, P. Gene conversions mediating antigenic variation in Trypanosoma brucei can occur in variant surface glycoprotein expression sites lacking 70-base-pair repeat sequences. *Molecular and Cellular Biology* **17,** 833–843 (1997).

116. Barry, J. D. & McCulloch, R. Antigenic variation in trypanosomes: enhanced phenotypic variation in a eukaryotic parasite. *Adv. Parasitol.* **49,** 1–70 (2001).

117. Dreesen, O., Li, B. & Cross, G. A. M. Telomere structure and function in trypanosomes: a proposal. *Nat. Rev. Microbiol.* **5,** 70–75 (2007).

118. Doyle, J. J., Hirumi, H., Hirumi, K., Lupton, E. N. & Cross, G. A. Antigenic variation in clones of animal-infective Trypanosoma brucei derived and maintained in vitro. *Parasitology* **80,** 359–369 (1980).

119. Lamont, G. S., Tucker, R. S. & Cross, G. A. Analysis of antigen switching rates in Trypanosoma brucei. *Parasitology* **92 (Pt 2),** 355–367 (1986).

120. Hall, J. P. J., Wang, H. & Barry, J. D. Mosaic VSGs and the scale of Trypanosoma brucei antigenic variation. *PLoS Pathog* **9,** e1003502 (2013).

121. Roth, C., Bringaud, F., Layden, R. E., Baltz, T. & Eisen, H. Active late-appearing variable surface antigen genes in Trypanosoma equiperdum are constructed entirely from pseudogenes. *Proc. Natl. Acad. Sci. U.S.A.* **86,** 9375–9379 (1989).

122. Kamper, S. M. & Barbet, A. F. Surface epitope variation via mosaic gene formation is potential key to long-term survival of Trypanosoma brucei. *Mol. Biochem. Parasitol.* **53,** 33–44 (1992).

123. Marcello, L. & Barry, J. D. Analysis of the VSG gene silent archive in Trypanosoma brucei reveals that mosaic gene expression is prominent in antigenic variation and is favored by archive substructure. *Genome Res.* **17,** 1344–1352 (2007).

124. Horn, D. & Cross, G. Analysis of Trypanosoma brucei vsg expression site switching in vitro. *Mol. Biochem. Parasitol.* **84,** 189–201 (1997).

125. Turner, C. M. & Barry, J. D. High frequency of antigenic variation in Trypanosoma brucei rhodesiense infections. *Parasitology* **99 Pt 1,** 67–75 (1989).

126. Turner, C. M. The rate of antigenic variation in fly-transmitted and syringe-passaged infections of Trypanosoma brucei. *FEMS Microbiol. Lett.* **153,** 227–231 (1997).

127. Miller, E. N. & Turner, M. J. Analysis of antigenic types appearing in first relapse populations of clones of Trypanosoma brucei. *Parasitology* **82,** 63–80 (1981).

128. Myler, P. J., Allen, A. L., Agabian, N. & Stuart, K. Antigenic variation in clones of Trypanosoma brucei grown in immune-deficient mice. *Infect. Immun.* **47,** 684–690 (1985).

129. Liu, A. Y., Michels, P. A., Bernards, A. & Borst, P. Trypanosome variant surface glycoprotein genes expressed early in infection. *J. Mol. Biol.* **182,** 383–396 (1985).

130. Magez, S. *et al.* Interferon-γ and Nitric Oxide in Combination with Antibodies Are Key Protective Host Immune Factors during Trypanosoma congolense Tc13 Infections. *J Infect Dis* **193,** 1575–1583 (2006).

131. Magez, S. *et al.* The Role of B-cells and IgM Antibodies in Parasitemia, Anemia, and VSG Switching in Trypanosoma brucei–Infected Mice. *PLoS Pathog* **4,** e1000122 (2008).

132. Reinitz, D. M. & Mansfield, J. M. T-cell-independent and T-cell-dependent B-cell responses to exposed variant surface glycoprotein epitopes in trypanosome-infected mice. *Infect. Immun.* **58,** 2337–2342 (1990).

133. Mond, J. J., Lees, A. & Snapper, C. M. T cell-independent antigens type 2. *Annu. Rev. Immunol.* **13,** 655–692 (1995).

134. Lutz, C. *et al.* IgD can largely substitute for loss of IgM function in B cells. *Nature* **393,** 797–801 (1998).

135. Shi, M., Pan, W. & Tabel, H. Experimental African trypanosomiasis: IFN-γ mediates early mortality. *Eur. J. Immunol.* **33,** 108–118 (2003).

136. MACASKILL, J. A. *et al*. Immunological clearance of 75Se-labelled Trypanosoma brucei in mice. II. Mechanisms in immune animals. *Immunology* **40,** 629–635 (1980).

137. Magez, S. *et al*. Specific uptake of tumor necrosis factor-alpha is involved in growth control of Trypanosoma brucei. *J. Cell Biol*. **137,** 715–727 (1997).

138. Magez, S., Radwanska, M., Beschin, A., Sekikawa, K. & De Baetselier, P. Tumor necrosis factor alpha is a key mediator in the regulation of experimental Trypanosoma brucei infections. *Infect. Immun*. **67,** 3128–3132 (1999).

139. Magez, S. *et al*. Murine tumour necrosis factor plays a protective role during the initial phase of the experimental infection with Trypanosoma brucei brucei. *Parasite Immunol*. **15,** 635–641 (1993).

140. Darji, A. *et al*. In vitro simulation of immunosuppression caused by Trypanosoma brucei: active involvement of gamma interferon and tumor necrosis factor in the pathway of suppression. *Infect. Immun*. **64,** 1937–1943 (1996).

141. Harris, T. H., Cooney, N. M., Mansfield, J. M. & Paulnock, D. M. Signal transduction, gene transcription, and cytokine production triggered in macrophages by exposure to trypanosome DNA. *Infect. Immun*. **74,** 4530–4537 (2006).

142. Drennan, M. B. *et al*. The induction of a type 1 immune response following a Trypanosoma brucei infection is MyD88 dependent. *J. Immunol*. **175,** 2501–2509 (2005).

143. Schofield, L. & Tachado, S. D. Regulation of host cell function by glycosylphosphatidylinositols of the parasitic protozoa. *Immunol. Cell Biol*. **74,** 555–563 (1996).

144. Schleifer, K. W., Filutowicz, H., Schopf, L. R. & Mansfield, J. M. Characterization of T helper cell responses to the trypanosome variant surface glycoprotein. *J. Immunol*. **150,** 2910–2919 (1993).

145. Fumoux, F., Traore-Leroux, T., Queval, R., Pinder, M. & Roelants, G. E. High and low responsiveness of bovine lymphocytes to Trypanosoma brucei in vitro: lack of correlation with resistance to trypanosomiasis. *Immunology* **54,** 195–203 (1985).

146. McKeever, D. J., Awino, E., Kairo, A., Gobright, E. & Nene, V. Bovine T cells specific for Trypanosoma brucei brucei variant surface glycoprotein recognize nonconserved areas of the molecule. *Infect. Immun*. **62,** 3348–3353 (1994).

147. Hertz, C. J., Filutowicz, H. & Mansfield, J. M. Resistance to the African trypanosomes is IFN-gamma dependent. *J. Immunol*. **161,** 6775–6783 (1998).

148. Liu, G. *et al*. Distinct Contributions of CD4 +and CD8 +T Cells to Pathogenesis of Trypanosoma brucei Infection in the Context of Gamma Interferon and Interleukin-10. *Infect. Immun*. **83,** 2785–2795 (2015).

149. De Muylder, G. *et al*. A Trypanosoma brucei kinesin heavy chain promotes parasite growth by triggering host arginase activity. *PLoS Pathog* **9,** e1003731 (2013).

150. Salmon, D. *et al*. Adenylate cyclases of Trypanosoma brucei inhibit the innate immune response of the host. *Science* **337,** 463–466 (2012).

151. Gómez Rodríguez, J. *et al*. Identification of a parasitic immunomodulatory protein triggering the development of suppressive M1 macrophages during African trypanosomiasis. *Journal of Infectious Diseases* **200,** 1849–1860 (2009).

152. Sacco, R. E., Hagen, M., Donelson, J. E. & Lynch, R. G. B lymphocytes of mice display an aberrant activation phenotype and are cell cycle arrested in G0/G1A during acute infection with Trypanosoma brucei. *J. Immunol.* **153,** 1714–1723 (1994).

153. Mayor-Withey, K. S., Clayton, C. E., Roelants, G. E. & Askonas, B. A. Trypanosomiasis leads to extensive proliferation of B, T and null cells in spleen and bone marrow. *Clin. Exp. Immunol.* **34,** 359–363 (1978).

154. Diffley, P. Trypanosomal surface coat variant antigen causes polyclonal lymphocyte activation. *J. Immunol.* **131,** 1983–1986 (1983).

155. Sparwasser, T. *et al*. Immunostimulatory CpG-oligodeoxynucleotides cause extramedullary murine hemopoiesis. *J. Immunol.* **162,** 2368–2374 (1999).

156. Bockstal, V. *et al*. T. brucei infection reduces B lymphopoiesis in bone marrow and truncates compensatory splenic lymphopoiesis through transitional B-cell apoptosis. *PLoS Pathog* **7,** e1002089 (2011).

157. Radwanska, M. *et al*. Comparative Analysis of Antibody Responses against HSP60, Invariant Surface Glycoprotein 70, and Variant Surface Glycoprotein Reveals a Complex Antigen-Specific Pattern of Immunoglobulin Isotype Switching during Infection by Trypanosoma brucei. *Infect. Immun.* **68,** 848–860 (2000).

158. Cnops, J. *et al*. IFN-γ mediates early B-cell loss in experimental African trypanosomosis. *Parasite Immunol.* **37,** 479–484 (2015).

159. Dempsey, W. L. & Mansfield, J. M. Lymphocyte function in experimental African trypanosomiasis. VI. Parasite-specific immunosuppression. *J. Immunol.* **130,** 2896–2898 (1983).

160. Radwanska, M. *et al*. Trypanosomiasis-Induced B Cell Apoptosis Results in Loss of Protective Anti-Parasite Antibody Responses and Abolishment of Vaccine-Induced Memory Responses. *PLoS Pathog* **4,** e1000078 (2008).

161. Esser, K. M. & Schoenbechler, M. J. Expression of two variant surface glycoproteins on individual African trypanosomes during antigen switching. *Science* **229,** 190–193 (1985).

162. Carrington, M. *et al*. The properties and function of the glycosylphosphatidylinositol-

phospholipase C in Trypanosoma brucei. *Mol. Biochem. Parasitol.* **91,** 153–164 (1998).

163. Carrington, M. *et al.* Variant specific glycoprotein of Trypanosoma brucei consists of two domains each having an independently conserved pattern of cysteine residues. *J. Mol. Biol.* **221,** 823–835 (1991).

164. Popp, M. W.-L., Antos, J. M. & Ploegh, H. L. *Site-Specific Protein Labeling via Sortase-Mediated Transpeptidation*. (John Wiley & Sons, Inc., 2001). doi:10.1002/0471140864.ps1503s56

165. Stavropoulos, P. & Papavasiliou, F. N. Using T. brucei as a biological epitope-display platform to elicit specific antibody responses. *Journal of Immunological Methods* **362,** 190–194 (2010).

166. Böhme, U. & Cross, G. A. M. Mutational analysis of the variant surface glycoprotein GPI-anchor signal sequence in Trypanosoma brucei. *Journal of Cell Science* **115,** 805–816 (2002).

167. Wirtz, E., Leal, S., Ochatt, C. & Cross, G. A. A tightly regulated inducible expression system for conditional gene knock-outs and dominant-negative genetics in Trypanosoma brucei. *Mol. Biochem. Parasitol.* **99,** 89–101 (1999).

168. Popp, M. W.-L. & Ploegh, H. L. Making and Breaking Peptide Bonds: Protein Engineering Using Sortase. *Angew. Chem. Int. Ed.* **50,** 5024–5032 (2011).

169. Strijbis, K., Spooner, E. & Ploegh, H. L. Protein Ligation in Living Cells Using Sortase. *Traffic* **13,** 780–789 (2012).

170. Schneewind, O., Mihaylova-Petkov, D. & Model, P. Cell wall sorting signals in surface proteins of gram-positive bacteria. *EMBO J.* **12,** 4803–4811 (1993).

171. Lyons, A. B. & Parish, C. R. Determination of lymphocyte division by flow cytometry. *Journal of Immunological Methods* **171,** 131–137 (1994).

172. Schwartz, A. *et al.* Formalization of the MESF unit of fluorescence intensity. *Cytometry* **57B,** 1–6 (2003).

173. Siegel, T. N., Tan, K. S. W. & Cross, G. A. M. Systematic Study of Sequence Motifs for RNA trans Splicing in Trypanosoma brucei. *Molecular and Cellular Biology* **25,** 9586–9594 (2005).

174. Hotz, H. R., Hartmann, C., Huober, K., Hug, M. & Clayton, C. Mechanisms of developmental regulation in Trypanosoma brucei: a polypyrimidine tract in the 3'-untranslated region of a surface protein mRNA affects RNA abundance and translation. *Nucleic Acids Research* **25,** 3017–3026 (1997).

175. Muñoz-Jordán, J. L., Davies, K. P. & Cross, G. A. Stable expression of mosaic coats of variant surface glycoproteins in Trypanosoma brucei. *Science* **272,** 1795–1797 (1996).

176. Baltz, T. *et al*. Stable expression of two variable surface glycoproteins by cloned Trypanosoma equiperdum. *Nature* **319,** 602–604 (1986).

177. Zahalsky, A. C. & Weinberg, R. L. Immunity to monomorphic Trypanosoma brucei: humoral response. *J. Parasitol.* **62,** 15–19 (1976).

178. Sarvas, H. & Mäkelä, O. Haptenated bacteriophage in the assay of antibody quantity and affinity: maturation of an immune response. *Immunochemistry* **7,** 933–943 (1970).

179. Feinstein, A., Munn, E. A. & Richardson, N. E. The three-dimensional conformation of γM and γA globulin molecules. *Annals of the New York Academy of Sciences* **190,** 104–121 (1971).

180. Czajkowsky, D. M. & Shao, Z. The human IgM pentamer is a mushroom-shaped molecule with a flexural bias. *Proc. Natl. Acad. Sci. U.S.A.* **106,** 14960–14965 (2009).

181. Mehlert, A., Bond, C. S. & Ferguson, M. A. J. The glycoforms of a Trypanosoma brucei variant surface glycoprotein and molecular modeling of a glycosylated surface coat. *Glycobiology* **12,** 607–612 (2002).

182. Dubois, M. E., Demick, K. P. & Mansfield, J. M. Trypanosomes Expressing a Mosaic Variant Surface Glycoprotein Coat Escape Early Detection by the Immune System. *Infect. Immun.* **73,** 2690–2697 (2005).

183. Kelley, L. A., Mezulis, S., Yates, C. M., Wass, M. N. & Sternberg, M. J. E. The Phyre2 web portal for protein modeling, prediction and analysis. *Nat Protoc* **10,** 845–858 (2015).

184. Mendonça-Previato, L., Todeschini, A. R., Heise, N. & Previato, J. O. Protozoan parasite-specific carbohydrate structures. *Current Opinion in Structural Biology* **15,** 499–505 (2005).

185. Vigerust, D. J. & Shepherd, V. L. Virus glycosylation: role in virulence and immune interactions. *Trends in Microbiology* **15,** 211–218 (2007).

186. Abe, Y. *et al*. Effect of the addition of oligosaccharides on the biological activities and antigenicity of influenza A/H3N2 virus hemagglutinin. *Journal of Virology* **78,** 9605–9611 (2004).

187. Gault, J. *et al*. Neisseria meningitidis Type IV Pili Composed of Sequence Invariable Pilins Are Masked by Multisite Glycosylation. *PLoS Pathog* **11,** e1005162 (2015).

188. Racine, R. & Winslow, G. M. IgM in microbial infections: Taken for granted? *Immunology Letters* **125,** 79–85 (2009).

189. Ochsenbein, A. F. *et al*. Control of early viral and bacterial distribution and disease by natural antibodies. *Science* **286,** 2156–2159 (1999).

190. Murugan, R. *et al*. Clonal selection drives protective memory B cell responses in

controlled human malaria infection. *Sci Immunol* **3,** eaap8029 (2018).

191. Cole, L. E. *et al*. Antigen-specific B-1a antibodies induced by Francisella tularensis LPS provide long-term protection against F. tularensis LVS challenge. *Proc. Natl. Acad. Sci. U.S.A.* **106,** 4343–4348 (2009).

192. Alugupalli, K. R. *et al*. B1b lymphocytes confer T cell-independent long-lasting immunity. *Immunity* **21,** 379–390 (2004).

193. Brändlein, S. *et al*. Natural IgM antibodies and immunosurveillance mechanisms against epithelial cancer cells in humans. *Cancer Res.* **63,** 7995–8005 (2003).

194. Vollmers, H. P. & Brändlein, S. Natural antibodies and cancer. *New Biotechnology* **25,** 294–298 (2009).

195. Grönwall, C. & Silverman, G. J. Natural IgM: Beneficial Autoantibodies for the Control of Inflammatory and Autoimmune Disease. *J Clin Immunol* **34,** 12–21 (2014).

196. Watzlawik, J. O., Wootla, B., Painter, M. M., Warrington, A. E. & Rodriguez, M. Cellular targets and mechanistic strategies of remyelination-promoting IgMs as part of the naturally occurring autoantibody repertoire. *Expert Rev Neurother* **13,** 1017–1029 (2013).

197. Witchell, T. D. *et al*. Post-translational modification of LipL32 during Leptospira interrogans infection. *PLoS Negl Trop Dis* **8,** e3280 (2014).

198. Hegge, F. T. *et al*. Unique modifications with phosphocholine and phosphoethanolamine define alternate antigenic forms of Neisseria gonorrhoeae type IV pili. *Proc. Natl. Acad. Sci. U.S.A.* **101,** 10798–10803 (2004).

199. De Greef, C. & Hamers, R. The serum resistance-associated (SRA) gene of Trypanosoma brucei rhodesiense encodes a variant surface glycoprotein-like protein. *Mol. Biochem. Parasitol.* **68,** 277–284 (1994).

200. Wiedemar, N. *et al*. Beyond immune escape: a variant surface glycoprotein causes suramin resistance in Trypanosoma brucei. *Mol. Microbiol.* **107,** 57–67 (2018).

201. Smith, J. D. The role of PfEMP1 adhesion domain classification in Plasmodium falciparum pathogenesis research. *Mol. Biochem. Parasitol.* **195,** 82–87 (2014).

202. Norris, S. J. Antigenic variation with a twist--the Borrelia story. *Mol. Microbiol.* **60,** 1319–1322 (2006).

203. Lisowska, E. The role of glycosylation in protein antigenic properties. *Cell. Mol. Life Sci.* **59,** 445–455 (2002).

204. Rangappa, S. *et al*. Effects of the multiple O-glycosylation states on antibody recognition of the immunodominant motif in MUC1 extracellular tandem repeats. *Med.*

Chem. Commun. **7,** 1102–1122 (2016).

205. Winter, H. C., Oscarson, S., Slättegård, R., Tian, M. & Goldstein, I. J. Banana lectin is unique in its recognition of the reducing unit of 3-O-beta-glucosyl/mannosyl disaccharides: a calorimetric study. *Glycobiology* **15,** 1043–1050 (2005).

206. Schulz, D., Zaringhalam, M., Papavasiliou, F. N. & Kim, H.-S. Base J and H3.V Regulate Transcriptional Termination in Trypanosoma brucei. *PLoS Genet* **12,** e1005762–21 (2016).

207. Burkard, G., Fragoso, C. M. & Roditi, I. Highly efficient stable transformation of bloodstream forms of Trypanosoma brucei. *Mol. Biochem. Parasitol.* **153,** 220–223 (2007).

208. Raz, A. & Fischetti, V. A. Sortase A localizes to distinct foci on the Streptococcus pyogenes membrane. *Proc. Natl. Acad. Sci. U.S.A.* **105,** 18549–18554 (2008).

209. Pinger, J., Chowdhury, S. & Papavasiliou, F. N. Variant surface glycoprotein density defines an immune evasion threshold for African trypanosomes undergoing antigenic variation. *Nature Communications* **8,** 828 (2017).